

# Empirical approaches to Fröhlich excitonic polarons in polar semiconductors with application to 3D halide perovskites

*Dedicated to the memory of Prof. Jozef T. Devreese [1937-2023]*

*Jacky Even<sup>1,\*</sup>, Simon Thebaud<sup>1</sup>, Aseem R. Kshirsagar<sup>2</sup>, Laurent Pedesseau<sup>1</sup>, Marios Zacharias<sup>1</sup>,  
Claudine Katan<sup>2,\*</sup>*

<sup>1</sup> Univ Rennes, INSA Rennes, CNRS, Institut FOTON, UMR 6082, Rennes, France.

<sup>2</sup> Univ Rennes, ENSCR, CNRS, ISCR-UMR 6226, Rennes F-35000, France.

AUTHOR INFORMATION

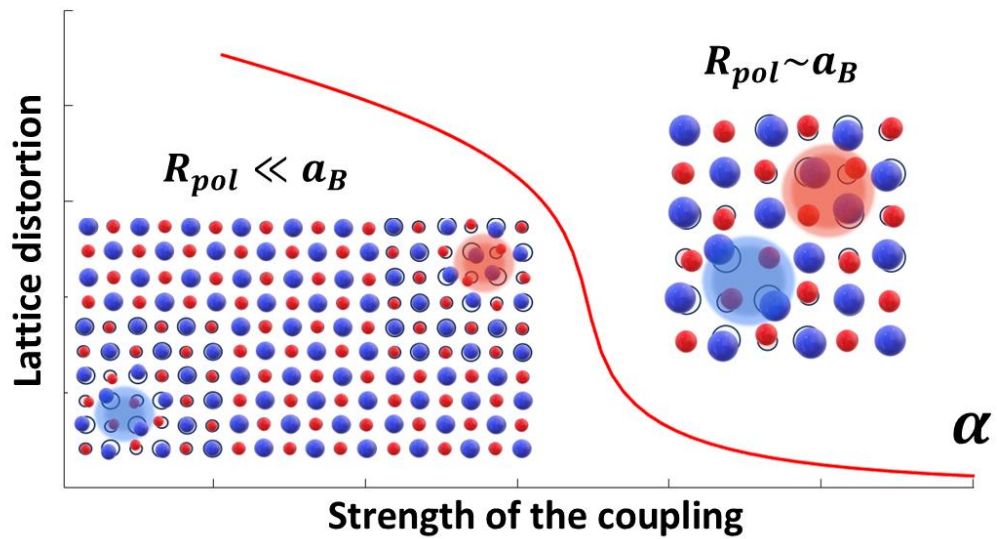
## **Corresponding Author**

Jacky Even, Email: [jacky.even@insa-rennes.fr](mailto:jacky.even@insa-rennes.fr)

Claudine Katan, Email: [claudine.katan@univ-rennes.fr](mailto:claudine.katan@univ-rennes.fr)

ABSTRACT. The paper reviews the physics of Fröhlich excitonic polarons from the viewpoint of empirical approaches with some original developments. Models for excitonic polarons in ionic semiconductors in the spirit of the Lee Low and Pines (LLP) model for free polarons were initiated by Toyozawa and Hermanson and extended by Pollman and Buttner (PB). The dominant electron-hole interaction with the lattice introduced by Fröhlich is represented by a long-range effective interaction with a single longitudinal optical polar mode. The properties of the excitonic polarons are characterized by various physical quantities such as effective dielectric constants, effective masses, virtual phonon populations, carrier self-energies and binding energies, and effective electron-hole interactions mediated by the lattice. In 3D perovskites, the excitonic polarons deviate from the simplified picture of weakly interacting (almost free) polarons, with sizeable effects of electron-hole correlations on all the physical properties. In the case of equal electron and hole masses, a new analytical expression of the approximated version of the PB effective interaction potential is derived and compared to the expression of Haken. The refined Kane approach to PB's model is further shown to bridge the regime between weakly interacting polarons and excitonic polarons with strong correlations, as well as to match LLP expressions for free polarons. An approximate scheme derived from Kane's model is also proposed for the regime of weakly interacting polarons. In the case of equal electron and hole masses, the expression of the excitonic polaron energy dispersion is analytically derived by analogy with the one of LLP for free polarons. The center of mass motion is studied, and analytical formulas are derived. Finally, Kane and PB's semi-empirical models are extended to include Fröhlich-like interactions with multiple polar phonons. Model results and limitations are illustrated in the case study of lead halide perovskites, for which almost equal electron and hole masses have been reported. Inclusion of multiple polar phonons reconciles various experimental observations related to exciton binding energies, reduced

masses, effective dielectric constants, multiple polar modes evidenced by infrared or THz spectroscopies, LO-TO splitting of polar modes, phonon side bands to exciton photoluminescence lines.



TOC GRAPHICS

In ionic materials such as 3D perovskites, a polar coupling to the lattice occurs for isolated charge carriers. The situation is more complex for bound electron-hole (e-h) pairs called excitons, since correlations between charge carriers may also additionally affect displacements of lattice ions. The polar coupling to the lattice can be treated as a perturbation to a single charge carrier in the weak electron-phonon (e-ph) coupling regime but eventually leads to the formation of a more complex quasiparticle known as a “polaron” often depicted as a charge surrounded by a lattice distortion (Figure 1) or a virtual phonon cloud. In recent years, the concept of polaron has witnessed renewed interest in different areas of physics and chemistry, including the highly fashionable context of halogenated perovskites. Unfortunately, the nature of polaron in question is not always clearly apprehended. However, the type of polaron must be well anticipated as it is essential to validate the theoretical model supporting experimental evidence.<sup>1,2</sup>

The original description of the polar coupling to a periodic lattice was introduced by Fröhlich as early as 1937.<sup>3</sup> In the case of a diatomic lattice with the approximation of a single undispersed optical phonon branch, he managed to relate in an elegant way the microscopic e-ph coupling Hamiltonian to the difference between macroscopic dielectric constants,  $\epsilon_\infty$  and  $\epsilon_s$ , the optical (high frequency) and static dielectric constants, respectively. This shall appear natural since  $\epsilon_s$  includes the additional contribution of ions to the lattice polarizability. The strength of the e-ph coupling in such a case is usually represented by the dimensionless constant<sup>4</sup>

$$\alpha_e = \frac{e^2}{4\pi\epsilon_0\hbar} \left( \frac{m_e}{2\hbar\omega_{LO}} \right)^{1/2} \frac{1}{\epsilon^*} \quad (1)$$

where  $m_e$  and  $e$  are the electron effective mass and charge, the polarizability of the ionic lattice is represented by  $\frac{1}{\epsilon^*} = \left( \frac{1}{\epsilon_\infty} - \frac{1}{\epsilon_s} \right)$  and  $\hbar\omega_{LO}$  is the energy of the characteristic polar longitudinal optical (LO) phonon at the  $\Gamma$  point of the Brillouin zone in the diatomic lattice. Herein, we use the international system of units (SI) with usual meanings of  $\epsilon_0$  and  $\hbar$ . It is worth noting that the  $\epsilon_\infty$

and  $\epsilon_s$  difference vanishes in conventional non-polar semiconductors such as Si, while the contribution of the polar mode appears as a small correction to  $\epsilon_\infty$  in polar III-V semiconductors such as GaAs, InP or InAs.  $\alpha_e \ll 1$  defines the weak coupling regime and is thus relevant for this class of semiconductors. For this regime, Fröhlich proposed initially a perturbative approach to evaluate the modification of the carrier effective mass and its stabilization energy (self-energy) due to the creation of a distortion field in the surrounding lattice. The extent of the distortion around the charge carrier can be evaluated by the characteristic length

$$R_e = \left( \frac{\hbar}{2m_e\omega_{LO}} \right)^{1/2} \quad (2)$$

which is the so called “free polaron radius”. In a very crude approximation, the polaron can thus be viewed as a quasi-particle surrounded by a spherical distortion field of radius  $R_e$  (Fig. 1). The radius is larger for particles with small masses and soft lattices. The dimensionless constant can be rewritten as  $\alpha_e = \frac{e^2}{8\pi\epsilon_0\hbar\omega_{LO}R_e} \frac{1}{\epsilon^*}$  evidencing that  $\alpha_e$  includes  $R_e$  as well as the lattice polarizability through  $\frac{1}{\epsilon^*}$ . The intermediate coupling regime usually extends roughly to  $\alpha_e \sim 3$ . The validity of the Fröhlich formulation has been tested for more complex polar semiconductors with state-of-the-art ab initio approaches,<sup>5-8</sup> and the coupling between excitons and phonons is progressively tackled at this level of theory.<sup>9-11</sup>

At the empirical level, the correlated motion of an e-h forming a bound exciton state can be modelled using a Wannier Hamiltonian based on charge carrier effective masses and the dielectric constant  $\epsilon_\infty$  of the background lattice. After decoupling the e-h pair center of mass motion, the wavefunction for the relative e-h motion ( $r$ ) of the exciton 1S ground state is found to correspond to the textbook solution for the electron state in the hydrogen atom:  $\varphi_{1S}(\vec{r}) = \frac{e^{-r/a_B}}{a_B^{3/2}\pi^{1/2}}$ .<sup>12</sup> The 1S exciton Bohr radius  $a_B$  corresponds to the average distance between the

electron and the hole in a simple picture. To account for the polar coupling of charge carriers and match the experimental result for the exciton binding energy, a relative effective dielectric constant is very often taken arbitrarily in the  $\epsilon_\infty \leq \epsilon_{eff} \leq \epsilon_s$  range. However, to get more insight into the physics of excitons and the various consequences of the coupling of charge carriers to the lattice, it is necessary to switch to more advanced theoretical descriptions.

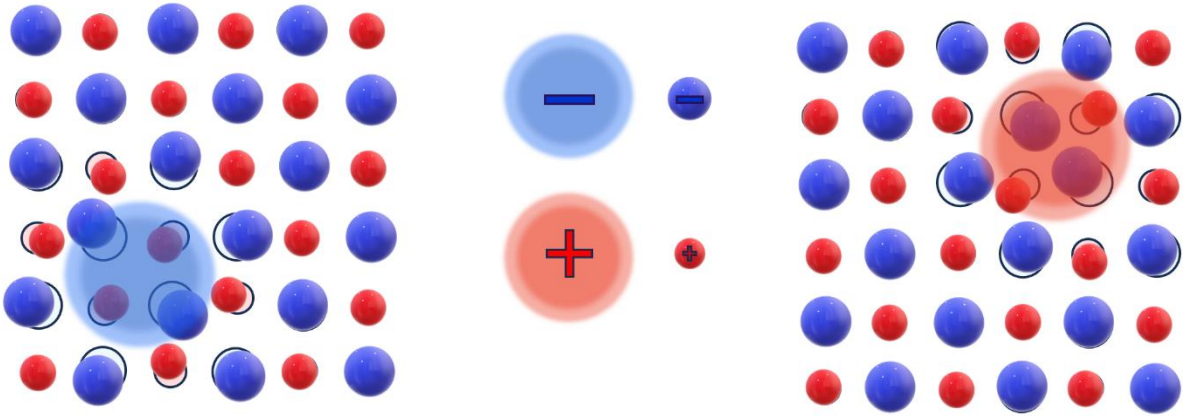


**Figure 1.** (left) Artist view of the polar lattice distortion for a negative Fröhlich polaron. (center) The electron and the hole are represented by large shallow spheres, while lattice anions or cations are represented by smaller negatively or positively charged spheres. (right) Artist view of the polar lattice distortion for a positive Fröhlich polaron.

A deep understanding of the physics of excitons in complex materials is still lacking, particularly in 3D halide perovskites which are the most promising class of new semiconductors for solar cell applications.<sup>13–16</sup> 3D halide perovskites are almost ideal direct band gap semiconductors by comparison to conventional III-V, II-VI or silicon semiconductors, with low effective masses and sizeable optical oscillator strengths. However, they exhibit distinct physical properties owing to their unusual softness of the crystal lattice and its strong ionicity. The latter

characteristic directly affects the magnitude of the carrier-lattice interactions and the dielectric properties, including the formation of exciton complexes. 3D halide perovskites form a novel class of semiconductors with a simple and original structure of the electronic band edges at the R point of its cubic Brillouin zone, that can be analyzed from an orbital combination viewpoint by tight binding models coupled with double group symmetry analyses.<sup>17</sup> As a consequence of the perovskite crystallographic structure, the formation of antibonding s-p states at the R point across the electronic band gap is leading to a  $S_z = \frac{1}{2}$  state at the top of the valence band ( $R_6^+$ ) and a  $J_z = \frac{1}{2}$  split-off band ( $R_6^-$ ) at the bottom of the conduction band due to the presence of a giant spin-orbit coupling<sup>18-22</sup>. It affords specific selection rules for carrier-phonon scattering mechanisms including a weak deformation potential mechanism related to acoustic phonons and stronger polar mechanisms related to optical phonons and low frequency relaxations, characterized by pseudo-spin variables.<sup>18,19,21,23</sup> Density functional theory (DFT) calculations including spin-orbit coupling predict that 3D halide perovskites exhibit approximately similar hole ( $h$ ) and electron effective masses, i.e.  $m_h \approx m_e$ .<sup>18,24-27</sup> To the best of our knowledge, the  $m_e = m_h$  approximation, which is quite unusual among other semiconductors, is consistent with most experimental observations in case of 3D halide perovskites.<sup>28-30</sup> Excitonic properties have been at the center of discussions since the beginning of the hype on perovskite photovoltaics in 2012. Early 2014, by fitting the line shape of the low temperature (LT) absorption, some of us predicted that  $E_{b,1S} \approx 15 \text{ meV}$ .<sup>19</sup> This motivated the direct measurement of the exciton binding energy in 2015,<sup>31</sup> which led to a value of  $16 \text{ meV}$ , significantly smaller than the experimental values reported earlier. Since then, photovoltaic mechanisms in perovskites are considered closer to the mechanism in classical semiconductors, than to Dye Sensitized Solar Cells, as initially envisioned. Thus, due to the low exciton binding energy in 3D halide perovskites, only a negligible proportion of charge carriers

form excitons at the temperatures and carrier densities corresponding to typical device operating conditions.<sup>32</sup> Under such conditions, discussions about the nature of the coupling between charge carriers and the lattice are essentially related to either electrons or holes. The understanding of the excitonic properties, especially the exciton fine structure and the nature of exciton complexes, was further questioned with the advent of perovskite quantum dots (QD) leading to prospects for LEDs and quantum light emission.<sup>33</sup> The recent controversy about the exciton fine structure reflects the importance of a proper description of perovskite excitonic properties. The dispute between the initial hypothesis of a fine structure related to a singlet dark ground state<sup>20,34</sup> and the alternative proposal of an inverted dark-bright ordering due to an effective exchange energy stemming from a Rashba effect,<sup>35,36</sup> was closed only recently in favor of the initial assertion.<sup>37–39</sup>

Several open questions remain, especially about the nature of the coupling between the charge carriers and the lattice dynamics. This coupling is very sensitive to the polar character of the lattice and exhibits specific selection rules with respect to conventional semiconductors.<sup>21,40</sup> Recently developed ab initio frameworks have contributed to unravelling the peculiar lattice dynamics in 3D halide perovskites at high temperature, notably identifying that polymorphous networks correspond to a more realistic description of these crystals than the highly symmetric reference cubic perovskite lattice.<sup>41,42</sup> The developed ab initio framework achieves simultaneous description of vibrational and optoelectronic properties of highly disordered semiconductors in a strong anharmonic regime.<sup>43–46</sup> Several aspects have to be considered for description of these properties, namely the stochastic nature, short range and anisotropic correlations of atomic motions, among others. This leads to smearing of the electronic and vibrational densities of states as well as a smooth change of the electronic band gap at high temperature. Thus, within the room temperature (RT) regime, conventional Hamiltonian expressions for e-ph interactions are

questionable. In the low-temperature range, the expression of the polar coupling between carriers and optical phonons in terms of conventional e-ph Hamiltonian<sup>47</sup> is reasonably justified, despite the softness of the lattice. However, the simple e-ph Hamiltonian historically introduced by Fröhlich<sup>3</sup> is also inadequate because of the multiplicity of optical vibrational modes that come into play. We stress that most studies assume that the polar coupling to optical modes is effectively dominated by a single one.<sup>48</sup> This is rigorously incorrect for the cubic phase of halide perovskites.<sup>20</sup> However, as described early by Toyozawa,<sup>49</sup> Fröhlich's semi-empirical approach to e-ph coupling can be extended to polar lattices with multiple optical modes assuming harmonic oscillators with a single frequency and without dissipation. The polaronic coupling in perovskite bulk and nanostructures modelled using this approach deserves assessment and clarification. Existing papers and reviews on polaronic effects in 3D halide perovskites are mainly focused on free polarons and seldom address specifically excitonic polarons.<sup>50-54</sup> The effect of e-h correlations is also often not considered in the analysis of experimental results on "polaronic" distortions.<sup>55</sup> There have been a few attempts to directly perform excitonic polaron calculations with interaction potentials designed for the weak coupling regime.<sup>56</sup> However, we will see that the intermediate coupling regime is more relevant to the physics of 3D halide perovskites.

As a matter of fact, several fundamental questions remain unanswered such as: what is the significance of the so-called phonon cloud and its relation to the free polaron radius (Figure 1)? Are these quantities still relevant when the correlated e-h motion is considered (*vide infra*)? Do we need to consider similar mass renormalizations for free polarons and excitonic polarons (also sometimes referred to as polaronic exciton or exciton-polaron)? What is the origin of the intermediate effective dielectric constant needed for the description of the exciton?<sup>19</sup> What are the consequences of the polaronic coupling regime in terms of electronic band gap renormalization?<sup>11</sup>

How is it possible to account explicitly for the complexity of the perovskite lattice dynamics in an excitonic polaron modelling, especially the multimode character of the perovskite lattice? What is the origin of phonon sidebands observed close to the photoluminescence peak? What is the connection between the temperature broadening of the lattice and the lattice dynamics in 3D halide perovskites? To address these questions, we use in this paper a complete non-atomistic and empirical theoretical framework that has not yet been exploited in the context of 3D perovskites. Its strength lies in the fact that the physics of free polarons (Figure 1) and excitonic polarons (Figure 4) are treated on an equal footing (Figure 3). It provides insights into physical properties without the need to resort to complex and computationally expensive first-principles or machine learning/artificial intelligence driven approaches. We will base our description of excitonic polarons<sup>57,58</sup> on the Pollman-Buttner's (PB) model,<sup>59,60</sup> later refined by Kane<sup>61</sup> (herein quoted as the Pollman-Buttner-Kane (PBK) model). The transformation introduced initially by Toyozawa and Hermanson (TH) for excitonic polarons<sup>57,58</sup> affords a proper connection to the Lee-Low-Pines (LLP) theory<sup>62,63</sup> developed for free polarons. **Our aim is to use the same theoretical framework for the various interaction regimes (Fig. 3).** Other frameworks exist, based for example on alternative variational approaches for free polarons<sup>64</sup> and excitonic polarons<sup>65</sup>, or on the integral method.<sup>66-68</sup> Importantly, our approach complements recent theoretical developments providing atomistic description of free and excitonic polarons<sup>7,11,69-73</sup>. Some recent developments might be already relevant to the weak to intermediate coupling regime discussed in this work, but thorough numerical demonstrations are needed.<sup>69</sup> Here, we will introduce the basic picture for excitonic polarons, within the PB's framework which has the advantage of being numerically very efficient and already extended to more complex problems including bipolarons,<sup>74</sup> biexcitons,<sup>75</sup> but also 2D quantum wells or 0D nanostructures, with inclusion of both dielectric and quantum confinement

effects for excitons and phonons.<sup>76-79</sup> We will use experimental data for semiconductors exhibiting the classical zinc-blende (GaAs, Fig. 2a), CsCl (TlCl, Fig.2.b) or perovskite (CsPbI<sub>3</sub>, Fig. 2.c) crystallographic structures. Various materials and structures studied in this work (Table 1) allow consideration of a wide range of electron-phonon coupling strengths and extension of the empirical models from single (LLP/PB/PBK) to multiple polar phonon modes (MLLP/MPB/MPBK vide infra). Among these materials, TlCl (Fig.2.b) constitutes an ideal playground to test the accuracy of the exciton-phonon coupling models as this material shares common features with more complex halide perovskite materials (Table 1) such as: 1) almost equal electron and hole masses, 2) strong ionicity, 3) intermediate coupling regime, and simplifying 4) in a simpler situation with only one polar optical phonon.

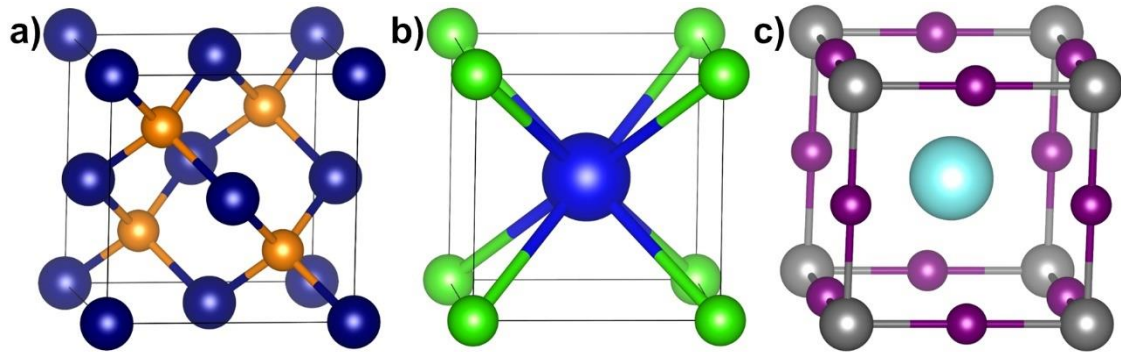


**Figure 2.** Schematic representations of (a) the zinc-blende structure of GaAs (b) the CsCl structure of TlCl (c) the perovskite structure of CsPbI<sub>3</sub>

Semiconductor	Structure Type	Lattice constant (Å)	$m_e$	$m_h$	$\epsilon_\infty$	$\epsilon_s$	$\hbar\omega_{LO}$ (meV)	$R_e$ (nm)	$R_h$ (nm)	$\alpha_e$	$\alpha_h$
GaAs	Zinc blende	5.7	0.0665	0.500	11.1	13.1	36.8	3.8	1.4	0.07	0.19
CdS	Zinc blende	5.4	0.185	0.700	5.3	8.6	36.8	2.4	1.0	0.61	1.48
TlCl	Caesium Chloride	3.8	0.365	0.365	5.1	37.6	21.5	2.2	2.2	2.58	2.58
MAPbI <sub>3</sub>	Perovskite	6.3	0.208	0.208	5.0	34.8	8.2*	4.7	4.7	3.18	3.18
MAPbBr <sub>3</sub>	Perovskite	5.9	0.234	0.234	4.3	25.5	13.1*	3.5	3.5	3.01	3.01
CsPbCl <sub>3</sub>	Perovskite	5.5	0.404	0.404	3.7	26.0	25.6*	1.9	1.9	3.40	3.40
LiF	Sodium Chloride	4.0	0.880	4.40	2.0	10.6	77	0.75	0.33	4.94	11.0

**Table 1. Ground state parameters for excitonic polaron calculations with a single polar optical phonon and corresponding data for free polarons.** Material parameters used for simulation with single phonon mode excitonic polaron models summarized in Figure 3, including the relative effective masses for the electron and the hole, the high frequency and static relative dielectric constants and the effective longitudinal optical phonon energies. All material parameters for GaAs, CdS, TlCl are obtained from ref. <sup>61</sup>, with a slight modification for TlCl, where the average of  $m_e = 0.37$  and  $m_h = 0.36$  is considered. For halide perovskites, effective longitudinal optical phonon energies  $\hbar\omega_{LO}$  (values given with an asterisk \*) are deduced within the PBK model so as to retrieve the experimental exciton binding energy of 16/25/64 meV for MAPbI<sub>3</sub><sup>31</sup>/MAPbBr<sub>3</sub><sup>29</sup>/CsPbCl<sub>3</sub><sup>80</sup>. The static and high frequency relative dielectric constants of MAPbI<sub>3</sub> and MAPbBr<sub>3</sub> are taken from ref. <sup>81</sup>,  $\epsilon_\infty = 3.7$  for CsPbCl<sub>3</sub> is obtained from ref. <sup>82</sup> and  $\epsilon_\infty = 3.7$  is estimated from the experimental optical LO and TO phonon frequencies<sup>82</sup> using Cochran-Cowley relation<sup>83</sup>, which is a generalization of Lyddane-Sachs-Teller equation<sup>84</sup> (Eq. 13). The relative effective masses are deduced from the experimentally determined reduced mass,<sup>29,31,80</sup> assuming  $m_e = m_h$ . Data for LiF are taken from Dai and coworkers.<sup>11</sup> Computed free polaron radii (Eq. 2) and  $\alpha$  values (Eq. 1) are also given.

We provide a critical comparison of various approximate models available in literature and provide several new analytical results for a specific case of  $m_h \approx m_e$ . The analytical description includes an effective interaction mediated by the lattice, self-energies, center of mass motion, virtual phonon populations, Huang-Rhys factors for phonon sidebands and total energy of the excitonic polarons. We extend PB's framework to include the multimode character of the lattice dynamics of halide perovskites using Toyozawa's generalization of Fröhlich semi-empirical approach to polar optical e-ph coupling Hamiltonian.<sup>49,85</sup> This allows analyzing the evolution of the exciton properties of 3D halide perovskites as a function of temperature and clarifies the limitations of PB framework.

### Limitations of the Wannier exciton model in a polar semiconductor

It is convenient to start with the classic Wannier Hamiltonian based on effective mass descriptions of the interacting electron and hole (exciton denoted by  $X$ ).<sup>86,87,12</sup>

$$\hat{H}_X = E_g + \frac{\hat{p}_e^2}{2m_e} + \frac{\hat{p}_h^2}{2m_h} - \frac{e^2}{4\pi\epsilon_0\epsilon_{eff}|\vec{r}_e - \vec{r}_h|}, \quad (3)$$

where  $\vec{r}_e$  ( $\vec{r}_h$ ) denotes the electron (hole) coordinates,  $\hat{p}_e$  ( $\hat{p}_h$ ) its momentum,  $m_e$  ( $m_h$ ) its effective mass,  $\epsilon_{eff}$  is a relative effective dielectric constant and  $E_g$  corresponds to the fundamental band gap of the semiconductor. At this stage, several points can be stressed. This Hamiltonian is formulated in real space, which allows an attractive analogy with the text-book quantum mechanical problem of the hydrogen atom. It approximates the more rigorous Bethe-Salpeter equation (BSE) for the exciton in a periodic solid, which is expressed in reciprocal space. In the

Wannier Hamiltonian framework, the description of a non-interacting electron (hole) is implicitly approximated by a wavefunction of the form:

$$\varphi_{\vec{k}_e}(\vec{r}_e) \approx u_{\vec{k}_e=0}(\vec{r}_e) \frac{e^{i\vec{k}_e \cdot \vec{r}_e}}{\sqrt{V}} \left( \varphi_{\vec{k}_h}(\vec{r}_h) \approx u_{\vec{k}_h=0}(\vec{r}_h) \frac{e^{i\vec{k}_h \cdot \vec{r}_h}}{\sqrt{V}} \right). \quad (4)$$

Here,  $\vec{k}_e$  ( $\vec{k}_h$ ) denotes the electron (hole) wavevector and  $V$  is the unit cell volume. The details of the lattice periodicity and atomic structure are accounted by the  $u_{\vec{k}_e=0}(\vec{r}_e)$  ( $u_{\vec{k}_h=0}(\vec{r}_h)$ ) Bloch function, while the effective mass  $m_e$  ( $m_h$ ) is derived from assumed parabolic electronic dispersion. Within this approximation, the wavevector  $\vec{k}_e$  ( $\vec{k}_h$ ) is expressed in spherical coordinates with a modulus extended to  $+\infty$ . It must be revised if multiband features or structural distortions need to be considered. The model can be further simplified by adopting center of mass coordinates, since the total momentum  $\hat{P}$  commutes with the Hamiltonian

$$\hat{H}_X = E_g + \frac{\hat{P}^2}{2M} + \frac{\hat{p}^2}{2\mu} - \frac{e^2}{4\pi\epsilon_0\epsilon_{eff}r}, \quad (5)$$

where  $M = m_e + m_h$  and  $\mu = \frac{1}{m_e} + \frac{1}{m_h}$  are the total and reduced masses, respectively. Solutions are thus products of wavefunctions for the center of mass coordinate  $\vec{R}$  and for the relative e-h motion given by  $\vec{r}$  ( $\vec{r} = \vec{r}_e - \vec{r}_h$ ), with a well-known expression for the 1S exciton ground state:

$$\varphi_{1S,K}(\vec{r}) = \frac{e^{-r/a_B}}{a_B^{3/2}\pi^{1/2}} \times \frac{e^{i\vec{K} \cdot \vec{R}}}{\sqrt{V}}, \quad (6)$$

where  $a_B$  is the 1S exciton Bohr radius, which scales as

$$a_B(\epsilon_{eff}, \mu) = a_B^{vac} \times \left( \frac{\epsilon_{eff}}{\mu} \right) \quad (7)$$

and  $\vec{K}$  is the sum of wavevectors. In quest for a simple picture for the Wannier exciton, it is tempting to assume that the electron and hole are point charges (Fig. 4). We stress that for such an oversimplified representation, the same limitations apply as those related to the Bohr model of the hydrogen atom.<sup>86,87,12</sup> Therefore, constructing e-h potential including effects of the Fröhlich interaction by assuming point charges<sup>88</sup> must be handled very carefully, especially for 1S exciton in the intermediate coupling regime.

The 1S ground state exciton energy is given by:

$$E_{1S, K} = E_{uncorr} - Ry, \quad (8)$$

where:

$$E_{uncorr} = E_g + \frac{\hbar^2 K^2}{2M}, \quad (9)$$

denotes the energy of uncorrelated carriers, and  $Ry$  is the Rydberg energy of the Wannier exciton, which scales as

$$Ry(\varepsilon_{eff}, \mu) = Ry^{vac} \times \left( \frac{\mu}{\varepsilon_{eff}^2} \right). \quad (10)$$

The 1S exciton binding energy is  $E_{b,1S} = Ry$  in this Wannier model. Independent measurements of Landau levels and exciton binding energy allow the determination of the effective reduced mass  $\mu^{eff}$  and dielectric constant  $\varepsilon_{eff}$  (Figure 3).<sup>31</sup> However, the choice of the value for  $\varepsilon_{eff}$  for a Wannier model is not obvious, and more, it is experimentally observed that  $\mu^{eff}$  may deviate from the bare reduced mass  $\mu$ .<sup>89</sup> But, these quantities can be theoretically derived using an approach that

explicitly includes electron-hole (e-h) correlations as well as the interactions between charge carriers and phonons (Figure 3 and vide infra).

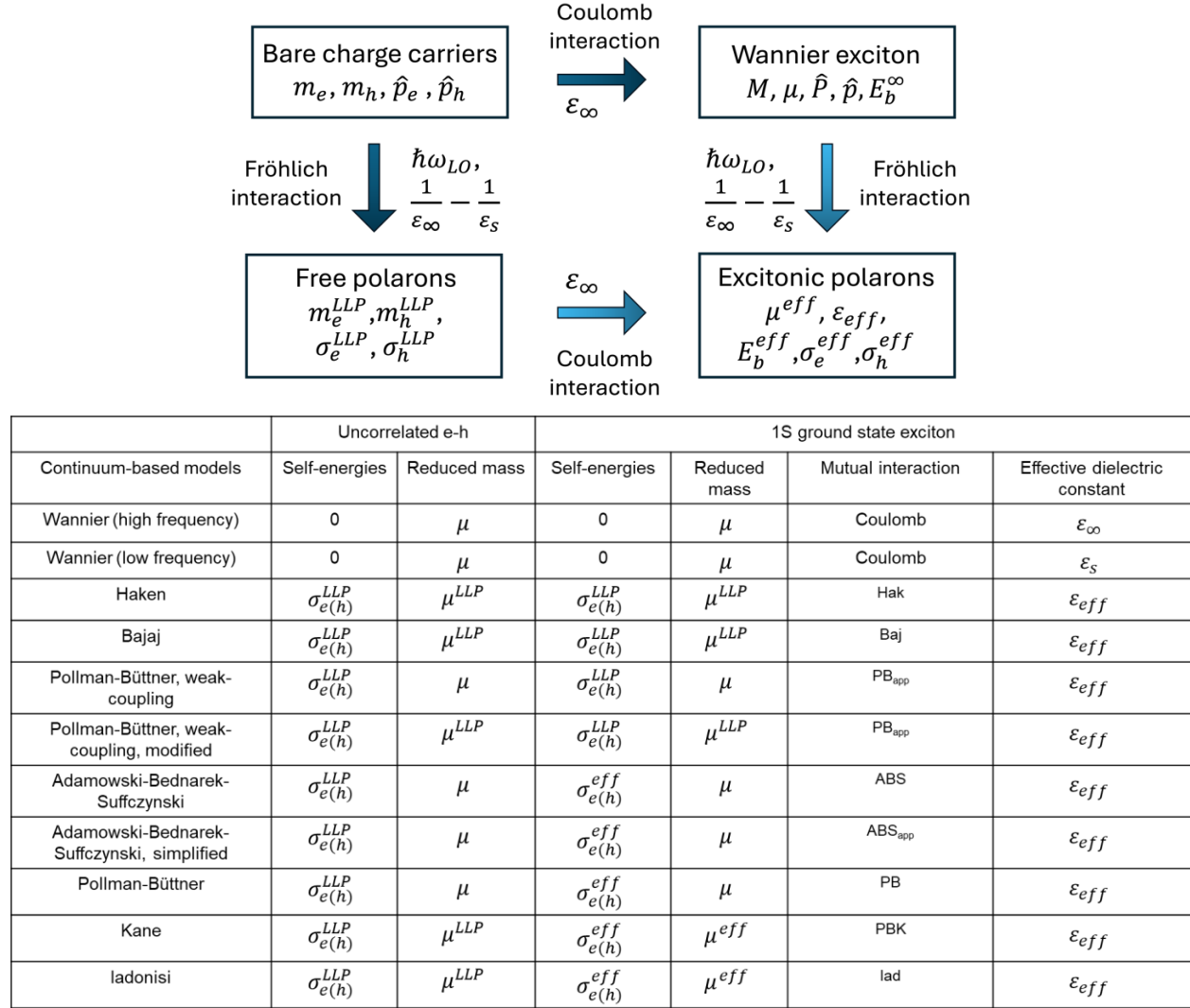


**Figure 3.** (Top) Various levels of theory analyzed in this work, with corresponding material parameters and physical observables. (Bottom) Continuum-based model parameters used for uncorrelated charge carriers and the 1S exciton ground state.

### Interplay between lattice distortion and electron-hole correlations

A more convenient way to understand qualitatively the difference between the weak and the intermediate coupling regimes for excitonic polarons, is to consider the value of the free polaron radius ( $R_{pol}$ ) with respect to the probability density of the 1S exciton wavefunction as a function of the e-h distance (Figure 4a). The dashed line in Figure 4b indicates that the crossover from the weak to intermediate exciton-polaron coupling regime occurs for  $\tilde{R}_{pol} = R_{pol}/a_B = 1/4$ . The intermediate exciton-polaron coupling regime can thus be schematically described as a regime, where the two dressed quasi-particles represented as spheres of radius  $R_{pol}$  cannot be contained into a sphere of diameter  $a_B$  without overlapping. This cross-over will be explored mathematically as follows. Regarding its physical interpretation, the intermediate exciton-polaron coupling regime represents a regime where the interplay between e-h correlations and their coupling to the lattice is complex. TlCl and all the halide perovskites studied in the present work (Tables 1 and 2) fall into this regime. Notice that for a free polaron, the classification of the coupling regime essentially refers to the value of the constant  $\alpha_e$  (Eq. (1)).<sup>90</sup>

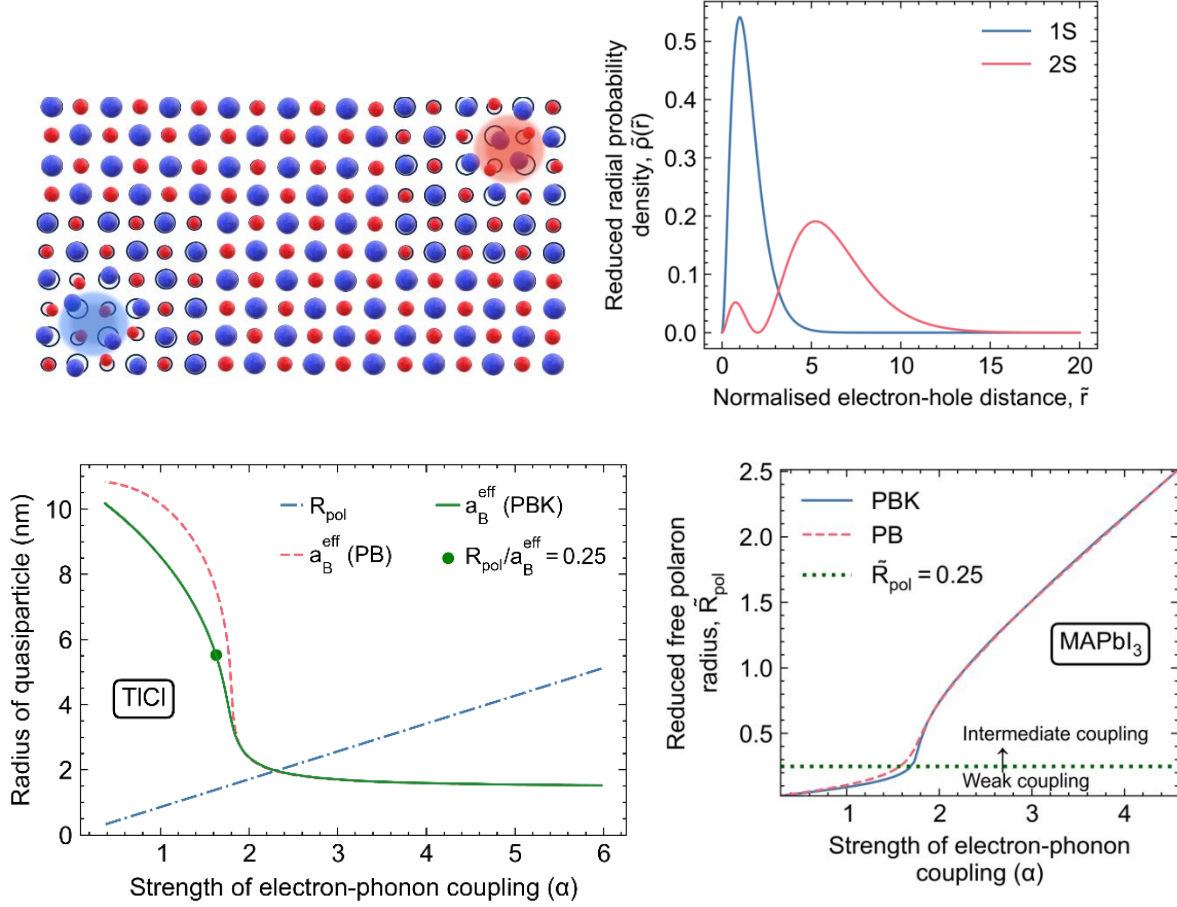


**Figure 4.** (Top left) Illustration of the regime where the e-h correlations weakly influence free polaronic distortions. The two charges are separated by a distance greater than the free polaron radius, with here the same radius  $R_e = R_h = R_{pol}$  for the electron and the hole.  $\tilde{R}_{pol}$  denotes the reduced free polaron radius  $\tilde{R}_{pol} = R_{pol}/a_B \ll 1$ .  $a_B$  is the 1S exciton Bohr radius. (Top right) Reduced radial probability densities  $\tilde{\rho}(\tilde{r}) = \rho(r) * a_B$  of hydrogenic 1S and 2S Wannier exciton wavefunctions as a function of the reduced e-h distance  $\tilde{r} = r/a_B$  (the same value of  $a_B$  is considered here for both 1S and 2S excitons) (Right) Artist view of two charges separated by a short distance, where the polaronic distortion differs from the simple superposition of the distortions related to free polarons. (Bottom left) Variation of the free polaron radius (blue line), Bohr radius within the PBK model (green line) and the PB model (red line) as a function of  $\alpha$

taking materials parameters for TlCl (Table 1). The variation of  $\alpha$  is obtained by varying the effective phonon frequency  $\hbar\omega_{LO}$ . (Bottom right) Variation of the reduced free polaron radius as obtained within the PBK model (blue straight line) and the PB model (red dashed line) as a function of  $\alpha$  taking materials parameters for MAPbI<sub>3</sub> (Table 1). The variation of  $\alpha$  is obtained by varying the effective phonon frequency  $\hbar\omega_{LO}$ . The differences between the two models are coming from small differences between the computed Bohr radii  $a_B$ . To match the experimentally determined exciton binding energy of 16 meV,<sup>31</sup> the effective longitudinal optical phonon energy derived within the PBK model amounts to 8.2 meV ( $\alpha = 3.18$ ). The dashed horizontal line indicates that the crossover from the weak to intermediate exciton-polaron coupling regime occurs for  $\tilde{R}_{pol} = 1/4$ , that is  $4R_{pol} = a_B$ .

Semiconductor	$\mu$	$\mu^{PBK}$	$\mu^{LLP}$	$E_b^\infty$ (meV)	$E_b^{Hak}$ (meV)	$E_b^{PBKapp}$ (meV)	$E_b^{PBK}$ (meV)	$E_b^{PB}$ (meV)	$E_b^{PBapp}$ (meV)	$E_b^s$ (meV)	$\varepsilon^{PBK}$	$a_B^{PBK}$ (nm)
GaAs	0.0614	0.0619	0.0623	6.8	5.1	5.0	5.0	4.9	4.9	4.9	13.0	11.0
CdS	0.158	0.161	0.180	78	50	40	38	38	35	29	7.6	2.1
TlCl	0.183	0.191	0.290	96	52	28	16	16	7.3	1.8	12.6	1.8
MAPbI <sub>3</sub>	0.104	0.106	0.184	57	40	27	16	16	9.4	1.1	9.4	2.9
MAPbBr <sub>3</sub>	0.117	0.119	0.200	86	60	41	25	25	15	2.4	8.0	2.2
CsPbCl <sub>3</sub>	0.202	0.205	0.372	201	149	105	64	63	38	4.1	6.6	1.1

**Table 2. Excitonic polaron properties.** Bare, PBK and LLP reduced masses. Exciton binding energies  $E_b^\infty$  and  $E_b^s$  are computed using the bare reduced mass  $\mu$  with  $\varepsilon_\infty$  or  $\varepsilon_s$ , respectively.  $E_b^{Hak}$ ,  $E_b^{PBKapp}$  are computed using the LLP reduced mass  $\mu_{LLP}$  and  $V_{latt}^{Hak}(\vec{r})$  (Eq. 64/65),  $V_{latt}^{PBapp}(\vec{r})$  (Eq. 63/66), respectively.  $E_b^{PBapp}$  are computed using the bare reduced mass  $\mu$  with  $V_{latt}^{PBapp}(\vec{r})$  (Eq. 63/66). The reduced mass  $\mu^{PBK}$  is obtained together with the binding energy  $E_b^{PBK}$ , the effective dielectric constant  $\varepsilon^{PBK}$  and the Bohr radius  $a_B^{PBK}$  in the PBK model.<sup>61</sup>

### Fröhlich electron-phonon coupling Hamiltonian in a polar semiconductor

A compact form for the Fröhlich (abbreviated by Frö) e-ph coupling Hamiltonian reads:

$$\hat{H}^{Fr\ddot{o}} = \sum_{\vec{k}} \left( e^{i\vec{k}\cdot\vec{r}_e} g_{\vec{k}} \hat{a}_{\vec{k}} + e^{-i\vec{k}\cdot\vec{r}_e} g_{\vec{k}}^* \hat{a}_{\vec{k}}^+ \right), \quad (11)$$

where  $g_{\vec{k}}$  is a scalar entering the Fröhlich e-ph coupling matrix element:

$$g_{\vec{k}} = -\frac{i}{k} \left( \frac{e^2 \hbar \omega_{LO}}{2V \epsilon_0 \epsilon^*} \right)^{1/2}, \quad (12)$$

$\hat{a}_{\vec{k}}$  ( $\hat{a}_{\vec{k}}^+$ ) is the creation (annihilation) operator for a longitudinal optical phonon of wave vector  $\vec{k}$  and energy  $\hbar\omega_{LO}$ .

A continuum approach such as the one chosen by Fröhlich reasonably grasps the physics because interaction has a long-range character through the  $\frac{1}{k}$  term in (12).<sup>5,91</sup> More, it allows performing analytic or semi-analytic summations over  $\vec{k}$  in spherical coordinates by extending the modulus to  $+\infty$ , since the most important contributions are related to  $k \rightarrow 0$ .<sup>63,91</sup> For more complex situations, where multiple optical phonon branches contribute, in a first approximation the longitudinal optical phonon  $\hbar\omega_{LO}$  has to be considered as an effective phonon. The macroscopic and microscopic physical quantities entering the Hamiltonian are related by the Lyddane-Sachs-Teller (LST) equation:<sup>84</sup>

$$\frac{\epsilon_s}{\epsilon_\infty} = \left( \frac{\omega_{LO}}{\omega_{TO}} \right)^2, \quad (13)$$

transverse optical modes being associated to the longitudinal one. Using the Fröhlich Hamiltonian (Eq. 9) requires the knowledge of only a few basic quantities namely the effective masses, the frequency of an effective polar optical mode and the static and infinite limits of the dielectric constant.<sup>92,93</sup> However, the precise experimental determination of these quantities is not an easy

task in many materials, and for complex materials such as 3D halide perovskites the definition of the effective polar optical mode is not straightforward. For 3D halide perovskites, existing data are often limited to bare carrier effective masses and effective dielectric constants for the exciton. The data concerning optical phonons are numerous, with data from Raman and neutron scattering, infrared and THz spectroscopies, or photoluminescence phonon side bands. But it appears that reported values show many inconsistencies. Clearly, there is a need to put the analysis in the wider context that includes both the multimode and polymorphous nature of halide perovskites, with strong anharmonicity and local disorder.<sup>42,94</sup>

The empirical e-ph Hamiltonian reads:

$$\hat{H}_{e-ph} = \frac{\hat{p}_e^2}{2m_e} + \sum_{\vec{k}} \left( e^{i\vec{k}\cdot\vec{r}_e} g_{\vec{k}} \hat{a}_{\vec{k}} + e^{-i\vec{k}\cdot\vec{r}_e} g_{\vec{k}}^* \hat{a}_{\vec{k}}^+ \right) + \hbar\omega_{LO} \sum_{\vec{k}} \hat{a}_{\vec{k}}^+ \hat{a}_{\vec{k}}. \quad (14)$$

Here, the term  $\frac{\hbar\omega_{LO}}{2}$  has been left out, as in the rest of the paper. From a perturbative calculation suitable for the regime of weak e-ph interaction, Fröhlich proposed to renormalize the expression of the energy of the electron as follows:

$$E_e(k_e) \approx \sigma_e + \frac{\hbar^2 k_e^2}{2m_e} \left( 1 - \frac{\alpha_e}{6} \right) + \dots \quad (15)$$

The electron ground state is stabilized by a self-energy term:<sup>4</sup>

$$\sigma_e \approx -\alpha_e \hbar\omega_{LO}, \quad (16)$$

A similar expression can be considered for a hole, leading together to corrections for the electronic band gap of the semiconductor. Noteworthy, these corrections are missing in standard DFT calculations. In addition, the quasiparticle acquires a heavier effective mass:

$$m_e^* \approx \frac{m_e}{\left(1 - \frac{\alpha_e}{6}\right)}, \quad (17)$$

where  $m_e$  is referred to as the ‘bare’ effective mass, that can be computed within DFT.  $m_e^*$  is the effective mass of the dressed quasiparticle.

The perturbation approach of Fröhlich turned out to provide reasonable approximations for the carrier self-energies and renormalized masses, not only in the weak coupling regime but also in the intermediate one.<sup>90</sup> From the materials viewpoint, the intermediate regime is usually present in polar ionic materials due to large differences between  $\epsilon_\infty$  and  $\epsilon_s$ . Noteworthy, soft materials such as 3D perovskites with low energy optical modes ( $\hbar\omega_{LO} < 10\text{meV}$ ) are more prone to exhibit an intermediate coupling regime.

#### Empirical Hamiltonian for free polarons in a polar semiconductor

Despite its apparent simplicity, Eq. (14) has no analytical solutions, and was the subject of intense research over decades due to its experimental and theoretical implications. Interested readers may consult the series of review papers by J. T. Devreese.<sup>90</sup> In their initial analysis, assuming that the electrons adiabatically follow the ionic motion, Landau and Pekar obtained expressions for the polaron self-energy and effective masses.<sup>95</sup> This approach valid for the strong e-ph coupling regime can be tackled by unitary transformations of the Hamiltonian represented in the basis of Gaussian trial functions for the electron wavefunction.<sup>90</sup> In the fifties, various theoretical approaches were developed to reshape the problem into forms suitable for efficient and accurate variational approaches. In 1953, LLP introduced a series of unitary transformations connected to shift operators that are determined from variational considerations. It also questioned the validity of the assumption of adiabaticity for low energy electrons.<sup>63</sup> As stated by Devreese and

coworkers, the polaron theory of LLP “essentially treats the opposite case, where the phonon field tends to follow the displacements of the electron”.<sup>96</sup> In 1955,<sup>66</sup> Feynman formulated the polaron problem in a different way using a Lagrangian form of quantum mechanics, referred to as the path-integral method, also coupled with a variational approach. The later has the advantage of recovering also the limits known for the strong coupling regime ( $\alpha_e \rightarrow +\infty$ ) and can be extended to tackle exciton-phonon coupling.<sup>67</sup> Unitary transformations were also utilized to bridge the gap between weak and strong coupling regimes for free polarons.<sup>97-99</sup>

Before commenting on the LLP approach for free polarons, let us consider the infinite mass limit of  $\widehat{H}_{e-ph}$

$$\widehat{H}_{e-ph}^{\infty} = \sum_{\vec{k}} \left( e^{i\vec{k}\cdot\vec{r}_e} g_{\vec{k}} \hat{a}_{\vec{k}} + e^{-i\vec{k}\cdot\vec{r}_e} g_{\vec{k}}^* \hat{a}_{\vec{k}}^{\dagger} \right) + \hbar\omega_{LO} \sum_{\vec{k}} \hat{a}_{\vec{k}}^{\dagger} \hat{a}_{\vec{k}}. \quad (18)$$

As shown by Devreese,<sup>90</sup> using the unitary transformation

$$\widehat{W} = e^{\sum_{\vec{k}} (F_{\vec{k}}^* \hat{a}_{\vec{k}} - F_{\vec{k}} \hat{a}_{\vec{k}}^{\dagger})}, \quad (19)$$

with a shift operator  $F_{\vec{k}}$ <sup>90</sup> which can be understood as the amplitude of the lattice distortion around the charge carrier (vide infra):

$$F_{\vec{k}} = \frac{g_{\vec{k}}^*}{\hbar\omega_{LO}}, \quad (20)$$

yields a transformed Hamiltonian:

$$\widehat{H}_{e-ph}^{\infty} = \widehat{W}^{\dagger} \widehat{H}_{e-ph}^{\infty} \widehat{W} = - \sum_{\vec{k}} \frac{|g_{\vec{k}}|^2}{\hbar\omega_{LO}} + \hbar\omega_{LO} \sum_{\vec{k}} \hat{a}_{\vec{k}}^{\dagger} \hat{a}_{\vec{k}}, \quad (21)$$

where the first term represents self-energy. The sign convention for the shift operator and the related unitary transformation follows the work by PB. Eigenvalues can be derived and read:

$$E_{\{n_{\vec{k}}\}} = -\sum_{\vec{k}} \frac{|g_{\vec{k}}|^2}{\hbar\omega_{LO}} + \hbar\omega_{LO} \sum_{\vec{k}} n_{\vec{k}}. \quad (22)$$

Phonon operators are shifted by  $F_{\vec{k}}$  (see supplementary information):

$$\widehat{W}^+ \widehat{a}_{\vec{k}} \widehat{W} = \widehat{a}_{\vec{k}} - F_{\vec{k}} \text{ and } \widehat{W}^+ \widehat{a}_{\vec{k}}^+ \widehat{W} = \widehat{a}_{\vec{k}}^+ - F_{\vec{k}}^*. \quad (23)$$

When considering the complete problem, LLP first noted that, when the e-ph interaction is included, the momentum  $\hat{p}_e$  does not commute with  $\widehat{H}_{e-ph}$ . The total momentum operator  $\widehat{\rho}$  is thus introduced:<sup>1</sup>

$$\widehat{\rho} = \hat{p}_e + \sum_{\vec{k}} \hbar \vec{k} \widehat{a}_{\vec{k}}^+ \widehat{a}_{\vec{k}}, \quad (24)$$

with  $[\widehat{\rho}, \widehat{H}_{e-ph}] = 0$ ,  $\widehat{H}_{e-ph}|\varphi\rangle = E|\varphi\rangle$  and  $\widehat{\rho}|\varphi\rangle = \hbar\vec{Q}|\varphi\rangle$ .

Therefore,  $\hbar\vec{Q}$ , the eigenvalue of  $\widehat{\rho}$ , is introduced into the Hamiltonian thanks to the unitary transformation (see supplementary information):

$$\widehat{U} = e^{i(\vec{Q} - \sum_{\vec{k}} \vec{k} \widehat{a}_{\vec{k}}^+ \widehat{a}_{\vec{k}}) \cdot \vec{r}_e} \quad (25)$$

$$\widehat{H}_{CM}^{LLP} = \widehat{U}^+ \widehat{H}_{e-ph} \widehat{U} = \frac{(\hbar\vec{Q} - \sum_{\vec{k}} \hbar \vec{k} \widehat{a}_{\vec{k}}^+ \widehat{a}_{\vec{k}})^2}{2m_e} + \sum_{\vec{k}} (g_{\vec{k}} \widehat{a}_{\vec{k}} + g_{\vec{k}}^* \widehat{a}_{\vec{k}}^+) + \hbar\omega_{LO} \sum_{\vec{k}} \widehat{a}_{\vec{k}}^+ \widehat{a}_{\vec{k}}. \quad (26)$$

The electron position and momentum have been removed from the Hamiltonian and replaced by the polaron momentum, provided that the unitary transformation is also applied to the eigenstates

$|\varphi_{CM}\rangle = \hat{U}^+|\varphi\rangle$ . Then a second unitary transformation (Eq. 19), which includes the shift operators, is applied. The LLP Hamiltonian reads:

$$\hat{H}^{LLP}\left(F_{\vec{k}}(\vec{Q})\right) = \hat{W}^+\hat{U}^+\hat{H}_{e-ph}\hat{U}\hat{W} = \hat{H}_{0_{ph}}^{LLP} + \hat{H}_{1_{ph}}^{LLP} + \hat{H}_{2_{ph}}^{LLP} + \hat{H}_{3_{ph}}^{LLP} + \hat{H}_{4_{ph}}^{LLP}. \quad (27)$$

where  $\hat{H}_{n_{ph}}^{LLP}\left(F_{\vec{k}}(\vec{Q})\right)$  are the  $n$ -phonon ( $n_{ph}$ ) contributions to the Hamiltonian. The eigenstates are now deduced from  $|\psi\rangle = \hat{W}^+\hat{U}^+|\varphi\rangle$ .  $F_{\vec{k}}(\vec{Q})$  is expected to be determined by minimization of energy. The resulting one-electron Hamiltonian is independent of the electronic coordinate  $\vec{r}$ . This preserves the polaron total momentum as a constant of motion and enables exact diagonalization of Hamiltonians of Fröhlich type with regard to the electronic subspace.<sup>100</sup> Exact diagonalization no longer applies for an equivalent treatment of the excitonic polarons by PB (vide infra). We also note that the exact diagonalization of the one-electron Hamiltonian through the LLP transformation is connected to the implicit absence of an electronic periodic potential in this Hamiltonian, and thus to the effective mass approximation (Eq. 3). Alternative complex approaches<sup>101</sup>, or unitary transformation such as the Fulton–Gouterman (FG) transformation capable of handling periodicity of potential, Umklapp terms and phonon anharmonicity do exist.<sup>100,102</sup> Introducing lattice periodicity may further reconcile semi-empirical approaches with on-going developments connected to DFT calculations.

### Variational approach for free polarons in a polar semiconductor

The one-electron  $\hat{H}^{LLP}\left(F_{\vec{k}}(\vec{Q})\right)$  Hamiltonian is applied to a ‘free vacuum’ e-ph ground state with zero (real) phonon ( $0_{ph}$ ) and thus considering only  $\hat{H}_{0_{ph}}^{LLP}\left(F_{\vec{k}}(\vec{Q})\right)$ , leading to the energy

dispersion of the polaron (for the validity of this approximate representation of the free polaron wavefunction beyond the weak coupling regime see ref.<sup>96,99</sup>):

$$E_{GS}(\vec{Q}) = \frac{\hbar^2 Q^2 - 2\vec{Q} \cdot (\sum_{\vec{k}} \hbar \vec{k} |F_{\vec{k}}(\vec{Q})|^2) + (\sum_{\vec{k}} \hbar \vec{k} |F_{\vec{k}}(\vec{Q})|^2)^2}{2m_e} - \sum_{\vec{k}} (g_{\vec{k}} F_{\vec{k}}(\vec{Q}) + c. c) + \sum_{\vec{k}} |F_{\vec{k}}(\vec{Q})|^2 \left( \hbar \omega_{LO} + \frac{\hbar^2 k^2}{2m_e} \right). \quad (28)$$

An additional relation between  $g_{\vec{k}}$  and  $F_{\vec{k}}^*$  can be derived by energy minimization  $\frac{\partial E_{GS}(\vec{Q})}{\partial F_{\vec{k}}(\vec{Q})} =$

$$\frac{\partial E_{GS}(\vec{Q})}{\partial F_{\vec{k}}(\vec{Q})} = 0 \text{ (see supplementary information):}$$

$$F_{\vec{k}}^{min}(\vec{Q}) = \frac{g_{\vec{k}}^*}{\hbar \omega_{LO} - \hbar^2 \frac{\vec{Q} \cdot \vec{k}}{m_e} + \frac{\hbar^2 k^2}{2m_e} + \frac{\hbar^2}{m_e} \vec{k} \cdot \sum_{\vec{k}'} \vec{k}' |F_{\vec{k}'}^{min}(\vec{Q})|^2} = \frac{g_{\vec{k}}^*}{\hbar \omega_{LO} (1 + K^2 - 2\vec{q} \cdot \vec{K})}. \quad (29)$$

$$\text{With } \vec{K} = R_e \vec{k} \text{ and } \vec{q} = R_e \vec{Q} (1 - \eta)$$

The total momentum is the only physical quantity associated with a symmetry-breaking.  $\sum_{\vec{k}} \vec{k} |F_{\vec{k}}^{min}(\vec{Q})|^2$  is thus set equal to  $\eta \vec{Q}$ , with a constant  $\eta$  that must be determined self-consistently. For zero (real) phonon, the mean number of phonons in the cloud around the electron<sup>63</sup> (also called virtual phonons<sup>63,60</sup>) can be related to the distortion field  $F_{\vec{k}}^{min}$  (see supplementary information):

$$N_e^{LLP}(\vec{Q}) = \langle \varphi_{GS} | \sum_{\vec{k}} \hat{a}_{\vec{k}}^+ \hat{a}_{\vec{k}} | \varphi_{GS} \rangle = \sum_{\vec{k}} |F_{\vec{k}}^{min}(\vec{Q})|^2. \quad (30)$$

At this stage the problem remains highly nonlinear and further developments are needed to find analytical expressions for the energy dispersion  $E_{GS}(\vec{Q})$  of the polaron.<sup>63</sup> Finding the energy

minimum  $E_{GS}(\vec{0})$  at the bottom of the polaron dispersion is easier. It is indeed possible to drastically simplify the problem by setting  $\sum_{\vec{k}} \vec{k} |F_{\vec{k}}^{min}(\vec{0})|^2 = \vec{0}$ ., since for zero center of mass momentum the free polaron wavefunction is symmetric. In that case,  $F_{\vec{k}}^{min}(\vec{0}) = \frac{g_{\vec{k}}^*}{\hbar\omega_{LO}(1+R_e^2k^2)}$  and the energy after integration is given by  $E_{GS}(\vec{0}) = \sigma_e^{LLP} = -\alpha_e \hbar\omega_{LO}$ , which is the self-energy correction considered by Fröhlich. This population of virtual phonons yields a simple metric for the amplitude of the lattice distortion around the charge carrier, leading to the elegant formula proposed by LLP:  $N_e^{LLP}(\vec{0}) = \frac{\alpha_e}{2}$ . **This formula highlights the connection between the strength of coupling and the induced lattice distortion.**

To get further theoretical expressions for the polaron energy and virtual phonon population close to the minimum of  $E_{GS}(\vec{Q})$  including the derivation of a polaron effective mass, it is necessary to go beyond the simple approximation the  $\sum_{\vec{k}} \vec{k} |F_{\vec{k}}^{min}(\vec{Q})|^2 = \vec{0}$ . The variable  $\eta$  mentioned above in the formula  $\sum_{\vec{k}} \vec{k} |F_{\vec{k}}^{min}(\vec{Q})|^2 = \eta\vec{Q}$  is introduced. Full analytical integrations is possible (see supplementary information), leading to  $\eta = \frac{\alpha_e(1-\eta)}{2q^3} \left( \frac{q}{\sqrt{1-q^2}} - a \sin(q) \right)$ ,  $N_e^{LLP}(\vec{Q}) = \frac{\alpha_e}{2\sqrt{1-q^2}}$  and  $E_{GS}(\vec{Q}) = \frac{\hbar^2 Q^2(1-\eta^2)}{2m_e} - \alpha_e \hbar\omega_{LO} \frac{a \sin(q)}{q}$ , with  $q = R_e Q(1-\eta)$ . Close to the bottom of the energy dispersion a parabolic expression can be obtained leading to a correction over the charge carrier mass:

$$E_{GS}(\vec{Q}) \approx -\alpha_e \hbar\omega_{LO} + \frac{\hbar^2 Q^2}{2m_e \left(1 + \frac{\alpha_e}{6}\right)} + \dots \quad (31)$$

The effective mass expression is thus slightly different from the one of Fröhlich:

$$m_e^{LLP} \approx m_e \left(1 + \frac{\alpha_e}{6}\right). \quad (32)$$

When treating the excitonic polarons within PB and PBK models, Eq. (31-32) of the LLP model will be our reference for uncorrelated e-h motion (Figure 5).

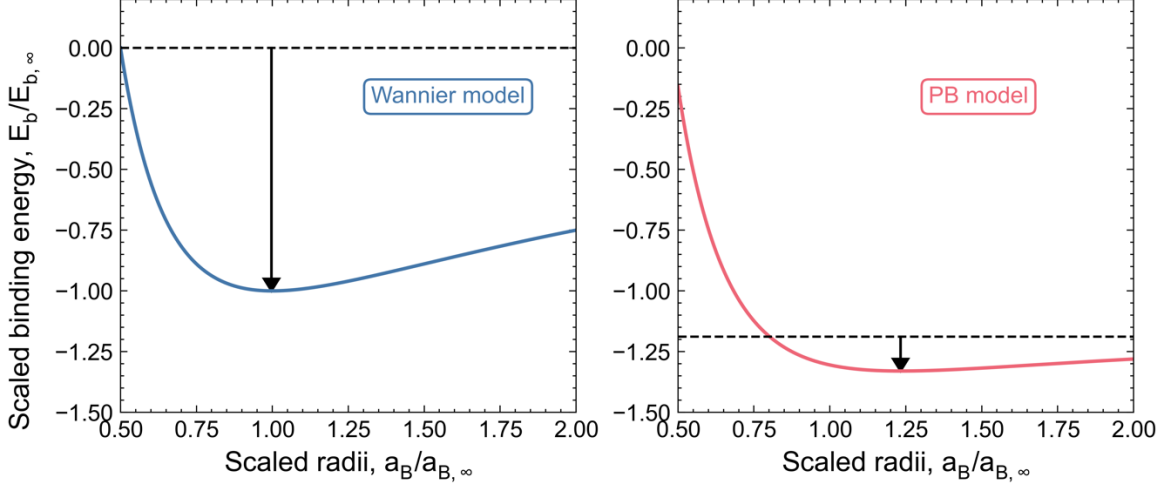


Figure 5. Illustration of the calculations of 1S exciton binding energies for TlCl. The variations of exciton energies are represented by straight lines as a function of the Bohr radius, for a Wannier exciton model (a) with  $\epsilon_{eff} = \epsilon_\infty$  and a PB excitonic polaron model (b). The Bohr radii are scaled by the value  $a_{B,\infty}$  at the minimum energy for (a). Energies are scaled by the minimum energy  $E_b^\infty$  for (a). The binding energies represented by arrows are computed at the energy minima by subtracting the energies for free carriers (a) or free polarons (b). The minimum energy for free carriers (band gap) is set as a reference to 0 to define the vertical axis. The minimum energy for free polarons is lowered by self-energy terms computed within LLP theory.

It is interesting to note that the LLP expressions for self-energy correction and virtual phonon population at the bottom of the polaron dispersion can be derived by considering:

$$F_{\vec{k}}^{min}(\vec{0}) = \frac{g_{\vec{k}}^*}{\hbar\omega_{LO}(1+R_e^2k^2)}. \quad (33)$$

Notice that the denominator of eq. (33) captures the tendency of the lattice (spatial extension) to undergo a distortion along a polar optical eigenvector. However,  $R_e$  does not account for the amplitude of the distortion, which is related to  $g_{\vec{k}}$  included in the numerator of Eq. (33). This is also true for the population of the virtual phonon cloud which is directly related to  $\alpha_e$  for a single particle.

### Empirical Hamiltonian for excitonic polarons in a polar semiconductor

Including explicitly the coupling between the e-h pairs and the lattice at the same level of theory is possible with an extension of the Wannier Hamiltonian in the center of mass coordinates:

$$\hat{H}_{X-ph} = E_g + \frac{\hat{p}^2}{2M} + \frac{\hat{p}^2}{2\mu} - \frac{e^2}{4\pi\epsilon_0\epsilon_\infty r} + \hbar\omega_{LO} \sum_{\vec{k}} \hat{a}_{\vec{k}}^+ \hat{a}_{\vec{k}} + \sum_{\vec{k}} \left[ \rho_{\vec{k}} e^{i\vec{k}\cdot\vec{R}} g_{\vec{k}} \hat{a}_{\vec{k}} + c.c \right], \quad (34)$$

Where the interplay between the correlated e-h motion and the coupling to the lattice is related to the exciton charge density operator<sup>58</sup>:

$$\rho_{\vec{k}} = e^{is_h\vec{k}\cdot\vec{r}} - e^{-is_e\vec{k}\cdot\vec{r}}, \quad (35)$$

$s_h = \frac{m_h}{M}$  and  $s_e = \frac{m_e}{M}$ . Another characteristic length, the exciton Bohr radius  $a_B$  thus enters the physics of polarons. The physics of the associated neutral quasiparticle, called excitonic polaron, strongly depends on the ratio of the free polaron radius  $R_{pol}$  to the exciton Bohr radius, motivating the definition of the reduced free polaron radius:

$$\tilde{R}_{pol} = R_{pol}/a_B. \quad (36)$$

This can be understood qualitatively by considering the free polaron radius with respect to the probability density curves of 1S and 2S excitons (Figure 4a). In the case where the lattice

distortions produced by a 1S excitonic polaron are strongly reduced by comparison to the sum of the distortions produced by the related free-like polarons then we have  $\tilde{R}_{pol} \geq 0.25$  (vide infra). This reduction is weaker for the 2S excitonic polaron. The variable extent of distortions underpins deviations from the Rydberg like series for nS excitons. This will be quantified later based on the virtual phonon populations and self-energies of the quasiparticles. The cross-over from the weak coupling regime ( $\alpha \rightarrow 0, a_B^{eff} \gg R_{pol}$ ) to the intermediate coupling regime ( $a_B^{eff} < 4R_{pol}$ ) is obtained in the present work by tuning the effective phonon frequency in the expression of  $\alpha$  (Eq. 1).

Early models for description of excitonic polarons were proposed by Meyer and Haken,<sup>103–105</sup>. Later, Toyozawa and Hermanson (TH) proposed models for excitonic polarons<sup>57,58</sup> which established a clear connection to the LLP theory<sup>63</sup> for free polarons, thanks to two unitary transformations of the initially proposed exciton-phonon Hamiltonian. PB<sup>59,60</sup> followed by Kane<sup>61</sup> and Iadonisi<sup>106</sup> further refined this approach to quantitatively predict the properties of excitonic polarons in simple semiconductors. TH introduced a unitary transformation to account for the excitonic polaron total momentum:

$$\hat{\rho} = \hat{P} + \sum_{\vec{k}} \hbar \vec{k} \hat{a}_{\vec{k}}^{\dagger} \hat{a}_{\vec{k}} \quad (37)$$

by choosing:

$$\hat{U} = e^{i(\vec{Q} - \sum_{\vec{k}} \vec{k} \hat{a}_{\vec{k}}^{\dagger} \hat{a}_{\vec{k}}) \cdot \vec{R}}, \quad (38)$$

where  $\hbar \vec{Q}$  is the eigenvalue of  $\hat{\rho}$ . The resulting Hamiltonian is comparable to  $\hat{H}_{CM}^{LLP}$  with additional terms (see supplementary information):

$$\hat{H}_{CM}^{TH} = \hat{U}^+ \hat{H}_{X-ph} \hat{U} = E_g + \frac{\hbar^2 Q^2}{2M} + \frac{\hat{p}^2}{2\mu} - \frac{e^2}{4\pi\epsilon_0\epsilon_\infty r} + \hbar\Omega_{CM}^{TH} \sum_{\vec{k}} \hat{a}_{\vec{k}}^+ \hat{a}_{\vec{k}} + \sum_{\vec{k}} \left[ \rho_{\vec{k}} e^{i\vec{k}\cdot\vec{R}} g_{\vec{k}} \hat{a}_{\vec{k}} + c.c \right] + \sum_{\vec{k}} \sum_{\vec{k}'} \frac{\hbar^2 \vec{k}\cdot\vec{k}'}{2M} \hat{a}_{\vec{k}}^+ \hat{a}_{\vec{k}'}^+ \hat{a}_{\vec{k}} \hat{a}_{\vec{k}'}$$
(39)

$$\text{with } \hbar\Omega_{CM}^{TH} = \hbar\omega_{LO} - \frac{\hbar^2}{M} \vec{k}\cdot\vec{Q} + \frac{\hbar^2 k^2}{2M}.$$

This transformed Hamiltonian was also used before PB's paper as a starting point for perturbative calculations.<sup>107</sup> The expression of  $\hbar\Omega_{CM}^{TH}$  indicates that the phonon spectrum may deviate from the one of the crystal ground state.<sup>106</sup> The last term also shows that for excited states beyond the excitonic polaron ground state, additional small energy contributions might be included<sup>60,108</sup>. The second unitary transformation was subsequently studied in detail by PB allowing a variational approach:

$$\hat{W} = e^{\sum_{\vec{k}} (F_{\vec{k}}^*(\vec{Q}, \vec{r}) \hat{a}_{\vec{k}} - F_{\vec{k}}(\vec{Q}, \vec{r}) \hat{a}_{\vec{k}}^+)}$$
(40)

It introduces a lattice distortion amplitude  $F_{\vec{k}}(\vec{Q}, \vec{r})$  function of the e-h relative positions which allows accounting for the influence of their correlated motions. This function replaces the distortion parameter  $F_{\vec{k}}(\vec{Q})$  of LLP, and must thus be determined by functional minimization, instead of the standard minimization against a parameter. The transformed Hamiltonian reads:

$$\hat{H}^{PB} (F_{\vec{k}}(\vec{Q}, \vec{r})) = \hat{S}^+ \hat{U}^+ \hat{H}_{X-ph} \hat{U} \hat{S} = \hat{H}_{0ph}^{PB} + \hat{H}_{1ph}^{PB} + \hat{H}_{2ph}^{PB} + \hat{H}_{3ph}^{PB} + \hat{H}_{4ph}^{PB},$$
(41)

where  $\hat{H}_{nph}^{PB} (F_{\vec{k}}(\vec{Q}, \vec{r}))$  are the n-phonon contributions to the Hamiltonian. The explicit expression of  $\hat{H}_{0ph}^{PB} (F_{\vec{k}}(\vec{Q}, \vec{r}))$  is given in the supplementary information. It should be noted that the PB Hamiltonian has a more complex form than the LLP one. In the intermediate coupling

regime, it does not allow full analytical derivation of approximate expressions for the excitonic polaron energy, effective mass and virtual phonon population.

PB's initial work is focused on the 1S exciton-phonon ground state ( $0_{ph}$ ) with  $|\psi_{GS}\rangle = \phi_{1S}(\vec{r})|0\rangle$  related to the energy minimum at the bottom of the excitonic polaron dispersion ( $\vec{Q} = \vec{0}$ ). In this case, a small first order contribution ( $\hat{H}_{1ph}^{PB}$ ) and very small higher order terms can be derived in principle after functional minimization:

$$\frac{\delta}{\delta F_{\vec{k}}(\vec{r})} \left\langle \phi_{1S}(\vec{r}) \left| \hat{H}_{0ph}^{PB} \left( F_{\vec{k}}(\vec{0}, \vec{r}) \right) \right| \phi_{1S}(\vec{r}) \right\rangle = 0 \quad . \quad (42)$$

In a second step, the 1S excitonic polaron wavefunction  $\phi_{1S}(\vec{r})$  is obtained by energy minimization:  $E_{1S} = \left\langle \phi_{1S}(\vec{r}) \left| \hat{H}_{0ph}^{PB} \left( F_{\vec{k}}^{min}(\vec{0}, \vec{r}) \right) \right| \phi_{1S}(\vec{r}) \right\rangle$  with respect to the quasi-particle Bohr radius, which is considered as the minimization parameter. A 1S wavefunction form

$$\phi_{1S}(\vec{r}) = \frac{e^{-r/a_B^{eff}}}{a_B^{eff 3/2} \pi^{1/2}} \quad (43)$$

is used for the energy minimization yielding the expected effective Bohr radius  $a_B^{eff}$ .

### Pollman Büttner variational approach for excitonic polarons in a polar semiconductor

The theoretical framework discussed in the previous section leads to an exact expression for the function  $F_{\vec{k}}^{min}(\vec{0}, \vec{r})$  that was completely achieved in 1983 by Iadonisi and coworkers for the ground state (quoted as Iad in the following),<sup>106</sup> thanks to infinite series of Legendre polynomials and integrals of confluent hypergeometric functions. Exact solutions for excited states were provided a few years later by the same authors.<sup>108,109</sup> Iad's fully analytical solution yields numerical

results close to the initial PB and PBK semi-analytical implementation, but at much higher computational cost (vide infra). To perform a semi-analytical treatment of the problem for  $F_{\vec{k}}(\vec{0}, \vec{r})$ , PB indeed initially assumed a simplified form for the function, namely:

$$F_{\vec{k}}(\vec{0}, \vec{r}) \approx \frac{g_{\vec{k}}^*}{\hbar\omega_{LO}} \left( f_{e,\vec{k}}(\vec{0}) e^{-is_h \vec{k} \cdot \vec{r}} - f_{h,\vec{k}}(\vec{0}) e^{is_e \vec{k} \cdot \vec{r}} \right), \quad (44)$$

replacing the complex functional minimization against the amplitude function  $F_{\vec{k}}(\vec{0}, \vec{r})$  by minimization with respect to the parameters  $f_{e(h),\vec{k}}$ :

$$\frac{\delta}{\delta f_{e(h),\vec{k}}(\vec{0})} \left\langle \phi_{1S}(\vec{r}) \left| \widehat{H}_{0ph}^{PB} \left( f_{e,\vec{k}}(\vec{0}), f_{h,\vec{k}}(\vec{0}) \right) \right| \phi_{1S}(\vec{r}) \right\rangle = 0. \quad (45)$$

It allows retrieving analytical expressions for the k-dependent parameters:

$$f_{e(h),\vec{k}}^{min}(\vec{0}) = \frac{(1 - G_{1S}(\vec{k}, a_B^{eff})) (1 + R_{h(e)}^2 k^2 + G_{1S}(\vec{k}, a_B^{eff}))}{(1 + R_{h(e)}^2 k^2) (1 + R_{e(h)}^2 k^2) - G_{1S}(\vec{k}, a_B^{eff})^2} \quad (46)$$

with

$$G_{1S}(\vec{k}, a_B^{eff}) = \iiint e^{i\vec{k} \cdot \vec{r}} |\phi_{1S}(\vec{r})|^2 d^3\vec{r}. \quad (47)$$

The resulting 1S excitonic polaron ground state energy for  $\vec{Q} = \vec{0}$  is given by:

$$E_{1S}(a_B^{eff}, \vec{0}) = \left\langle \phi_{1S}(\vec{r}) \left| E_g + \frac{p^2}{2\mu} - \frac{e^2}{4\pi\epsilon_0\epsilon_\infty r} + V_{latt}^{PB} \left( \vec{r}, f_{e,\vec{k}}^{min}(\vec{0}), f_{h,\vec{k}}^{min}(\vec{0}) \right) \right| \phi_{1S}(\vec{r}) \right\rangle + \sigma_{h,1S} \left( f_{e,\vec{k}}^{min}(\vec{0}), f_{h,\vec{k}}^{min}(\vec{0}) \right) + \sigma_{e,1S} \left( f_{e,\vec{k}}^{min}(\vec{0}), f_{h,\vec{k}}^{min}(\vec{0}) \right), \quad (48)$$

including an effective lattice-mediated repulsive interaction in addition to the e-h Coulomb attraction:

$$V_{latt}^{PB}(\vec{r}, f_{e,\vec{k}}^{min}(\vec{0}), f_{h,\vec{k}}^{min}(\vec{0})) = 2 \sum_{\vec{k}} \frac{|g_{\vec{k}}|^2}{\hbar\omega_{LO}} \left( f_{e,\vec{k}}^{min}(\vec{0}) + f_{h,\vec{k}}^{min}(\vec{0}) - f_{e,\vec{k}}^{min}(\vec{0})f_{h,\vec{k}}^{min}(\vec{0}) \right) \cos(\vec{k} \cdot \vec{r})$$

(49)

and a sum of self-energy corrections  $\sigma_{h,1S}(\vec{0}) + \sigma_{e,1S}(\vec{0})$  in the presence of the exciton with:

$$\sigma_{e(h),1S}(\vec{0}) = - \sum_{\vec{k}} \frac{|g_{\vec{k}}|^2}{\hbar\omega_{LO}} \left( 2f_{e(h),\vec{k}}^{min}(\vec{0}) - (1 + R_{e(h)}^2 k^2) f_{e(h),\vec{k}}^{min}(\vec{0})^2 \right). \quad (50)$$

It may be noted that the expression of  $E_{1S}(a_B^{eff}, \vec{0})$  depends self-consistently on  $a_B^{eff}$  through  $\phi_{1S}(\vec{r})$  and  $f_{e(h),\vec{k}}^{min}(\vec{0})$ . Energy minimization is finally performed with respect to the quasi-particle Bohr radius  $a_B^{eff}$ , which is considered as the minimization parameter. The case of a bipolaron (either two electrons or two holes) is instructive. By comparison to an excitonic polaron, the Coulomb interaction is repulsive, but the lattice mediated interaction is attractive. At this level of theory, the effect of this additional interaction is not sufficient to create bound states as in the case of excitonic polarons (Fig. S1).

For the  $m_h = m_e$  case relevant for halide perovskites, we derive for excitonic polarons exact analytic expressions of the effective interaction  $V_{latt}^{PB}(\vec{r}, f_{e,\vec{k}}^{min}(\vec{0}), f_{h,\vec{k}}^{min}(\vec{0}))$  and total energy  $E_{1S}(a_B^{eff}, \vec{0})$  assuming Eq. 43 for the 1S wavefunction and simplifying the expressions of  $f_{e(h),\vec{k}}^{min}(\vec{0})$ :

$$f_{e(h),\vec{k}}^{min}(\vec{0}) = \frac{1 - G_{1S}(\vec{k}, a_B^{eff})}{1 + R_{pol}^2 k^2 - G_{1S}(\vec{k}, a_B^{eff})}. \quad (51)$$

After analytical integration over  $\vec{k}$ , we find:

$$\begin{aligned} \tilde{V}_{latt,m_e=m_h}^{PB}(\vec{r}, \vec{0}) &= \frac{V_{latt,m_e=m_h}^{PB}(\vec{r}, \vec{0})}{e^2} = f_a^+ \frac{1 - e^{-2\sqrt{-\lambda_+} \tilde{r} \tilde{R}_{pol}}}{\tilde{r}} - f_b^+ \sqrt{-\lambda_+} \tilde{R}_{pol} e^{-2\sqrt{-\lambda_+} \tilde{r} \tilde{R}_{pol}} \\ &+ f_a^- \frac{1 - e^{-2\sqrt{-\lambda_-} \tilde{r} \tilde{R}_{pol}}}{\tilde{r}} - f_b^- \sqrt{-\lambda_-} \tilde{R}_{pol} e^{-2\sqrt{-\lambda_-} \tilde{r} \tilde{R}_{pol}}, \end{aligned} \quad (52)$$

$$\text{With } -\lambda_{\pm} f_b^{\pm} = \frac{(2-1/\eta) \lambda_{\pm} + \frac{3\eta-2}{2\eta-1}}{1-4\eta} \frac{1}{\lambda_{\pm}} \quad \text{and} \quad -\lambda_{\pm} f_a^{\pm} = -\lambda_{\pm} f_b^{\pm} - \frac{(2-1/\eta)}{1-4\eta} \pm \frac{2(\lambda_{\pm} + 2 - 1/2\eta)}{\sqrt{1-4\eta}} \pm$$

$$\frac{2\eta(2-1/\eta)(\lambda_{\pm} + \frac{3\eta-2}{2\eta-1})}{(1-4\eta)^{3/2}}.$$

The internal excitonic polaron energy first reads:

$$E_{1S}(a_B^{eff}, \vec{0}) = E_g + \frac{\hbar^2}{2\mu a_B^{eff^2}} - \frac{e^2}{4\pi\epsilon_0\epsilon_{\infty} a_B^{eff}} - \frac{e^2}{2\pi^2\epsilon_0\epsilon^* R_{pol}} \int_0^{+\infty} dK \frac{(1-G_{1S})^2}{(1+K^2-G_{1S})} \quad (53)$$

where  $\vec{K} = R_{pol} \vec{k}$ . Effective interaction and self-energies have been merged into a single integral.

Getting analytic expressions for the internal excitonic polaron energy allows to better highlight the crossover from the weak to the intermediate excitonic polaron coupling regimes (Fig. 4) due to variation of the effective interaction and self-energies (Eq. 48-50):

- $\tilde{R}_{pol} \leq 1/4$

$$\frac{E_{1S}(a_B^{eff}, \vec{0})}{Ry^{vac}} = \frac{a_B^{vac^2}}{\mu a_B^{eff^2}} - \frac{2a_B^{vac}}{\epsilon_{\infty} a_B^{eff}} - \frac{4a_B^{vac}}{\epsilon^* a_B^{eff}} \left( \frac{1}{\sqrt{1-4\eta}} \left( \frac{\lambda_+ + \eta + 2}{\sqrt{-\lambda_+}} - \frac{\lambda_- + \eta + 2}{\sqrt{-\lambda_-}} \right) - \frac{1}{2} \right). \quad (54)$$

- $\tilde{R}_{pol} \geq 1/4$

$$\frac{E_{1S}(a_B^{eff}, \vec{0})}{Ry^{vac}} = \frac{a_B^{vac^2}}{\mu a_B^{eff^2}} - \frac{2a_B^{vac}}{\epsilon_{\infty} a_B^{eff}} - \frac{4a_B^{vac}}{\epsilon^* a_B^{eff}} \left( \frac{1}{2\eta \sin(\vartheta/2)} \left( \frac{1}{Z^{1/2}} - \frac{\eta+2}{Z^{3/2}} \right) - \frac{1}{2} \right). \quad (55)$$

Here,  $\eta = 4\tilde{R}_{pol}^2$ ,  $\lambda_{\pm} = \frac{1}{2\eta}(-1 + 2\eta) \pm \sqrt{1 - 4\eta}$ ,  $\sin(\vartheta/2) = \sqrt{\frac{1 - \cos(\vartheta)}{2}}$ ,  $\cos(\vartheta) = \frac{-(1 + \frac{1}{2\eta})}{Z}$ ,

$$Z = \sqrt{\frac{2}{\eta} + 1}.$$

Analyzing the effects of the excitonic polaron center of mass motion on the excitonic polaron energy  $E_{GS}(\vec{Q})$ , virtual phonon population  $N_{1S}(\vec{Q})$  and effective total mass close to the minimum of  $E_{GS}(\vec{Q})$  is more complex than in the case of free polarons and has been seldom considered.<sup>61,110</sup> Few attempts based on PB approach start indeed by neglecting terms describing e-h correlations in the expression of  $\hat{H}_{0_{ph}}^{PB}(F_{\vec{k}}(\vec{Q}, \vec{r}))$  to allow deriving analytical expressions.<sup>110,111</sup> In order to avoid any approximation we propose here a different calculation, also based on the PB approach, while assuming  $m_e = m_h$ , as for TlCl or halide perovskites. Then, the expressions of the PB parameters  $f_{e(h),\vec{k}}^{min}(\vec{Q})$  can be simplified and read (see supplementary information):

$$f_{e(h),\vec{k}}^{min}(\vec{Q}) = \frac{1 - G_{1S}(\vec{k}, a_B^{eff})}{1 + K^2 - \vec{q} \cdot \vec{K} - G_{1S}(\vec{k}, a_B^{eff})} \quad (56)$$

with  $\vec{K} = R_{pol}\vec{k}$ ,  $\vec{q} = R_{pol}\vec{Q}(1 - \eta)$  and  $\eta\vec{Q} = \left\langle \phi_{1S}(\vec{r}) \left| \sum_{\vec{k}} \vec{k} \left| F_{\vec{k}}^{min}(\vec{Q}, \vec{r}) \right|^2 \right| \phi_{1S}(\vec{r}) \right\rangle$ .

Semi analytic expressions for  $E_{1S}(a_B^{eff}, \vec{Q})$  and  $\eta\vec{Q}$  are given in supplementary information. For small Q values, these expressions can be simplified to a parabolic energy dispersion for the center of mass motion:

$$E_{1S}(a_B^{eff}, \vec{Q}) \approx E_{1S}(a_B^{eff}, \vec{0}) + \frac{\hbar^2 Q^2 (1 - \eta)^2}{2M} + \frac{\alpha \hbar^2 Q^2}{2M} (I_3(a_B^{eff}) - \eta I_2(a_B^{eff})) \quad (57)$$

with

$$\eta \approx \frac{\alpha I_4(a_B^{eff})}{1 + \alpha I_3(a_B^{eff})} \quad (58)$$

and

$$I_n(a_B^{eff}) = \int_0^{+\infty} \frac{8K^2 dK}{3\pi} \left( \frac{(1-G_{1S})^n}{(1+K^2-G_{1S})^3} \right) \text{ and } G_{1S} = \frac{1}{\left(1 + \left(\frac{K}{2R_{pol}}\right)^2\right)^2} \quad (59)$$

In the weak coupling limit  $G_{1S} \rightarrow 0$ , using  $\int_0^{+\infty} \frac{K^2 dK}{(1+K^2)^3} = \frac{\pi}{16}$  one retrieves an effective mass for the center of mass motion consistent with the LLP model (free polarons) and renormalized to  $M^{PB} \approx M \left(1 + \frac{\alpha}{6}\right) \approx m_e^{LLP} + m_h^{LLP}$ .

Figure 6 illustrates the variation of the total excitonic polaron mass as a function of  $\alpha$  computed for TlCl. A cross-over is observed from the weak coupling regime where the LLP limit is valid, to the intermediate coupling regime where the mass of bare charges is recovered. For similar  $\alpha$  values,  $\alpha \sim 1 - 2$ , a similar crossover is obtained for the reduced mass (Figure 7) and other physical quantities (vide infra).

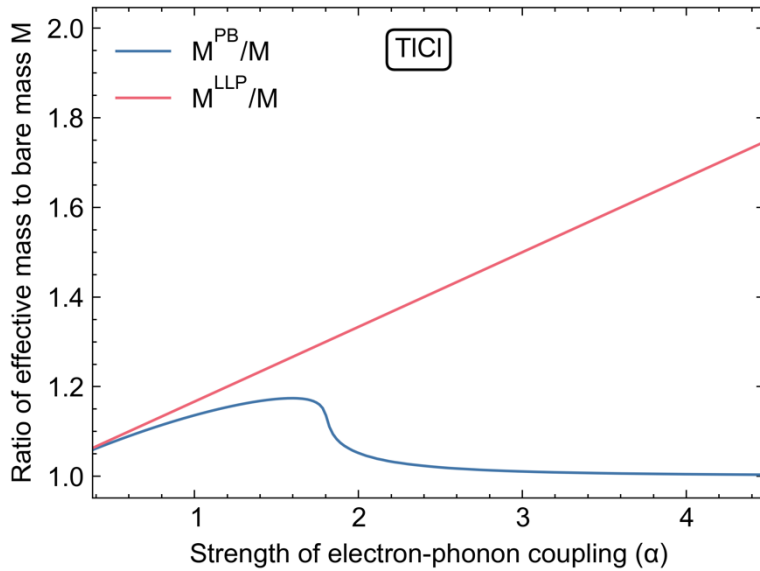


Figure 6. Total excitonic polaron mass (in unit of the bare mass  $M$ ) computed within PB (blue) model for TlCl. The cross-over from the weak ( $\alpha \rightarrow 0, a_B^{eff} \gg R_{pol}$ ) to the intermediate coupling regime ( $a_B^{eff} < 4R_{pol}$ ) is obtained by tuning the effective phonon frequency in the expression of  $\alpha$ . The red line represents the mass computed using the LLP expression for free polarons  $M^{LLP} = m_e^{LLP} + m_h^{LLP}$ .

### Alternative variational approaches for excitonic polarons in a polar semiconductor

The excitonic polaron PB model led historically to the first quantitative predictions of the dielectric constant relevant for the exciton in various semiconductors, ranging from conventional semiconductors to ionic materials, and from the weak to the intermediate-coupling regime.<sup>59</sup> However, unlike free polaron self-energies (Eq. 16), reduced e-h masses corresponding to the masses of free polarons (Eq. 32) are not recovered in the weak-coupling regime within the initial semi-analytical implementation by PB. This is a direct consequence of the approximate form chosen for  $F_{\vec{k}}(\vec{r}, \vec{0})$  with s-like trial functions for the phonon displacements (Eq. 44).<sup>61</sup> This technical and fundamental issue, well-identified by PB,<sup>61</sup> was solved a few years later by Kane<sup>61</sup> improving the shift operator variational expression by going beyond s-like trial functions:

$$f_{e(h),\vec{k}}(\vec{0}) \rightarrow f_{e(h),\vec{k}}(\vec{0}) \left( 1 - i\lambda_{e(h),\vec{k}} \left( \frac{\vec{k} \cdot \vec{r}}{r} \right) \right). \quad (60)$$

The additional refinement parameters  $\lambda_{e(h),\vec{k}}$  allow to recover a reduced e-h mass consistent with free polarons (LLP model) in the weak coupling regime (Figure 7, left). When the coupling is increased the e-h reduced mass recovers its bare value, due to the compensation of the distortion fields produced by the two charges in the excitonic polaron.

We illustrate the flexibility of the full PBK model considering the specific case of TlCl in Figure

7.

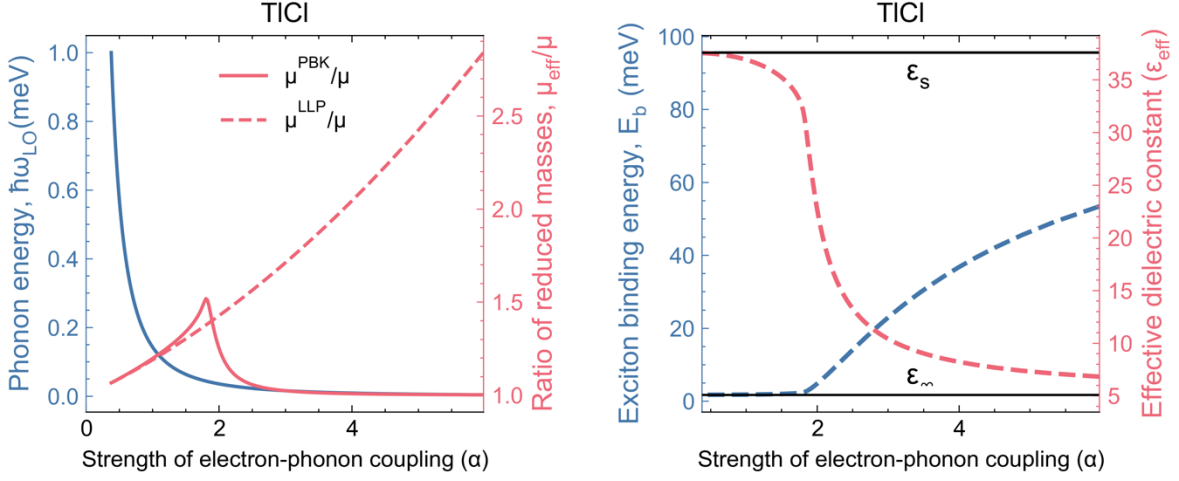


Figure 7. Excitonic polaron characteristics computed within the PBK model considering material parameters for TlCl from the weak coupling regime ( $\alpha \rightarrow 0, a_B^{eff} \gg R_{pol}$ ) to the intermediate coupling regime ( $a_B^{eff} < 4R_{pol}$ ). (Left, blue line) The cross-over from the weak to the intermediate coupling regime is obtained by tuning the effective phonon frequency in the expression of  $\alpha$  (Eq. 1). (Left, red line) The exciton reduced mass compared to the reduced mass of free-like polarons (Left red dotted line). (Right, blue dotted line) Exciton binding energy and effective dielectric constant (red dotted line) as a function of  $\alpha$ . The lower ( $\epsilon_\infty$ ) and upper ( $\epsilon_s$ ) bounds of the effective dielectric constant ( $\epsilon_{eff}$ ) are indicated by black horizontal lines.

These additional corrections defining the PBK model are yielding sizeable relative deviations from the PB model for the exciton binding energy only in the weak coupling regime (Figure 8).

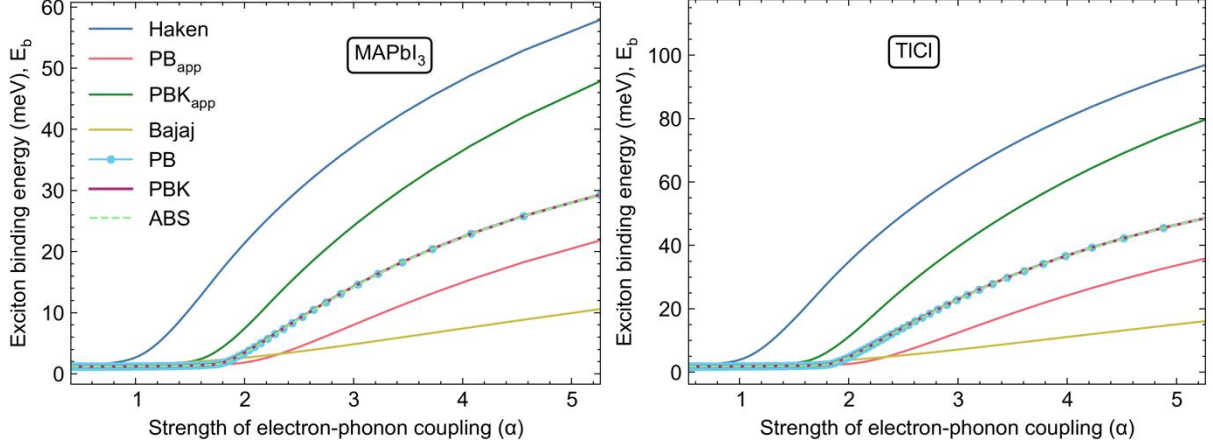


Figure 8: Exciton binding energies computed at various levels of theory for increasing coupling strength  $\alpha$ . Materials parameters are taken from Table 1 for TlCl and MAPbI<sub>3</sub> except the effective phonon frequencies  $\hbar\omega_{LO}$  for both materials, which allows considering different coupling strength  $\alpha$  (Figure 7a). The results of the full PBK<sup>61</sup> and PB<sup>60</sup> models (blue dotted and cyan lines, Eq. 50-55, 60) are almost identical at this scale. This is true also for the results of the ABS method<sup>112</sup> ( $E_b^{ABS}$ ) and a simplified version of the ABS method introduced in this work ( $E_b^{ABS_{app}}$ ) represented by the same green dashed line. Red and green lines correspond to the approximation of PB potential proposed in the present work (Eq. 66), respectively with ( $E_b^{PBK_{app}}$ ) and without ( $E_b^{PB_{app}}$ ) LLP reduced masses. The blue line correspond to Haken's historical derivation ( $E_b^{Hak}$ , Eq. 64/67).<sup>104</sup> The yellow line corresponds to Bajaj's approximate potential ( $E_b^{Baj}$ , Eq. 68).

It is interesting at this point to compare the PB or PBK approaches to alternative solutions for Eq. 34. The exact Iad solution for  $F_{\vec{k}}(\vec{r}, \vec{0})$ <sup>106</sup> can be written in a compact form using Whittaker functions instead of confluent hypergeometric functions:

$$\begin{aligned}
F_{\vec{k}}^{min}(\vec{r}, \vec{0}) = & \\
& \frac{g_{\vec{k}}^*}{\hbar\omega_{LO}} \sum_{l=0}^{+\infty} \left( (-1)^{l+1} \int_0^{+\infty} e^{\tilde{r}-\tilde{u}} \left( \frac{\tilde{u}}{s_e \tilde{k} \tilde{r}^2} \right)^{\frac{1}{2}} M_{\frac{\tilde{\zeta}}{2}, l+\frac{1}{2}}^1(2\tilde{\zeta}\tilde{r}) M_{\frac{\tilde{\zeta}}{2}, l+\frac{1}{2}}^2(2\tilde{\zeta}\tilde{u}) J_{l+\frac{1}{2}}(s_e \tilde{k} \tilde{u}) d\tilde{u} \right. \\
& \left. + \int_0^{+\infty} e^{\tilde{r}-\tilde{u}} \left( \frac{\tilde{u}}{s_h \tilde{k} \tilde{r}^2} \right)^{\frac{1}{2}} M_{\frac{\tilde{\zeta}}{2}, l+\frac{1}{2}}^1(2\tilde{\zeta}\tilde{r}) M_{\frac{\tilde{\zeta}}{2}, l+\frac{1}{2}}^2(2\tilde{\zeta}\tilde{u}) J_{l+\frac{1}{2}}(s_h \tilde{k} \tilde{u}) d\tilde{u} \right) \times \\
& \left( \frac{(-i)^l \sqrt{\frac{\pi}{8}} (2l+1) \Gamma\left(l+1-\frac{1}{\tilde{\zeta}}\right) P_l(\cos(\theta))}{(\tilde{R}_e^2 + \tilde{R}_h^2) \tilde{\zeta} \Gamma(2(l+1))} \right) \tag{61}
\end{aligned}$$

where  $(M^1, M^2)$  stand for the Whittaker functions  $(M, W) / (W, M)$  when  $(\tilde{u} > \tilde{r}) / (\tilde{r} > \tilde{u})$ ,  $\Gamma$  for the gamma function,  $P_l$  for a Legendre polynomial and  $\tilde{\zeta} = \sqrt{1 + \frac{1}{\tilde{R}_e^2 + \tilde{R}_h^2} + \frac{\mu}{M} \tilde{k}^2}$ . All the variables are expressed in reduced units with respect to the effective Bohr radius  $a_B^{eff}$ . As pointed out by Iadonisi, this series has unfortunately a very slow convergence as a function of  $l$ . Iadonisi performed a partial exact summation over an infinite number of terms to recover the LLP limit for free polarons.<sup>106</sup> A similar partial summation using Lommel integrals for the Whittaker functions in Eq. 61 also leads to the LLP limit (Supplementary information). For  $m_h = m_e$ , relevant to halide perovskites, all the terms with even  $l$  values vanish, and this reduces the computational burden. However, these exact solutions cannot be used for nanostructures. However, approximate methods derived from the PB model can be extended to account for quantum confinement effects in nanostructures (vide infra).

Self-energy corrections like those obtained by LLP for free polarons (Eq. 16) are recovered within the PB model in the weak-coupling regime since the expression derived for  $f_{e(h), \vec{k}}^{min}(\vec{0})$  (Eq. 46) reduces to approximate expressions that do not depend anymore on  $a_B^{eff}$ :

$$f_{e(h), \vec{k}}^{min}(\vec{0}) \approx \frac{1}{(1 + R_{e(h)}^2 k^2)}. \tag{62}$$

These expressions lead indeed to  $\sigma_{e(h),1S}(\vec{0}) \approx -\alpha_{e(h)}\hbar\omega_{LO}$  (see supplementary information). A way to extract an approximate effective interaction for the weak coupling regime was proposed by PB in 1977.<sup>60</sup> By inserting the approximate form of the coefficients  $f_{e(h),\vec{k}}^{min}$  (Eq. 62), in the expression of  $V_{latt}^{PB}(\vec{r}, \vec{0})$ , Eq. (49), and after analytical integration over  $\vec{k}$ , PB obtained a real space expression for the case where  $m_e \neq m_h$  that reads:

$$V_{latt,m_e \neq m_h}^{PBapp}(\vec{r}, \vec{0}) \approx \frac{e^2}{4\pi\epsilon_0\epsilon^*r} \left( 1 + \frac{m_e}{\Delta m} e^{-r/R_e} - \frac{m_h}{\Delta m} e^{-r/R_h} \right), \quad (63)$$

with  $\Delta m = m_h - m_e$ . This expression, which is convenient for a numerical implementation into a Wannier-like equation, is often improperly referred to as the ‘‘PB potential’’, whereas the true expression of the PB potential  $V_{latt}^{PB}(\vec{r}, \vec{0})$  is Eq. (49). For the simulation of materials with roughly equal masses, the presence of  $\Delta m$  in the denominators of  $V_{latt,m_e \neq m_h}^{PBapp}(\vec{r}, \vec{0})$  may be problematic. In this work, we propose a suitable expression for this specific case (vide infra). Finally as pointed out by Kane,<sup>61</sup> expressions for  $f_{e(h),\vec{k}}^{min}(\vec{0})$  such as Eq. 62 are not sufficient to derive effective masses consistent with the LLP model in the weak-coupling regime.

Haken’s historical model (abbreviated as Hak) is also based on eq. 62.<sup>104</sup> Hak self-energies are thus the ones of a pair of free polarons. In addition, Haken considered a reduced mass consistent with the LLP model. Among approximate methods, the approximated potential proposed by Haken for the effective interaction in the weak-coupling regime<sup>104</sup> is still very popular. But it must be used with great care since its validity is limited to the very weak coupling regime,  $\alpha \ll 1$ . This is illustrated in Figure 8 for TlCl and MAPbI<sub>3</sub> with the comparison to the more complete PB/PBK approaches. Haken’s approximate expression for the effective interaction reads:

$$V_{latt}^{Hak}(\vec{r}, f_{e,\vec{k}}^{min}(\vec{0}), f_{h,\vec{k}}^{min}(\vec{0})) \approx \sum_{\vec{k}} \frac{|g_{\vec{k}}|^2}{\hbar\omega_{LO}} (f_{e,\vec{k}}^{min}(\vec{0})e^{-i\vec{k}\cdot\vec{r}} + f_{h,\vec{k}}^{min}(\vec{0})e^{i\vec{k}\cdot\vec{r}}), \quad (64)$$

where the coefficients  $f_{e(h),\vec{k}}^{min}(\vec{0})$  (Eq. (62)) are consistent with the LLP model for free polarons and do not depend self-consistently on the exciton properties.<sup>104</sup> After analytical integration over  $\vec{k}$ , Eq. (64) leads to an effective interaction term expressed in real space (see supplementary information):

$$V_{latt}^{Hak}(\vec{r}, \vec{0}) \approx \frac{e^2}{4\pi\epsilon_0\epsilon^*r} \left(1 - \frac{1}{2}e^{-r/R_e} - \frac{1}{2}e^{-r/R_h}\right). \quad (65)$$

Such a real space expression for the effective interaction is attractive for a numerical implementation in a Wannier-like equation and is often referred to as the ‘‘Haken potential’’.

To understand the differences between Hak and PB approximate expressions, we provide expressions specifically designed for the case where  $m_e = m_h$  ( $R_e = R_h = R_{pol}$ )

$$\tilde{V}_{latt,m_e=m_h}^{PBapp}(\vec{r}, \vec{0}) = \frac{V_{latt,m_e=m_h}^{PBapp}(\vec{r}, \vec{0})}{\frac{e^2}{4\pi\epsilon_0\epsilon^*R_{pol}}} \approx \left(\frac{1-e^{-\tilde{r}}}{\tilde{r}} + \frac{e^{-\tilde{r}}}{2}\right), \quad (66)$$

with  $\tilde{r} = r/R_{pol}$ . Comparison of this expression to Haken one (Eq. 65) considering  $R_e = R_h =$

$R_{pol}$ :

$$\tilde{V}_{latt,m_e=m_h}^{Hak}(\vec{r}, \vec{0}) = \frac{V_{latt,m_e=m_h}^{Hak}(\vec{r}, \vec{0})}{\frac{e^2}{4\pi\epsilon_0\epsilon^*R_{pol}}} \approx \left(\frac{1-e^{-\tilde{r}}}{\tilde{r}}\right), \quad (67)$$

evidences that the Haken potential is missing the  $\frac{e^{-\tilde{r}}}{2}$  contribution. The influence of this term is expected to vanish only in the very weak coupling limit where  $a_B^{eff} \gg R_{pol}$  (Figure 8,  $\alpha \ll 1$ ).

For larger coupling regimes, Hak approach significantly deviates from the complete PBK model (Table 2, Figure 8). In many reports, Haken's potential (Eq. 65) is combined in an ad hoc manner with a kinetic energy term based on LLP effective masses as proposed by Haken himself.<sup>105</sup> On the contrary, PB approximated potential  $V_{latt}^{PB_{app}}(\vec{r}, \vec{0})$  (Eq. 63) is usually implemented<sup>56</sup> with bare effective masses, in line with PB's initial paper (dashed green line in Figure 7).<sup>59</sup> As quoted by PB,<sup>60</sup> we stress here again that bare effective masses are not justified in the weak coupling regime. Consistently with the results of the PBK refined approach (vide infra), we propose instead to **use  $V_{latt}^{PB_{app}}(\vec{r}, \vec{0})$  together with the LLP effective masses**, in the spirit of Haken's suggestion. This new approach, which is mathematically justified in the present work, appears to be the **best approximation to the full PBK model for the weak coupling regime**. It can be used for a numerical implementation into a Wannier-like equation neglecting self-consistency necessary for full PB and PBK approaches (dashed blue line in Figure 8).<sup>61</sup> As shown in figure 9, the approximate expressions  $\tilde{V}_{latt, m_e=m_h}^{PB_{app}}(\vec{r}, \vec{0})$  (Eq. 66) and  $\tilde{V}_{latt, m_e=m_h}^{Hak}(\vec{r})$  (Eq. 67) deviate strongly from the exact expression of the effective interaction  $\tilde{V}_{latt, m_e=m_h}^{PB}(\vec{r})$  (Eq. 52) in the intermediate exciton polaron coupling regime ( $\tilde{R}_{pol} \geq 1/4$ ,  $a_{B,eff} < 2(R_e + R_h)$ ).

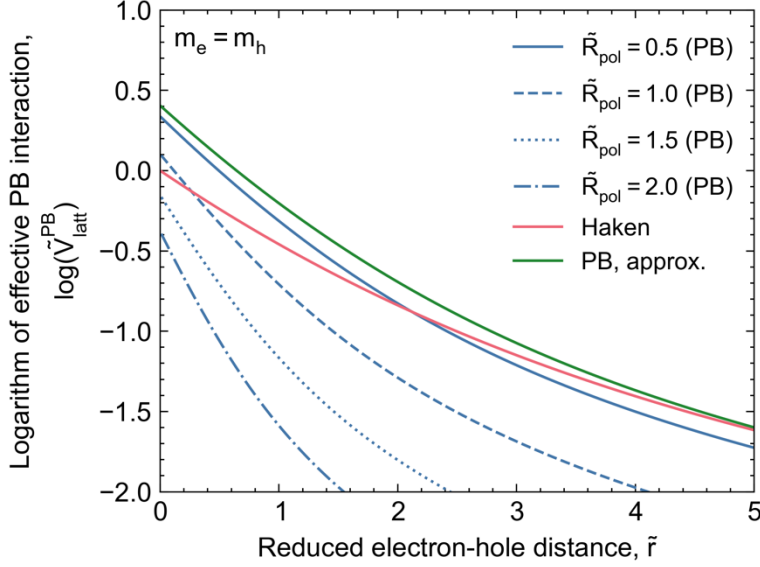


Figure 9.  $\log(\tilde{V}_{latt}^{PB})$  represented for  $m_e = m_h$  as the function of the e-h distance, for various expressions of the effective potential. The full PB effective interaction  $\tilde{V}_{latt,m_e=m_h}^{PB}(\vec{r})$  (Eq. 52, green lines) represented for various values of  $\tilde{R}_{pol}$  is compared with the approximate expressions  $\tilde{V}_{latt,m_e=m_h}^{PBapp}(\vec{r})$  (Eq. 66, red line) and  $\tilde{V}_{latt,m_e=m_h}^{Hak}(\vec{r})$  (Eq. 67, blue line) relevant for the weak coupling regime  $\tilde{R}_{pol} \rightarrow 0$ . The e-h distance is expressed in reduced units:  $\tilde{r} = r/R_{pol}$ .

Bajaj (abbreviated as Baj) proposed<sup>113</sup> an ad hoc modification of Haken's potential to avoid the overestimation of the exciton binding energy that it entails:

$$V_{latt}^{Baj}(\vec{r}, \vec{0}) \approx \frac{e^2}{4\pi\epsilon_0\epsilon^*r} - \frac{e^2}{8\pi\epsilon_0\epsilon^*r} \left(\frac{\epsilon_\infty}{\epsilon_s}\right)^\gamma \left(e^{-r/R_e} + e^{-r/R_h}\right) \quad (68).$$

In this modified potential  $\gamma = 3/5$ , whereas  $\gamma = 0$  in the Haken potential. But this expression still deviates significantly from the PB and PBK potentials (Fig. 8) and is invalid beyond the weak-coupling regime, because self-energies and effective masses of free polarons are used. Another attempt was made later on by the same author to extend perturbatively the Haken's

approach beyond the free polaron limit,<sup>65</sup> but this extension is again limited by comparison to the complete PB and PBK approaches.

A more flexible approach was introduced by Adamowski, Bednarek and Suffczynski (ABS).<sup>112,114,115</sup> It aims at reproducing PB's results with a variational approach for the  $f_{e(h),\vec{k}}^{min}(\vec{0})$  coefficients, replacing the full expression in Eq. 46. This method modifies not only the effective interaction but also the self-energies and thus its validity extends beyond the weak coupling regime. Beyond the exciton ground state, it has also been tested by the authors for the excited states of the exciton as well as for exciton complexes. To illustrate the ABS method, we consider here excitonic polarons and use notations consistent with the rest of the paper. The derivation of the effective interaction and self-energies can be found in the supplementary information in general cases. In the main text, we illustrate the specific case where  $m_e = m_h$ , for which the full

expression of PB  $f_{e(h),\vec{k}}^{min}(\vec{0}) = \frac{1-G_{1S}(\vec{k},a_B^{eff})}{1+R_{pol}^2 k^2 - G_{1S}(\vec{k},a_B^{eff})}$  is replaced by:

$$f_{e(h),\vec{k}}^{min}(\vec{0}) = \frac{\lambda\rho}{1+(\rho R_{pol})^2 k^2}. \quad (69)$$

The two parameters  $(\lambda, \rho)$  must be determined by minimization of the total energy. For  $m_e = m_h$ , the effective interaction can be for example expressed as (see supplementary information for additional analytical expressions):

$$\tilde{V}_{latt,m_e=m_h}^{ABS}(\vec{r}, \vec{0}) = \frac{V_{latt,m_e=m_h}^{ABS}(\vec{r}, \vec{0})}{\frac{e^2}{4\pi\epsilon_0\epsilon^*R_{pol}}} = \frac{1}{\rho} \left( \frac{(2\lambda\rho - \lambda^2\rho^2)(1 - e^{-\tilde{r}/\rho})}{\tilde{r}/\rho} + \frac{\lambda^2\rho^2 e^{-\tilde{r}/\rho}}{2} \right). \quad (70)$$

Considering  $\lambda \rightarrow 1, \rho \rightarrow 1$ , one retrieves the weak-coupling limit, the free polaron self-energies as well as the approximate PB effective interaction Eq. 66. The ABS expressions for  $f_{e(h),\vec{k}}^{min}(\vec{0})$  do not exhibit explicitly the influence of e-h correlations. However, the influence of the lattice distortions is introduced in the medium coupling regime, by a reduction of the effective polaron

radii ( $0 < \rho < 1$ ) and the amplitudes of distortions ( $0 < \lambda < 1$ ) (Fig. S2). The relative error on the excitonic polaron binding energy versus PB's model is less than 1.5% (Fig. S3).

The ABS variational approach is numerically less efficient than the direct computation of the effective interaction, self-energies and total energies within the PB model when one uses the analytical solutions derived in the present work (Eq. 52-55). However, it provides an accurate approach for excited states and exciton complexes, that are very hard to tackle with extensions of the PB model. From Fig. S2 we see that the variations of the two parameters of the ABS approach are very similar. We propose here to further reduce the numerical cost of the variational calculation by considering a single parameter, assuming  $\lambda = \rho$ :

$$\tilde{V}_{latt, m_e=m_h}^{ABS_{app}}(\vec{r}, \vec{0}) = \frac{V_{latt, m_e=m_h}^{ABS_{app}}(\vec{r}, \vec{0})}{\frac{e^2}{4\pi\epsilon_0\epsilon^*R_{pol}}} = \frac{1}{\rho} \left( \frac{(2\rho^2 - \rho^4)(1 - e^{-\tilde{r}/\rho})}{\tilde{r}/\rho} + \frac{\rho^4 e^{-\tilde{r}/\rho}}{2} \right). \quad (71)$$

Despite this additional simplification, the relative error on the excitonic polaron binding energy versus PB's model remains moderate and less than 2.5% (Fig. S3). **The ABS and simplified ABS approaches are the most attractive solutions in the intermediate coupling regime** as compared to the full PB and PBK models (Figure 8).

### Connection with first principles approaches for excitonic polarons

Progress has been made in the recent years on the development of exciton coupling theory from first principles<sup>116,117,9</sup>, including approaches to excitonic polarons.<sup>11,71,72</sup> Some last developments are connected to first-principles approaches for free polarons.<sup>118</sup> It is thus interesting to make a comparison between the empirical PBK model used in the present work and recent state-of-the-art atomistic modelling approaches to Fröhlich excitonic polarons. In their introduction, based on the papers of Iadonisi and coworkers the authors of ref. <sup>11,72</sup> state that the empirical

formalism is biased to find only localized solutions, since the dispersions of the exciton bands are not considered. If indeed the excitonic polaron dispersion is not accounted by the Iad analytical solution for the ground state,<sup>106</sup> this is generally not true for the PB formalism, which is precisely based on a unitary transformation that introduce the excitonic polaron total momentum (Eq. 38). Besides, as shown in the present work, it is possible to analyze the change of the excitonic polaron total mass from PB's formalism, something that has not yet been performed in detail from first principles (Figure 6, Eq. 56-59). Indeed, first-principles approaches allow assessing the exciton<sup>119</sup> or the excitonic polaron dispersion,<sup>11</sup> but the calculation needs to be performed for each value of the exciton momentum, and the computational cost scales linearly with the size of the momentum grid used for sampling.

For free polarons, first principles approaches give access to envelop functions for the atomic displacements of the phonon mode  $\nu$ :

$$B_{\vec{q},\nu} = \frac{1}{N_p} \sum_{m,n,\vec{k}} A_{m,\vec{k}+\vec{q}}^* \frac{g_{mn,\nu}(\vec{k},\vec{q})}{\hbar\omega_{\vec{q},\nu}} A_{n,\vec{k},\nu} \quad (72)$$

where the  $g_{mn,\nu}(\vec{k},\vec{q})$  are the e-ph coupling matrix elements. Using these envelop functions and eigenvectors for the phonon modes, the atomic displacements in the polaron cloud can be computed.<sup>118,120</sup> This envelop function is connected to  $F_{\vec{k},\nu}^{min}(\vec{Q})$  in the LLP empirical approach to free polarons extended to multiple phonons (MLLP model, vide infra, Eq. 86).

The recent DFT-based formalism for excitonic polarons starts by combining the electronic ground state and BSE excitation energies with a quadratic expression for the elastic energy associated with the lattice distortion and atomic displacements. It involves a BSE Hamiltonian which depends on the atomic displacements and thus allows to account for a distorted structure. This Hamiltonian is then expanded linearly as a function of the displacements, and the total energy

is minimized with respect to the exciton wavefunction  $\Psi(\vec{r}_e, \vec{r}_h)$  and atomic displacements. This is formally equivalent to the functional and wavefunction minimization at the heart of PB's formalism (Eq. 42,43). We may note that self-consistency is important for the simulation of the free carrier polaron from first principles<sup>7</sup> on par with the empirical calculations within LLP's formalism (Eq. 26-27).

To reduce the computational cost of the DFT-based approach, the excitonic polaron Hamiltonian is expressed<sup>11</sup> in an exciton (e-h pair) basis  $\Psi(\vec{r}_e, \vec{r}_h) = \sum_{s\vec{Q}} A_{s,\vec{Q}} \sum_{v\vec{k}} a_{v\vec{k}}^{s,\vec{Q}} \varphi_{c,\vec{k}+\vec{Q}}(\vec{r}_e) \varphi_{v,\vec{k}}^*(\vec{r}_h)$ . This basis choice brings the first principles formalism close to the empirical one:

$$\sum_{s'\vec{Q}'} \left[ E_{s\vec{Q}}^0 \delta_{ss'} - \frac{2}{N_p} \sum_v B_{\vec{Q}-\vec{Q}',v} \mathcal{G}_{ss',v}(\vec{Q}', \vec{Q} - \vec{Q}') \right] A_{s',\vec{Q}'} = E A_{s,\vec{Q}} \quad (73)$$

With the envelop function

$$B_{\vec{Q},v} = \frac{1}{N_p} \sum_{ss'\vec{Q}'} A_{s',\vec{Q}'}^* \frac{\mathcal{G}_{ss',v}^*(\vec{Q}', \vec{Q})}{\hbar\omega_{\vec{Q},v}} A_{s,\vec{Q}+\vec{Q}'} \quad (74)$$

$E_{s\vec{Q}}^0$  are the eigenvalues of the undistorted structure.  $\mathcal{G}_{ss',v}$  are the exciton-phonon matrix element:

$$\mathcal{G}_{ss',v}(\vec{Q}, \vec{q}) = \sum_{v\vec{k}} a_{v\vec{k}}^{s,\vec{Q}+\vec{q}*} \left[ \sum_{c'} g_{cc',v}(\vec{k} + \vec{Q}, \vec{q}) a_{v\vec{k}}^{s,\vec{Q}} - \sum_{c'} g_{vv',v}(\vec{k}, \vec{q}) a_{v'\vec{k}+\vec{q}}^{s',\vec{Q}} \right] \quad (75)$$

As shown by the authors of ref. <sup>11</sup>, in the framework of the Wannier exciton and Fröhlich interaction models, also considered in the present work, the e-ph coupling matrix elements finally correspond to Eq. 11 and an hydrogenic wavefunction for the 1S ground state can be considered

$$\Psi_{1S}(\vec{R}_e, \vec{R}_h) \approx \frac{e^{i\vec{Q}\cdot\vec{R}_e} e^{-r/a_B^{eff}}}{a_B^{eff3/2} \pi^{1/2}}. \text{ Here, } (\vec{R}_e, \vec{R}_h) \text{ refer to various unit cell positions whereas } (\vec{R}, \vec{r}) \text{ are}$$

the center of mass and relative e-h positions. This envelop function is connected to  $F_{\vec{k},\nu}^{min}(\vec{Q},\vec{r})$  in the empirical approach to excitonic polarons extended to multiple phonons (MPB/MPBK models, Eq. 86). These last considerations bridge the DFT-based approach of Refs. <sup>11,72</sup> with the PB or MPB (vide infra) formalisms.

In ref. <sup>11</sup> the authors used the case of LiF to illustrate their novel DFT-based approach. The polaron radii and  $\alpha$  values of LiF reported in Table 1 show that it corresponds to the case of a strongly bound exciton, which is clearly beyond the validity limit of the LLP model suitable for free polarons. This is especially true for the hole polaron as pointed out by the authors. The hole polaron radius is smaller than the lattice constant. LiF hosts strongly bound Fröhlich electron polarons and Holstein hole polarons, respectively. It is nevertheless interesting to compare the excitonic polaron properties of LiF computed using the present PBK model and results obtained using the atomistic approach of Dai and coworkers (Table 3). In such a case where the interaction with the lattice is very strong, the self-energies computed by the LLP model deviate from the DFT ones, as expected, especially for the Holstein hole polaron. However, the self-energy computed for the excitonic polaron shows a better agreement. This results from the strong reduction of the polaronic distortions due to e-h correlations beyond the weak-coupling regime, an effect which is captured within PB's formalism (Fig. 4). The exciton binding energy is significantly underestimated in PB formalism. Numerical accuracy is indirectly affected by the inadequacies of the LLP approach in description of free polarons in the strong coupling regime. Future studies deserve to further compare results from atomistic approaches with those derived within empirical models, for materials more adapted to their respective limitations.

LiF	$\mu$	$\mu^{PBK}$	$\mu^{LLP}$	$E_{b,1S}$ (eV)	$\sigma_e$ (eV)	$\sigma_h$ (eV)	$\sigma_{e,1S} + \sigma_{h,1S}$ (eV)
Dai et al <sup>8</sup>				1.88	0.23	1.98	0.46
PBK	0.158	0.161	0.180	1.35	0.38	0.85	0.42

**Table 3. Excitonic polaron properties for LiF.** The first line reports the results obtained with the first principles approach by Dai and coworkers.<sup>11</sup> The second line shows results obtained for LiF within the LLP free polaron and PBK excitonic polaron empirical models considered in this work. Exciton binding energies  $E_{b,1S}$ , electron ( $\sigma_e$ ) and hole ( $\sigma_h$ ) free polarons, and excitonic polaron self-energies  $\sigma_{e,1S} + \sigma_{h,1S}$  are given in eV.

Extending the standard empirical approach for excitonic polarons to multiple polar phonon modes

When applied to excitonic polarons in halide perovskites and more generally to polar lattices with atomic motifs containing more than two atoms, empirical approaches treat the exciton-lattice coupling by means of a single optical polar mode. For 3D halide perovskites it is known both theoretically<sup>20</sup> and experimentally<sup>44,81</sup> that multiple polar modes play a role. This is one of the specific features of this class of polar semiconductors (Table 1). The single mode approximation is related to the use of the original expression of the Fröhlich interaction. It can be partially overcome by treating this mode as an effective one, but this effective frequency is not directly related to an experimental one, except that they fall roughly in the low-energy range of the lattice modes (Table 2). It is also proven experimentally that couplings of excitons to multiple phonons are systematically observed.<sup>34,121</sup> To include these effects, one may either rely on an atomistic approach or make approximations in order to turn the multimode polaronic calculation into a tractable problem. The later approach, for example, has been implemented in the past for free polarons to compute carrier mobilities.<sup>81,85,122,123</sup>

We propose here a multimode extension of PB, PBK and Iad frameworks (quoted as MPB, MPBK, MIad models hereafter) for excitonic polaron. Let's start first by describing how the empirical approaches for the dielectric properties and the Fröhlich interaction have been originally extended to multiple polar modes in literature. As reported in earlier reports<sup>81,124</sup>, polar modes and lattice anharmonicity are included using the semi-empirical expression of Gervais and coworkers:<sup>125</sup>

$$\varepsilon(\omega) = \varepsilon'(\omega) + i\varepsilon''(\omega) = \varepsilon_\infty + \sum_v \frac{\omega_{TO,v}^2 \Delta\varepsilon_v}{\omega_{TO,v}^2 - \omega^2 - i\omega\gamma_{TO,v}} \quad (76)$$

where  $\omega_{TO,v}$  and  $\gamma_{TO,v}$  are the frequency of the TO-mode  $v$  and the corresponding damping parameter, respectively. With negligible anharmonicity, this equation is reduced to Toyozawa's

multimode expression:<sup>49</sup>  $\varepsilon(\omega) = \varepsilon_\infty + \sum_v \frac{\omega_{TO,v}^2 \Delta\varepsilon_v}{\omega_{TO,v}^2 - \omega^2}$ . For a single polar mode:  $\varepsilon(\omega) = \varepsilon_\infty + \frac{\omega_{TO}^2(\varepsilon_s - \varepsilon_\infty)}{\omega_{TO}^2 - \omega^2}$ . A generalization of the LST equation (13) to multimodes can also be derived:<sup>125</sup>

$$\frac{\varepsilon(\omega)}{\varepsilon_\infty} = \prod_v \left( \frac{\omega_{LO,v}^2 - \omega^2 + i\omega\gamma_{LO,v}}{\omega_{TO,v}^2 - \omega^2 + i\omega\gamma_{TO,v}} \right) \quad (77)$$

where  $\omega_{LO,v}$  and  $\gamma_{LO,v}$  are the frequency of the LO mode  $v$  and the corresponding damping parameter, respectively. Longitudinal optical modes appear as poles of  $\frac{1}{\varepsilon(\omega)}$ , while transverse optical modes are poles of  $\varepsilon(\omega)$ . In a cubic crystal, the longitudinal component of the dielectric tensor can be combined with the general expression of  $\varepsilon(\omega)$  and the LST equation because  $\varepsilon_{//}(\omega) = \varepsilon(\omega)$ . More importantly as detailed by Toyozawa, a semi-empirical calculation based on Poisson equation allows computing independently the longitudinal component of the dielectric tensor as a function of various contributions to the Fourier transform of the polarization:<sup>49</sup>

$$\frac{1}{\varepsilon_\infty} - \frac{1}{\varepsilon_{//}(\omega)} = \sum_{\nu} \frac{2\omega_{LO,\nu}\varepsilon_0 k^2 |g_{\vec{k},\nu}|^2}{\hbar e^2 (\omega_{LO,\nu}^2 - \omega^2)}. \quad (78)$$

Toyozawa pushed forward the analysis in the multimode case with negligible phonon damping (harmonic approximation) by expanding  $\frac{1}{\varepsilon_{//}(\omega)}$  close to  $\omega = \omega_{LO,\nu}$  (see supplementary information), in order to get the k-dependent e-ph matrix element for each optical phonon

$$k^2 |g_{\vec{k},\nu}|^2 = \frac{\hbar e^2}{\varepsilon_0 \frac{\partial \varepsilon}{\partial \omega} |_{\omega_{LO,\nu}}}.^{49}$$

This multimode extension of the Fröhlich e-ph coupling matrix element (Eq. 12) was used for alloys of conventional semiconductors<sup>126,127</sup> and, more recently to investigate free carrier mobility in MAPbI<sub>3</sub>.<sup>85</sup> Multimode coupling strength  $\alpha_{e,\nu}$  can be introduced with respect to the matrix element by analogy with the standard theory:

$$k |g_{\vec{k},\nu}| = \hbar \omega_{LO,\nu} \left( \frac{4\pi\alpha_{e,\nu}}{V} \right)^{1/2} \left( \frac{\hbar}{2m_e \omega_{LO,\nu}} \right)^{1/4}. \quad (79)$$

In the harmonic approximation, the strength of the coupling of an electron to each polar optical mode of the lattice can then be obtained as (see supplementary information):<sup>49,126,85</sup>

$$\alpha_{e,\nu} = \frac{e^2}{4\pi\varepsilon_0\hbar} \left( \frac{m_e}{2\hbar\omega_{LO,\nu}} \right)^{1/2} \frac{1}{\varepsilon_\infty} \left( 1 - \frac{\omega_{TO,\nu}^2}{\omega_{LO,\nu}^2} \right) \prod_{\mu \neq \nu} \left( \frac{\omega_{LO,\nu}^2 - \omega_{TO,\mu}^2}{\omega_{LO,\nu}^2 - \omega_{LO,\mu}^2} \right). \quad (80)$$

By expanding the general expression of  $\varepsilon(\omega)$  close to  $\omega = \omega_{TO,\nu}$  (see supplementary information) we can demonstrate that (see supplementary information):

$$\Delta\varepsilon_\nu = \varepsilon_\infty \left( \frac{\omega_{LO,\nu}^2}{\omega_{TO,\nu}^2} - 1 \right) \prod_{\mu \neq \nu} \left( \frac{\omega_{TO,\nu}^2 - \omega_{LO,\mu}^2}{\omega_{TO,\nu}^2 - \omega_{TO,\mu}^2} \right). \quad (81)$$

For the treatment of the excitons in the MPB/MPBK/MIad models, we extend the PB approach to multiple branches introducing a generalized unitary transformation:

$$\hat{S} = e^{\sum_{\vec{k},\nu} (F_{\vec{k},\nu}^*(\vec{Q},\vec{r})\hat{a}_{\vec{k},\nu} - F_{\vec{k},\nu}(\vec{Q},\vec{r})\hat{a}_{\vec{k},\nu}^\dagger)} \quad (82)$$

assuming independent lattice distortions produced by the various polar optical modes:

$$F_{\vec{k},\nu}(\vec{Q},\vec{r}) \approx \frac{g_{\vec{k},\nu}^*}{\hbar\omega_{LO}} (f_{e,\vec{k},\nu} e^{-is_{\vec{k},\nu}\vec{r}} - f_{h,\vec{k},\nu} e^{is_{\vec{k},\nu}\vec{r}}) \quad (83)$$

The e-h effective interaction potential includes a summation over the mode contributions:

$$V_{latt}^{MPB}(\vec{r}) = 2 \sum_{\vec{k},\nu} \frac{|g_{\vec{k},\nu}|^2}{\hbar\omega_{LO,\nu}} (f_{e,\vec{k},\nu}^{min} + f_{h,\vec{k},\nu}^{min} - f_{e,\vec{k},\nu}^{min} f_{h,\vec{k},\nu}^{min}) \cos(\vec{k} \cdot \vec{r}) \quad (84)$$

and the total self-energy corrections read:

$$\sigma_{e(h),1S} = - \sum_{\vec{k},\nu} \frac{|g_{\vec{k},\nu}|^2}{\hbar\omega_{LO,\nu}} (2f_{e(h),\vec{k},\nu}^{min} - (1 + R_{e(h),\nu}^2 k^2) f_{e(h),\vec{k},\nu}^{min}) \quad (85)$$

with mode dependent free polaron radii  $R_{e(h),\nu} = \left( \frac{\hbar}{2m_{e(h)}\omega_{LO,\nu}} \right)^{1/2}$ .

To provide a reference to computing the binding energies, we extend the LLP empirical approach for free polarons (Eq. 40) to multiple phonons (MLLP), thanks to a unitary transformation:

$$\hat{S} = e^{\sum_{\vec{k},\nu} (F_{\vec{k},\nu}^*(\vec{Q})\hat{a}_{\vec{k},\nu} - F_{\vec{k},\nu}(\vec{Q})\hat{a}_{\vec{k},\nu}^\dagger)} \quad (86)$$

At this stage, it is interesting to notice that one of the limitations of the present multiple phonons implementation is the use of a generalized LST equation connected to independent harmonic oscillators (Eq. 77). The simplified expression of the coupling strength (Eq. 80) is therefore derived assuming that the LO/TO resonances in the dielectric response are not overlapping, and the mode damping parameters are small. For that reason, the MLLP/MPB/MPBK/MIad models are expected

to be valid mostly in the LT range of metal halide perovskites, where lattice anharmonicity is reduced. However, while experimental data on exciton binding energies, reduced effective masses and effective dielectric constants are usually obtained at LT,<sup>28–30,80,128,89</sup> vibrational optical spectroscopy on lattice polar modes is essentially reported at RT.<sup>82,81,50,129–134,48,135,124</sup> Experiments at LT performed so far on MA-based 3D perovskites, are leading to more complex results, because LT structural phase transitions are leading to a large number of closely spaced polar optical resonances in the dielectric responses.<sup>136–138,130,133,135,124,139</sup> We will consider at the end of this section one of the very few THz experiment performed over a large temperature range.

To gauge the differences between the original versions of PB/PBK models based on a single effective mode and the proposed MPB/MPBK extensions, let's first consider the fully inorganic 3D halide perovskite CsPbCl<sub>3</sub>. Cs-based perovskites are less prone to phonon resonance splitting at LT than MA-based compounds.<sup>130</sup> Wakamura's paper on CsPbCl<sub>3</sub> is, to our knowledge, the first detailed report on multiple mode resonances and LO/TO splitting in inorganic 3D perovskites especially at LT.<sup>82</sup>

CsPbCl <sub>3</sub> modes		$\hbar\omega_{LO}/\hbar\omega_{TO}$ (meV)	number of modes	$\mu^{LLP}$	$\mu^{PBK}$	$E_{b,1S}$ (eV)	$\epsilon_{eff}$
PB model	effective	25.6 / 9.6	1 effective	0.372	0.205	64 (exp. 2K)	6.6 (exp. 2K)
exp. 40K	mode 1	27.5 / 13.6	1	0.299	0.204	76	6.0
exp. 40K	mode 2	13.3 / 11.5	2	0.308	0.205	67	6.4
exp. 40K	mode 3	9.9 / 9.8	3	0.309	0.205	66	6.5
exp. 40K	mode 4	5.5 / 4.8	4	0.318	0.205	62	6.7

**Table 5. Influence of the presence of multiple polar phonon modes on excitonic polarons in CsPbCl<sub>3</sub> at LT computed within the MPB model.** Experimental values of the exciton binding energy, effective dielectric constants and bare effective mass ( $\mu = 0.404$ ) at T=2K

are taken from ref. <sup>80</sup> and the experimental values of the LO/TO optical mode frequencies at T=40K from ref <sup>82</sup>. For each line the number of phonons is indicated, In the second line, a single effective LO mode is tuned within the PB model to match the experimental exciton binding energy. For the MPB calculations (lines 3-6), the experimental LO/TO optical mode frequencies are used and included progressively. The experimental LO/TO optical energies are given in the second column. Computed binding energies are given in the fourth column.

Interestingly as shown in Table 5 for CsPbCl<sub>3</sub>, both experimental LO/TO optical frequencies and exciton characteristics are available from the literature at LT. The binding energy can be evaluated within PB's model by adjusting the energy of a single effective phonon (Table 2). Within the MPB model, similar values for the exciton binding energy and effective dielectric constant values are retrieved, provided that all 4 experimental phonon resonances are considered. We may notice that, in such a case, the free polaron effective mass  $\mu^{LLP}$  is smaller than the one derived with a single effective phonon. It means that the PB approximation of a single effective phonon tends to overestimate the matrix element of the e-ph interaction in a multimode situation, by attributing to this mode all the polarizability responsible for the difference between  $\epsilon_{\infty}$  and  $\epsilon_S$ . A more physical description such as the MPB model, accounts for the various contributions of the experimental phonon lines to the total polarizability. It is also clear from table 5 that the various modes do not equally contribute to the physical properties of the excitonic polarons in CsPbCl<sub>3</sub>. Mode 1, located at high energy, is the dominant one. The mode-dependent  $\alpha_{(e,v)}$  correspond respectively to 0.269, 0.010, 0.025 3.14, while for a single effective mode, a value of 3.4 is needed.

MAPbBr <sub>3</sub> modes		$\hbar\omega_{LO}/\hbar\omega_{TO}$ (meV)	number of modes	$\mu^{LLP}$	$\mu^{PBK}$	$E_{b,1S}$ (eV)	$\epsilon_{eff}$
PB model	effective	13.1 / 5.4	1 effective	0.200	0.119	25 (exp. 2K)	7.5 (exp. 2K)
exp. 300K	mode 1	21.3 / 14.6	1	0.146	0.118	40	6.3
exp. 300K	mode 2	13.8 / 9.1	2	0.162	0.121	18	9.4
exp. 300K	mode 3	6.2 / 5.6	3	0.165	0.122	16	10.0

**Table 6. Influence of the presence of multiple polar phonon modes on the excitonic polarons in MAPbBr<sub>3</sub>.** Experimental values of the exciton binding energy, effective dielectric constants and bare effective mass ( $\mu = 0.202$ ) at T=2K are taken from ref.<sup>29</sup> and the experimental values of the LO/TO optical mode frequencies at T=300K from ref<sup>124</sup>. For each line the number of phonons is indicated, In the second line, a single effective LO mode is tuned within the PB model to match the experimental exciton binding energy. For the MPB calculations (lines 3-5), the experimental LO/TO optical mode frequencies are used and included progressively. The experimental LO/TO optical energies are given in the second column. Computed binding energies are given in the fifth column.

Table 6 describes another example of a 3D halide perovskite (MAPbBr<sub>3</sub>) where data on phonons have been collected at RT,<sup>124</sup> while experimental exciton characteristics are available from the literature at LT.<sup>29</sup> The binding energy was first computed within PB's model by adjusting the energy of a single effective phonon (see Table 2). Using PB's model, it is possible to almost perfectly match the LT exciton characteristics, however the model provides little insight into the significance of the extracted effective phonon energy (13.1 meV) compared to known spectroscopic data. When the contributions of the phonon resonances at RT are progressively included within the MPB model, the corresponding binding energy decreases as the effective dielectric constant increases. Mode 1, located at high energy is again the dominant one. The mode-

dependent  $\alpha_{e,\nu}$  correspond respectively to 0.11, 0.18, 2.2, while for a single effective mode, a value of 3.0 is needed. But the computed binding energy (16meV) finally ends up being smaller than the LT experimental one (25meV). This is not a surprise because a temperature induced dielectric screening effect was predicted early for MA-based 3D perovskites.<sup>19</sup>

MAPbI <sub>3</sub> modes		$\hbar\omega_{LO}/\hbar\omega_{TO}$ (meV)	number of modes	$\mu^{LLP}$	$\mu^{PBK}$	$E_{b,1S}$ (eV)	$\epsilon_{eff}$
PB model	effective	8.2 / 3.1	1 effective	0.184	0.106	16 (exp. 2K)	9.4 (exp. 2K)
PB model	effective	10.8 / 4.1	1 effective	0.171	0.107	12 (exp. 155-190K)	10.9 (exp. 155-190K)
exp. 300K	mode 1	16.5 / 7.8	1	0.139	0.109	11	11.6
exp. 300K	mode 2	5.0 / 4.0	2	0.144	0.111	8	14.1

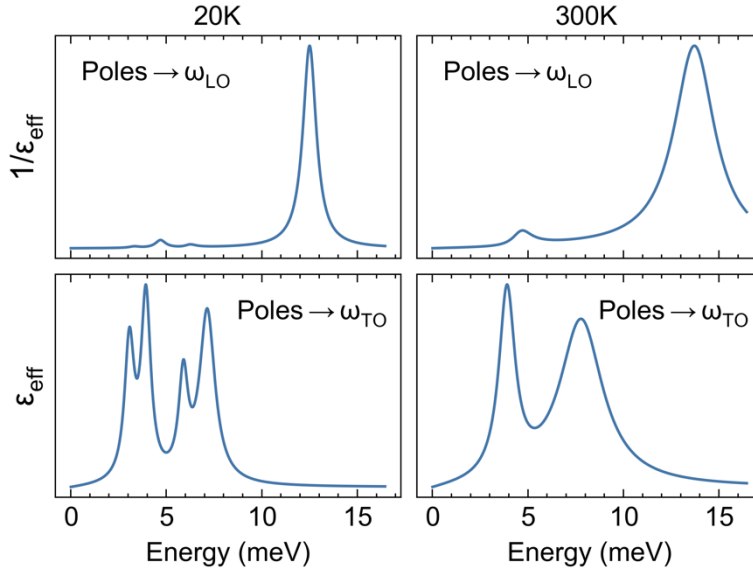
**Table 7. Influence of the presence of multiple polar phonon modes on the excitonic polarons in MAPbI<sub>3</sub>.** Experimental values of the exciton binding energy, effective dielectric constants and bare effective mass ( $\mu = 0.202$ ) at T=2K and 155-190K are taken from ref. <sup>29</sup> and the experimental values of the LO/TO optical mode frequencies at T=300K from ref <sup>81</sup>. For the MPB calculations (lines 4-5), the experimental LO/TO optical mode frequencies are used and included progressively. The experimental LO/TO optical energies are given in the second column. Computed binding energies are given in the fifth column.

Table 7 describes the results computed for MAPbI<sub>3</sub> from RT phonon spectroscopic data<sup>81</sup> with experimental exciton characteristics from the literature reported at 2K and 155-190K.<sup>31</sup> The binding energy was first computed from the PB model by adjusting the energy of a single effective phonon for each temperature. For the MPB model we used several phonon resonances, but the computed RT binding energy (7meV) is smaller than the one at very LT (16meV), but closer to

the one in the intermediate temperature range (12meV). Mode 1, located at high energy is again the dominant one.

To verify whether temperature effects are correctly captured by our approach, it is necessary to have experimental spectroscopic reference data for a wide range of temperature, from RT down to LT. It would also be necessary to know in detail the temperature and frequency dependence of the dielectric properties of the lattice. To our knowledge, the paper of La-o-vorakiat and coworkers on MAPbI<sub>3</sub><sup>138</sup> is the only one providing an extended set of spectroscopic data regarding phonons, necessary for such analysis. The authors performed complete THz time-domain investigations tracking the effect of the orthorhombic to tetragonal structural phase transition in MAPbI<sub>3</sub> observed at LT (about 160K in their study) on the polar optical modes at the  $\Gamma$  point. As expected from the symmetry of the two phases, the splitting of the two phonon lines measured at RT is observed, leading to four modes at LT. This transition is associated with a redistribution of  $\Delta\varepsilon_\nu$  between the modes, when the mode-specific contributions to the dielectric constant are considered (Eq. 81). We note that only the frequencies of the TO modes  $\omega_{TO,\nu}$  are provided as a function of temperature together with  $\Delta\varepsilon_\nu$  and the TO mode damping  $\gamma_{TO,\nu}$ , whereas the frequencies of the LO modes  $\omega_{LO,\nu}$  and the e-ph coupling matrix elements  $g_{\vec{k},\nu}$ , which are required for the implementation of the MPB model, are extracted by analyzing the frequency-dependent dielectric constant. For such analysis, we assume that the structural deviations from the cubic symmetry (MAPbI<sub>3</sub> undergoes a continuous phase transition from the I4mcm tetragonal space group to the Pm $\bar{3}$ m cubic one slightly above RT at 327K) are not significant to ensure validity of Toyozawa's analysis as well as the MPB model. Based on the experimental data of Ref.<sup>138</sup> and the frequency dependent expression for  $\varepsilon(\omega)$  (Eq. 76), Fig. 10 shows  $\text{Im}(1/\varepsilon)$  and  $\text{Im}(\varepsilon)$  as a function of energy for the lowest (20K) and the highest (300K) temperatures considered

in Ref. <sup>138</sup>. The only piece of experimental information that is missing is the temperature dependent value of  $\epsilon_\infty$ , which we approximate to a temperature independent value of 5. In fig. 10, the LO modes frequencies  $\omega_{LO,\nu}$  correspond to the poles of  $1/\epsilon$ , while the TO mode frequencies  $\omega_{TO,\nu}$  correspond to the poles of  $\epsilon$ . Both the influence of mode damping at RT and the splitting of the modes at LT are evident from the plots. It is evident from Fig. 10 that the highest frequency TO mode at about 13-14 meV undergoes the largest LO-TO splitting and its LO component yields the largest contribution to  $\frac{1}{\epsilon(\omega)}$ .



**Figure 10:**  $\text{Im}(1/\epsilon)$  and  $\text{Im}(\epsilon)$  of  $\text{MAPbI}_3$  obtained from THz time-domain spectroscopy and plotted as a function of energy for the lowest (20K) and the highest (300K) temperatures considered in ref.<sup>138</sup> The LO modes frequencies  $\omega_{LO,\nu}$  correspond to the poles of  $1/\epsilon$ , while the TO modes frequencies  $\omega_{TO,\nu}$  correspond to the poles of  $\epsilon$ .

Starting from the experimental data, the first step within Toyozawa's approach which neglects phonon damping, consists in finding numerically the values LO modes frequencies  $\omega_{LO,\nu}$  leading to a good match with the experimentally observed dielectric jump  $\Delta\epsilon_\nu$  (Eq. 81). The

extracted LO modes energies together with the experimental TO modes energies are represented as a function of temperature in Fig. 11. Despite neglecting the experimental damping, the LO modes frequencies extracted from this procedure coincide well at the maxima of  $Im(1/\epsilon)$  (Fig. 10). The second step of Toyozawa's analysis consists in using the LO and TO frequencies to evaluate the e-ph coupling matrix elements  $g_{\vec{k},\nu}$  using Eq. 79-80. As expected from Fig. 10 and 11, the highest frequency LO mode at about 13-14 meV arises from the largest LO-TO splitting and corresponds to the largest e-ph coupling matrix elements  $g_{\vec{k},\nu}$  over the entire temperature range.

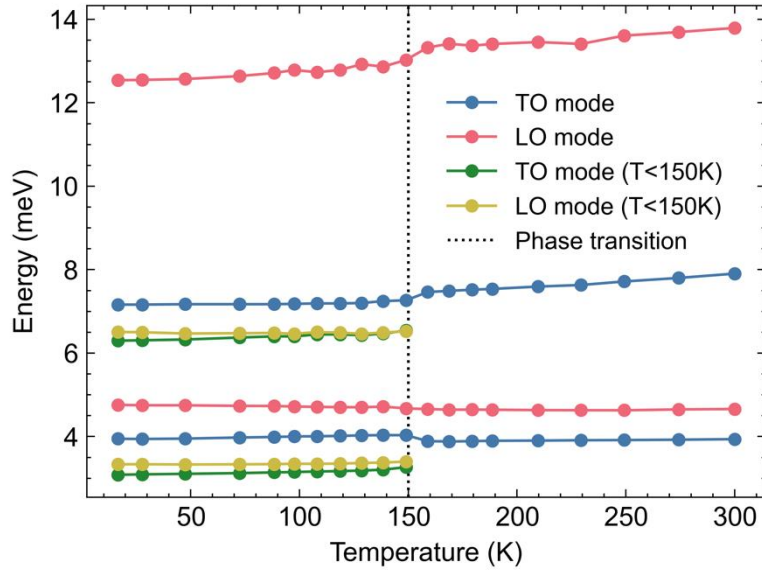


**Figure 11:** Energies of the LO modes as a function of temperature of MAPbI<sub>3</sub> obtained by a numerical analysis of experimental data<sup>138</sup> using Toyozawa's approximate expression for  $\epsilon(\omega)$ . Experimental<sup>138</sup> energies of TO modes are also shown.

Using the values of the e-ph coupling matrix elements  $g_{\vec{k},\nu}$ , we evaluate the exciton binding energy and effective dielectric constant as a function of temperature over the entire temperature

range based on the MPB model (Fig. 12). Both the calculated quantities undergo a continuous variation across the temperature range without exhibiting a discontinuity at the first order phase transition around 160K. It indicates that oscillator strengths are smoothly redistributed between the vibrational modes, when the number of phonon modes increases from 2 in the tetragonal phase to 4 in the orthorhombic phase because of the folding of the Brillouin zone.<sup>42</sup> However, the experimentally observed temperature evolution of both these quantities is not well described within the the MPB model. The model predicts a slight increase of the exciton binding energy from LT to RT, whereas a sizeable reduction has been experimentally observed between 2K and the intermediate temperature range of 155-190K.<sup>31</sup> This reduction is thus clearly related to the lattice disorder and to the strong anharmonicity at higher temperatures that affect the phonon spectral properties, but also the electronic states.<sup>42</sup> These effects are not accounted for within the PB or the MPB frameworks, which remain basically 0K theories. Nevertheless, these models can be utilized to predict the Huang-Rhys factors for side bands, evidenced at LT in photoluminescence experiments, related to virtual phonon populations (vide infra). Further theoretical developments are needed to incorporate temperature effects in the description of excitonic polarons.

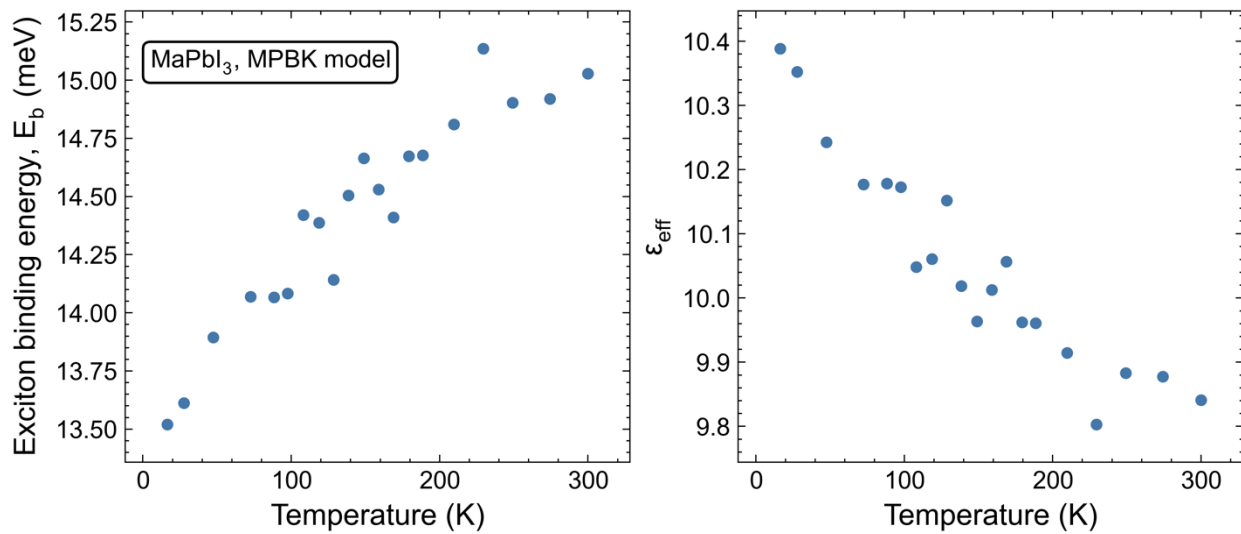


**Figure 12:** Effective exciton binding energy (left) and dielectric constant (right) computed as a function of temperature for MAPbI<sub>3</sub> using the MPB model and input data from ref. <sup>138</sup>.

### Physical observables for excitonic polarons

High resolution and time resolved diffraction experiments such as ultrafast electron diffraction (UED) can be used in principle to extract the details of the envelop functions of the distortion fields represented in MLLP/MPB/MPBK/MIad empirical models by  $F_{\vec{k},\nu}^{min}(\vec{Q})$  for free polarons and  $F_{\vec{k},\nu}^{min}(\vec{r},\vec{Q})$  for excitonic polarons.<sup>120</sup> But the practical task of analyzing these quantities is not easy in complex materials such as halide perovskites since this information is mostly related to diffuse scattering, which is a weak component in many experiments.<sup>140-144</sup> To simply gauge the importance of the lattice distortion induced by free polarons or excitonic polarons, the virtual phonon cloud population provides a simple dimensionless quantity related to the entire distortion field:

$$N_{1S,\nu}(\vec{0}) = \left\langle \varphi_{1S}(\vec{r}) \left| \sum_{\vec{k}} \left| F_{\vec{k},\nu}^{min}(\vec{r},\vec{0}) \right|^2 \right| \varphi_{1S}(\vec{r}) \right\rangle. \quad (87)$$

A partial cancellation of lattice distortions induced by the correlations between electron and hole  $N_{1S,\nu}(\vec{0}) \neq N_{e,\nu}^{LLP}(\vec{0}) + N_{h,\nu}^{LLP}(\vec{0})$  is predicted for excitonic polarons <sup>103</sup> (Figure 4). This is one important difference between excitonic polarons and free (or non-interacting) polarons. Similar considerations hold for bipolaronic states (bound states formed from pairs of particles with the same charge).<sup>74,90</sup> The PB or MPBs approaches further provides convenient ways to quantify the lattice distortion for both the ground state and the excited states of excitonic polarons. In Figure 13, the virtual phonon populations are reported as a function of  $\alpha$ , for both 1S and 2S excitons in TlCl (the variation of  $\alpha$  is obtained by tuning the phonon energy) and for free polarons. The case

of a 2S exciton has been studied by replacing the function  $G_{1S}(\vec{k}, a_B^{eff})$  (Eq. 47) for a 1S exciton by a similar expression for the 2S exciton.<sup>145</sup> As expected from the qualitative picture in figure 4, the e-h correlations in a 1S exciton more significantly affect the distortions than in case of a 2S exciton. Significant deviations from the hydrogen-like Rydberg series for the nS excitonic state energies are thus expected in the intermediate coupling regime.<sup>145</sup> In this coupling regime, the e-h correlations begin to have an impact on the interaction between the charge carriers and the lattice, in the case of a 2S exciton.

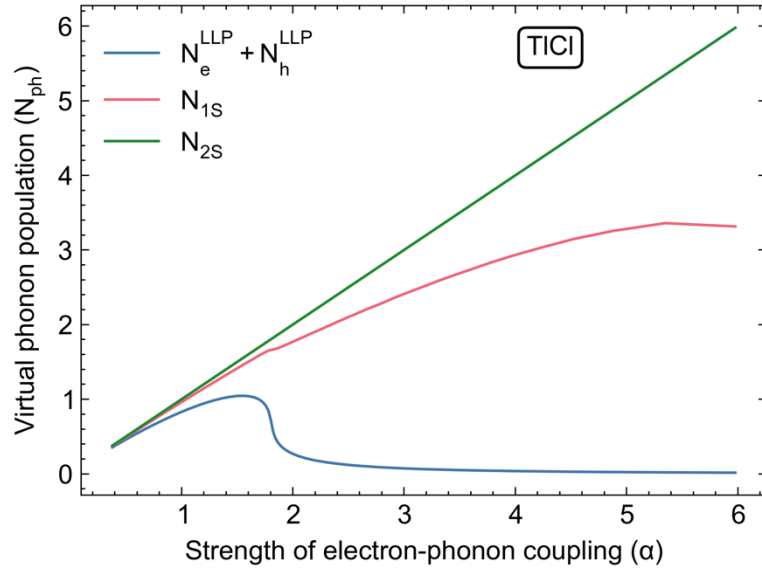


**Figure 13.** Virtual phonon populations of excitonic polarons in TlCl as a function of  $\alpha$ , for both 1S (blue line) and 2S (red line) excitons, compared to those obtained for free polarons (black line). The variation of  $\alpha$  is obtained by tuning the phonon energy. The vertical dotted line indicates the actual  $\alpha$  value relevant for TlCl (Table 1).

To further illustrate that the interplay between e-h correlated motions and the polaronic coupling depends on the extension of the exciton wavefunction, we plot for TlCl the effective dielectric constants computed for both 1S (blue) and 2S (red) excitons as a function of  $\alpha$ , keeping

the same parameters (Figure 14). As expected, both 1S and 2S effective dielectric constants tends toward  $\epsilon_\infty$  in the strong coupling limit, i.e.  $\alpha \rightarrow +\infty$ . Interestingly, within this model a plateau is predicted for  $\epsilon_{eff,2S}$  in the intermediate coupling regime. Such plateau is related to the first lobe in the radial probability density of a 2S exciton wavefunction in the range of small  $\tilde{r}$  values (Figure 4a).

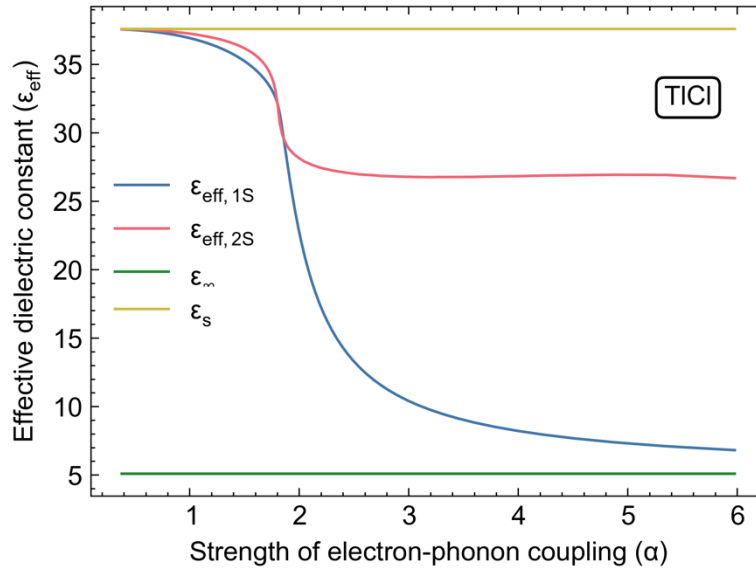


**Figure 14.** Effective dielectric constants for 1S (blue) and 2S (red) excitons as a function of  $\alpha$  for TlCl. The variation of  $\alpha$  is obtained by tuning the phonon energy. The vertical dotted line indicates the actual  $\alpha$  value relevant for TlCl (Table 1).

A physical observable, very often used to gauge the importance of the coupling between an exciton and the lattice, is the strength of the phonon side bands referred to as the Huang-Rhys factor ( $S$ ). This factor corresponds to the oscillator strength of the optical transition from the crystal ground state to an excitonic polaron plus one (real) phonon ( $1_{ph}$ ) divided by the oscillator strength of the excitonic polaron ground state related to the zero-phonon ( $0_{ph}$ ) line. The latter is usually

evaluated from a PL experiment. At the level of the PB model with one LO mode, this ratio is given by:<sup>145</sup>

$$S_{1ph} = S = \sum_{\vec{k}} \frac{|g_{\vec{k}}|^2}{(\hbar\omega_{LO})^2} \left( f_{\vec{k}}^e(\vec{0}) - f_{\vec{k}}^h(\vec{0}) \right)^2 \quad (88)$$

and the ratios for the n-phonons ( $n_{ph}$ ) side bands are given by

$$S_{n_{ph}} = (S)^n/n!. \quad (89)$$

These expressions show that the ratio is proportional to the strength of the interaction and depends on the phonon frequency. This simple expression will be generalized to multiple phonon branches within the MPB model (vide infra). It is affected by the correlations between the electron and hole through the factors  $f_{e(h),\vec{k}}(\vec{0})$ . But when the two factors are identical, i.e. for equal masses, they cancel each other. Figure 15 reports the computed Huang-Rhys factor as a function of  $\alpha$  for the 1S exciton in TlCl for different values of the relative difference between the electron and hole effective masses. Evidently, Huang-Rhys factors are very sensitive to the peculiarities of the electronic structure, and at  $\alpha > 1.5$ , they undergo the renormalization due to the onset of stronger e-h correlations at the cross-over between the weak and medium coupling regimes.

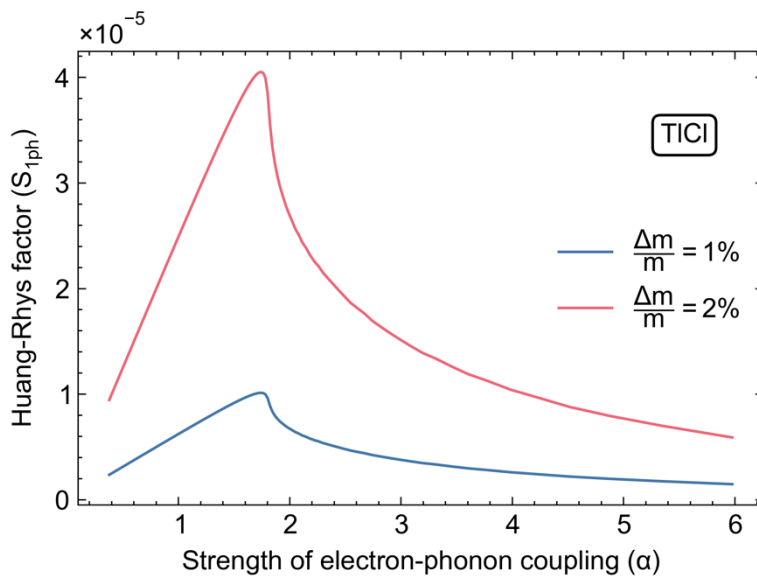


**Figure 15.** Variation of the Huang-Rhys factor ( $S_{1_{ph}}$ ) as a function of  $\alpha$  for the 1S exciton for TlCl considering few cases with different electron and hole effective masses (the relative mass ratio is given by  $\Delta m/m$ ). The variation of  $\alpha$  is obtained by tuning the phonon energy.

We further propose extending the calculation of Huang-Rhys factors to the case of multiple phonon lines within the present MPB model. We derive a sum rule (see supplementary information):

$$e^{-S}e^S = e^{-S} \sum_{n=0}^{+\infty} \frac{1}{n!} (\sum_{\nu} S_{1_{\nu}})^n = e^{-S} \left( 1 + (\sum_{\nu} S_{1_{\nu}}) + \frac{1}{2} (\sum_{\nu} S_{1_{\nu}})^2 + \dots \right) \quad (90)$$

where  $S_{1_{\nu}} = \sum_{\vec{k}} |F_{\vec{k},\nu}(\vec{0})|^2$  is the ratio of the one phonon sideband intensity for phonon branch  $\nu$  divided by the  $0_{ph}$  line and  $S = \sum_{\nu} S_{1_{\nu}}$ . The last term on the right hand side of Eq. 90 corresponds to both two-phonon side band intensities for the same phonon branch ( $\nu_1 = \nu_2$ ) and overtones involving two different phonon branches ( $\nu_1 \neq \nu_2$ ). As an example, Figure 16 represents the first-order side band absorption (red line) and second-order side bands and overtones intensity (green line) as a function of the energy for the case of MAPbI<sub>3</sub> at LT.

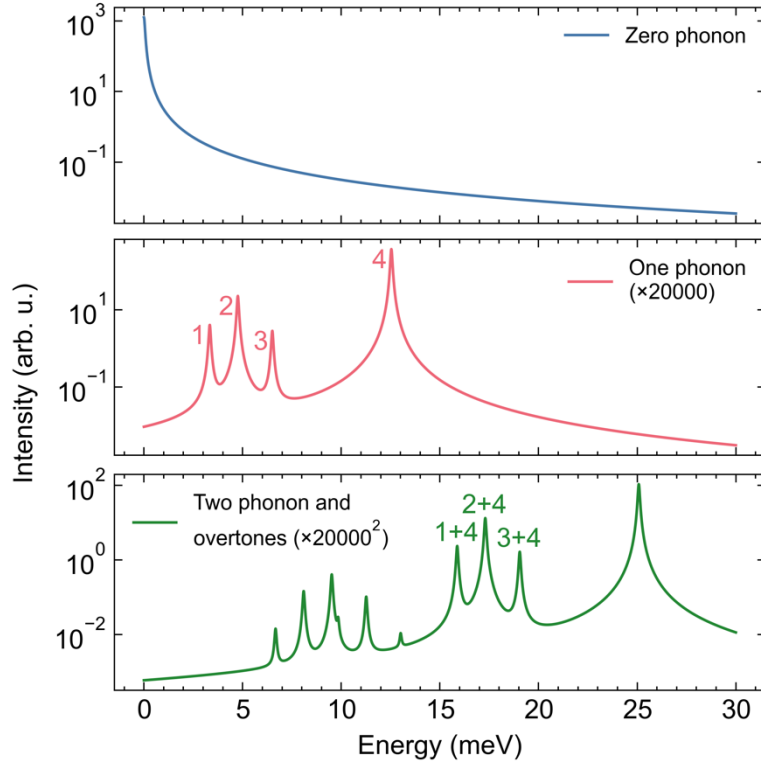


**Figure 16.** Simulation of the intensity as a function of the energy of the  $0_{ph}$  absorption (top), the first-order (middle) and second-order (bottom) side band absorptions including overtones. The experimental parameters for  $\text{MAPbI}_3$  at  $T=20\text{K}$  have been used (Figures 10,11). The theoretical expressions have been arbitrarily convoluted by Lorentzian function with a broadening of  $50\mu\text{eV}$ . The four experimental LO modes (Figures 10, 11) are indicated on the first-order side-band absorption curve. Some overtones combining the LO mode  $n^{\circ}4$  and the three other modes are indicated by 1+4, 2+4, 3+4.

### Extension of the empirical approach for excitonic polarons to quantum nanostructures

We will briefly discuss how the method of shift operators and the PB empirical framework can be transferred to analyze excitonic polarons in quantum nanostructures focusing on 2D quantum-wells and 0D quantum dot nanostructures. For 2D quantum well structures, the

continuous variation of the  $\vec{k}$  wavevector is lost along the stacking direction because of quantum confinement and must be replaced by discrete quantum numbers. This has been initially used to predict 2D excitons binding energies using effective mass model for the charge carriers and Wannier Hamiltonian for the excitons, including dielectric confinement, optical anisotropy, electronic sub-bands and envelope functions along the stacking axis.<sup>146–148</sup> Such approaches which do not explicitly account for the e-ph coupling can also be fruitfully used for 2D layered halide perovskites to study the dependence of the exciton binding energy on the quantum well thickness or deviations from the 2D Rydberg series.<sup>149</sup> Extension of the PB framework to explicitly account for excitonic polarons in 2D quantum wells was introduced by Matsuura and coworkers.<sup>76,150</sup> Based on unitary transformations related to bulk like phonons and e-ph coupling,<sup>151</sup> the methodology was developed<sup>152,76,150</sup> to include also the quantization of bulk-like optical phonons, and additional interface phonons.<sup>153</sup> In some situations where the weak-coupling regime is justified (Bohr radius larger than the sum of polaron radii), an approximate bulk-like PB model is appropriate to account for the exciton-phonon coupling at a reduced computational cost.<sup>154</sup> More generally, four characteristic lengths must be compared for a quantum well instead of three for corresponding bulk material: the exciton Bohr radius, the polaron radii and the quantum well thickness. The 2D halide perovskites are rather unusual compared to the conventional semiconductor quantum wells studied in the past: the equivalent quantum confinement thickness is extremely small and the bulk reference materials (3D halide perovskite) belong to the intermediate regime for the strength of exciton-phonon coupling. Future theoretical studies based on empirical models for excitonic polarons in 2D halide perovskites would benefit from including a complete PB-like description combined with quantized bulk-like optical phonons and interface optical phonons.

We will now describe in detail the extension of the PB framework for the case of QDs. 0D quantum confinement shall affect all the properties, including electron, hole and exciton states, as well as the undispersed bulk optical LO phonons. Surface effects related to the localization of polarization at the interface between the QD and the outer medium, potentially add dielectric confinement effects and a coupling with surface optical (SO) vibrations. For bulk-like quantities, the continuous variation of the  $\vec{k}$  wavevector is absent due to quantum confinement and must be replaced by discrete quantum numbers. A crude approximation consists in neglecting implicitly all the effects of quantum confinement except for electronic and excitonic states.<sup>155</sup> This leads to effective potentials that include the exciton-polaron coupling but as derived for bulk materials. Moreover, the effect of quantum confinement on self-energy terms and reduced mass cannot be included straightforwardly.

At the semi-empirical level the effect of quantum confinement can be included both for vibrations and e-ph couplings.<sup>156</sup> In the case of a spherical QD embedded in a non-polar medium, bulk-like phonons are replaced by localized phonons with quantum numbers  $(n, l, m)$  with  $n = 1, 2, 3, \dots \infty$ ;  $l = 0, 1, 2, \dots \infty$  ( $S, P, D, \dots$ );  $m = -l, \dots l$ . For surface phonons, the spherical symmetry corresponds to doublets  $(l, m)$  with  $l = 1, 2, \dots \infty$ ;  $m = -l, \dots l$ . For quantum confined bulk-like polar phonon, the e-ph Hamiltonian is modified and the Fröhlich expression of the matrix element (Eq. 12) transforms to

$$g_{LO,n,l} = \frac{1}{k_{n,l}} \left( \frac{e^2 \hbar \omega_{LO}}{j_{l+1}(k_{n,l}R)^2 R^3 \epsilon_0} \right)^{1/2} \left( \frac{1}{\epsilon_\infty} - \frac{1}{\epsilon_s} \right)^{1/2}. \quad (91)$$

The wavevectors  $k_{n,l}$  are now discretized according to the zeros of the spherical Bessel function ( $j_l(k_{n,l}R) = 0$ ) where R is the radius of the QD. Noteworthy, the first zeros yield the most

important contributions due to the  $\frac{1}{k_{n,l}}$  term. Effective interaction and self-energies are also affected. The PB expressions for the LO self-energies obtained for bulk (Eq. 50) can also be reshaped in a similar way for QDs:

$$\sigma_{e(h),1S,LO} = -\sum_{n,l,m} \frac{|g_{LO,n,l}|^2}{\hbar\omega_{LO}} \left( 2f_{e(h),LO,n,l,m}^{min} A_{LO,n,l,m}(k_{n,l}) - \left( A_{LO,n,l,m}(k_{n,l}) + R_{e(h)}^2 c_{LO,n,l,m}(k_{n,l}) \right) f_{e(h),LO,n,l,m}^{min} \right). \quad (92)$$

These self-energies now depend on the characteristics of the exciton (Bohr radius, ...), the polaron radii, but also the geometry (radius) of the QD. They involve more complex functions such as  $A_{LO,n,l,m}(k_{n,l})$  and  $c_{LO,n,l,m}(k_{n,l})$  in place of 1 and  $k^2$ , and build from various combinations of spherical Harmonics.<sup>77</sup>

## Conclusion

The paper reviews empirical approaches to Fröhlich polarons and excitonic polarons in polar semiconductors based on unitary transformations. These approaches are relevant for the weak and intermediate coupling regimes and can be extended from bulk 3D materials to 2D and 0D nanostructures. Several new analytical results are also provided, with detailed derivation of the most important formulae. The validity of various popular but approximate approaches for the simulation of excitonic polarons is further assessed. It is found that these approaches are mainly relevant for the weak coupling regime. Among approximate models, the ABS model and our simplified implementation (ABS<sub>app</sub>) are attractive to tackle excited states or exciton complexes. PB, PBK and Iad models appear to be the most accurate, the Iad model being slightly more precise

than the two others, but computationally much more expensive and hardly transferable to lower dimensions. Comparison with state-of-the-art first-principles developments for polarons and excitonic polarons has further been made. But the numerical tests of the implementations reported in the literature are currently made on materials belonging to the strong coupling regime. This hampers fair comparison to the various empirical approaches considered in this review. Nevertheless, the recent developments based on first principles open new perspectives for improved calibration of empirical approaches. So far, work along this line essentially relied on experimental data that are often insufficiently accurate, or in some cases, even conflicting. Combining first-principle and empirical approaches is thus promising for future developments provided those new experimental techniques such as THz spectroscopy or high-resolution diffraction have progressed rapidly. Last, the empirical approaches have further been extended in this work to include multiple phonon branches, which is demonstrated to be important in more complex materials such as the halide perovskite family of semiconductors. Numerical tests show that other developments are still needed to enable more quantitative comparisons with experimental results, with for instance methods capable of accounting for temperature effects or lattice disorder.

#### AUTHOR INFORMATION

[Jacky.even@insa-rennes.fr](mailto:Jacky.even@insa-rennes.fr), <https://cv.hal.science/jacky-even>.

[claudine.katan@univ-rennes.fr](mailto:claudine.katan@univ-rennes.fr)

#### Notes

The authors declare no competing financial interest.

#### ACKNOWLEDGMENT

J.E. acknowledges the financial support from the Institut Universitaire de France.

## REFERENCES

- (1) Devreese, J. T. Fröhlich Polarons. Lecture Course Including Detailed Theoretical Derivations -- 10th Edition. arXiv 2016. <https://doi.org/10.48550/ARXIV.1611.06122>.
- (2) Franchini, C.; Reticcioli, M.; Setvin, M.; Diebold, U. Polarons in Materials. *Nat. Rev. Mater.* **2021**, *6* (7), 560–586. <https://doi.org/10.1038/s41578-021-00289-w>.
- (3) Fröhlich, H. Theory of Electrical Breakdown in Ionic Crystals. *Proc. R. Soc. Lond. Ser. - Math. Phys. Sci.* **1937**, *160* (901), 230–241. <https://doi.org/10.1098/rspa.1937.0106>.
- (4) Fröhlich, H.; Pelzer, H.; Zienau, S. XX. Properties of Slow Electrons in Polar Materials. *Lond. Edinb. Dublin Philos. Mag. J. Sci.* **1950**, *41* (314), 221–242. <https://doi.org/10.1080/14786445008521794>.
- (5) Verdi, C.; Giustino, F. Fröhlich Electron-Phonon Vertex from First Principles. *Phys. Rev. Lett.* **2015**, *115* (17), 176401. <https://doi.org/10.1103/PhysRevLett.115.176401>.
- (6) Vasilchenko, V.; Gonze, X. Polarons in the Cubic Generalized Fröhlich Model: Spontaneous Symmetry Breaking. *Phys. Rev. B* **2024**, *109* (18), 184301. <https://doi.org/10.1103/PhysRevB.109.184301>.
- (7) Lafuente-Bartolome, J.; Lian, C.; Sio, W. H.; Gurtubay, I. G.; Eiguren, A.; Giustino, F. Unified Approach to Polarons and Phonon-Induced Band Structure Renormalization. *Phys. Rev. Lett.* **2022**, *129* (7), 076402. <https://doi.org/10.1103/PhysRevLett.129.076402>.
- (8) Lafuente-Bartolome, J.; Lian, C.; Giustino, F. Topological Polarons in Halide Perovskites. *Proc. Natl. Acad. Sci.* **2024**, *121* (21), e2318151121. <https://doi.org/10.1073/pnas.2318151121>.
- (9) Antonius, G.; Louie, S. G. Theory of Exciton-Phonon Coupling. *Phys. Rev. B* **2022**, *105* (8), 085111. <https://doi.org/10.1103/PhysRevB.105.085111>.
- (10) Adamska, L.; Umari, P. Bethe-Salpeter Equation Approach with Electron-Phonon Coupling for Exciton Binding Energies. *Phys. Rev. B* **2021**, *103* (7), 075201. <https://doi.org/10.1103/PhysRevB.103.075201>.
- (11) Dai, Z.; Lian, C.; Lafuente-Bartolome, J.; Giustino, F. Theory of Excitonic Polarons: From Models to First-Principles Calculations. *Phys. Rev. B* **2024**, *109* (4), 045202. <https://doi.org/10.1103/PhysRevB.109.045202>.
- (12) Knox, R. S. Introduction to Exciton Physics. In *Collective Excitations in Solids*; Bartolo, B., Ed.; Springer US: Boston, MA, 1983; pp 183–245. [https://doi.org/10.1007/978-1-4684-8878-4\\_5](https://doi.org/10.1007/978-1-4684-8878-4_5).
- (13) Kojima, A.; Teshima, K.; Shirai, Y.; Miyasaka, T. Organometal Halide Perovskites as Visible-Light Sensitizers for Photovoltaic Cells. *J. Am. Chem. Soc.* **2009**, *131* (17), 6050–6051. <https://doi.org/10.1021/ja809598r>.
- (14) Im, J.-H.; Lee, C.-R.; Lee, J.-W.; Park, S.-W.; Park, N.-G. 6.5% Efficient Perovskite Quantum-Dot-Sensitized Solar Cell. *Nanoscale* **2011**, *3* (10), 4088–4093. <https://doi.org/10.1039/c1nr10867k>.
- (15) Lee, M. M.; Teuscher, J.; Miyasaka, T.; Murakami, T. N.; Snaith, H. J. Efficient Hybrid Solar Cells Based on Meso-Superstructured Organometal Halide Perovskites. *Science* **2012**, *338* (6107), 643–647. <https://doi.org/10.1126/science.1228604>.

- (16) Kim, H.-S.; Lee, C.-R.; Im, J.-H.; Lee, K.-B.; Moehl, T.; Marchioro, A.; Moon, S.-J.; Humphry-Baker, R.; Yum, J.-H.; Moser, J. E.; Grätzel, M.; Park, N.-G. Lead Iodide Perovskite Sensitized All-Solid-State Submicron Thin Film Mesoscopic Solar Cell with Efficiency Exceeding 9%. *Sci. Rep.* **2012**, *2* (1), 591. <https://doi.org/10.1038/srep00591>.
- (17) Boyer-Richard, S.; Katan, C.; Traoré, B.; Scholz, R.; Jancu, J.-M.; Even, J. Symmetry-Based Tight Binding Modeling of Halide Perovskite Semiconductors. *J. Phys. Chem. Lett.* **2016**, *7* (19), 3833–3840. <https://doi.org/10.1021/acs.jpcclett.6b01749>.
- (18) Even, J.; Pedesseau, L.; Jancu, J.-M.; Katan, C. Importance of Spin–Orbit Coupling in Hybrid Organic/Inorganic Perovskites for Photovoltaic Applications. *J. Phys. Chem. Lett.* **2013**, *4* (17), 2999–3005. <https://doi.org/10.1021/jz401532q>.
- (19) Even, J.; Pedesseau, L.; Katan, C. Analysis of Multivalley and Multibandgap Absorption and Enhancement of Free Carriers Related to Exciton Screening in Hybrid Perovskites. *J. Phys. Chem. C* **2014**, *118* (22), 11566–11572. <https://doi.org/10.1021/jp503337a>.
- (20) Even, J. Pedestrian Guide to Symmetry Properties of the Reference Cubic Structure of 3D All-Inorganic and Hybrid Perovskites. *J. Phys. Chem. Lett.* **2015**, *6* (12), 2238–2242. <https://doi.org/10.1021/acs.jpcclett.5b00905>.
- (21) Even, J.; Pedesseau, L.; Saponi, D.; Rolland, A.; Kepenekian, M.; Katan, C. Electronic Properties of Metal Halide Perovskites. In *Unconventional Thin Film Photovoltaics*; Da Como, E., De Angelis, F., Snaith, H., Walker, A., Eds.; The Royal Society of Chemistry, 2016; pp 202–233. <https://doi.org/10.1039/9781782624066-00202>.
- (22) Even, J.; Katan, C. Ab Initio and First Principles Studies of Halide Perovskites. In *Halide Perovskites*; Sum, T., Mathews, N., Eds.; Wiley, 2018; pp 25–53. [https://doi.org/10.1002/9783527800766.ch1\\_02](https://doi.org/10.1002/9783527800766.ch1_02).
- (23) Nie, W.; Blancon, J.-C.; Neukirch, A. J.; Appavoo, K.; Tsai, H.; Chhowalla, M.; Alam, M. A.; Sfeir, M. Y.; Katan, C.; Even, J.; Tretiak, S.; Crochet, J. J.; Gupta, G.; Mohite, A. D. Light-Activated Photocurrent Degradation and Self-Healing in Perovskite Solar Cells. *Nat. Commun.* **2016**, *7*, 11574. <https://doi.org/10.1038/ncomms11574>.
- (24) Brivio, F.; Butler, K. T.; Walsh, A.; van Schilfhaarde, M. Relativistic Quasiparticle Self-Consistent Electronic Structure of Hybrid Halide Perovskite Photovoltaic Absorbers. *Phys. Rev. B* **2014**, *89* (15), 155204. <https://doi.org/10.1103/PhysRevB.89.155204>.
- (25) Giorgi, G.; Yamashita, K. Organic–Inorganic Halide Perovskites: An Ambipolar Class of Materials with Enhanced Photovoltaic Performances. *J. Mater. Chem. A* **2015**, *3* (17), 8981–8991. <https://doi.org/10.1039/C4TA05046K>.
- (26) Umari, P.; Mosconi, E.; De Angelis, F. Relativistic GW Calculations on CH<sub>3</sub>NH<sub>3</sub>PbI<sub>3</sub> and CH<sub>3</sub>NH<sub>3</sub>SnI<sub>3</sub> Perovskites for Solar Cell Applications. *Sci. Rep.* **2014**, *4* (1), 4467. <https://doi.org/10.1038/srep04467>.
- (27) Filip, M. R.; Verdi, C.; Giustino, F. GW Band Structures and Carrier Effective Masses of CH<sub>3</sub>NH<sub>3</sub>PbI<sub>3</sub> and Hypothetical Perovskites of the Type APbI<sub>3</sub>: A = NH<sub>4</sub>, PH<sub>4</sub>, AsH<sub>4</sub>, and SbH<sub>4</sub>. *J. Phys. Chem. C* **2015**, *119* (45), 25209–25219. <https://doi.org/10.1021/acs.jpcc.5b07891>.
- (28) Miyata, A.; Mitioglu, A.; Plochocka, P.; Portugall, O.; Wang, J. T.-W.; Stranks, S. D.; Snaith, H. J.; Nicholas, R. J. Direct Measurement of the Exciton Binding Energy and Effective Masses for Charge Carriers in Organic–Inorganic Tri-Halide Perovskites. *Nat. Phys.* **2015**, *11* (7), 582–587. <https://doi.org/10.1038/nphys3357>.
- (29) Galkowski, K.; Mitioglu, A.; Miyata, A.; Plochocka, P.; Portugall, O.; Eperon, G. E.; Wang, J. T.-W.; Stergiopoulos, T.; Stranks, S. D.; Snaith, H. J.; Nicholas, R. J. Determination

- of the Exciton Binding Energy and Effective Masses for Methylammonium and Formamidinium Lead Tri-Halide Perovskite Semiconductors. *Energy Environ. Sci.* **2016**, *9* (3), 962–970. <https://doi.org/10.1039/C5EE03435C>.
- (30) Yang, Z.; Surrante, A.; Galkowski, K.; Miyata, A.; Portugall, O.; Sutton, R. J.; Haghighirad, A. A.; Snaith, H. J.; Maude, D. K.; Plochocka, P.; Nicholas, R. J. Impact of the Halide Cage on the Electronic Properties of Fully Inorganic Cesium Lead Halide Perovskites. *ACS Energy Lett.* **2017**, *2* (7), 1621–1627. <https://doi.org/10.1021/acsenergylett.7b00416>.
- (31) Miyata, A.; Mitioglu, A.; Plochocka, P.; Portugall, O.; Wang, J. T.-W.; Stranks, S. D.; Snaith, H. J.; Nicholas, R. J. Direct Measurement of the Exciton Binding Energy and Effective Masses for Charge Carriers in Organic–Inorganic Tri-Halide Perovskites. *Nat. Phys.* **2015**, *11* (7), 582–587. <https://doi.org/10.1038/nphys3357>.
- (32) Fu, J.; Ramesh, S.; Melvin Lim, J. W.; Sum, T. C. Carriers, Quasi-Particles, and Collective Excitations in Halide Perovskites. *Chem. Rev.* **2023**, *123* (13), 8154–8231. <https://doi.org/10.1021/acs.chemrev.2c00843>.
- (33) Kovalenko, M. V.; Protesescu, L.; Bodnarchuk, M. I. Properties and Potential Optoelectronic Applications of Lead Halide Perovskite Nanocrystals. *Science* **2017**, *358* (6364), 745–750. <https://doi.org/10.1126/science.aam7093>.
- (34) Fu, M.; Tamarat, P.; Huang, H.; Even, J.; Rogach, A. L.; Lounis, B. Neutral and Charged Exciton Fine Structure in Single Lead Halide Perovskite Nanocrystals Revealed by Magneto-Optical Spectroscopy. *Nano Lett.* **2017**, *17* (5), 2895–2901. <https://doi.org/10.1021/acs.nanolett.7b00064>.
- (35) Becker, M. A.; Vaxenburg, R.; Nedelcu, G.; Sercel, P. C.; Shabaev, A.; Mehl, M. J.; Michopoulos, J. G.; Lambrakos, S. G.; Bernstein, N.; Lyons, J. L.; Stöferle, T.; Mahrt, R. F.; Kovalenko, M. V.; Norris, D. J.; Rainò, G.; Efros, A. L. Bright Triplet Excitons in Caesium Lead Halide Perovskites. *Nature* **2018**, *553* (7687), 189–193. <https://doi.org/10.1038/nature25147>.
- (36) Sercel, P. C.; Lyons, J. L.; Wickramaratne, D.; Vaxenburg, R.; Bernstein, N.; Efros, A. L. Exciton Fine Structure in Perovskite Nanocrystals. *Nano Lett.* **2019**, *19* (6), 4068–4077. <https://doi.org/10.1021/acs.nanolett.9b01467>.
- (37) Tamarat, P.; Bodnarchuk, M. I.; Trebbia, J.-B.; Erni, R.; Kovalenko, M. V.; Even, J.; Lounis, B. The Ground Exciton State of Formamidinium Lead Bromide Perovskite Nanocrystals Is a Singlet Dark State. *Nat. Mater.* **2019**, *18* (7), 717–724. <https://doi.org/10.1038/s41563-019-0364-x>.
- (38) Tamarat, P.; Hou, L.; Trebbia, J.-B.; Swarnkar, A.; Biadala, L.; Louyer, Y.; Bodnarchuk, M. I.; Kovalenko, M. V.; Even, J.; Lounis, B. The Dark Exciton Ground State Promotes Photon-Pair Emission in Individual Perovskite Nanocrystals. *Nat. Commun.* **2020**, *11* (1), 6001. <https://doi.org/10.1038/s41467-020-19740-7>.
- (39) Tamarat, P.; Prin, E.; Berezovska, Y.; Moskalenko, A.; Nguyen, T. P. T.; Xia, C.; Hou, L.; Trebbia, J.-B.; Zacharias, M.; Pedesseau, L.; Katan, C.; Bodnarchuk, M. I.; Kovalenko, M. V.; Even, J.; Lounis, B. Universal Scaling Laws for Charge-Carrier Interactions with Quantum Confinement in Lead-Halide Perovskites. *Nat. Commun.* **2023**, *14* (1), 229. <https://doi.org/10.1038/s41467-023-35842-4>.
- (40) Yu, P. Y.; Cardona, M. *Fundamentals of Semiconductors: Physics and Materials Properties*; Graduate Texts in Physics; Springer Berlin Heidelberg: Berlin, Heidelberg, 2010. <https://doi.org/10.1007/978-3-642-00710-1>.

- (41) Zhao, X.-G.; Dalpian, G. M.; Wang, Z.; Zunger, A. Polymorphous Nature of Cubic Halide Perovskites. *Phys. Rev. B* **2020**, *101* (15), 155137. <https://doi.org/10.1103/PhysRevB.101.155137>.
- (42) Zacharias, M.; Volonakis, G.; Giustino, F.; Even, J. Anharmonic Electron-Phonon Coupling in Ultrasoft and Locally Disordered Perovskites. *Npj Comput. Mater.* **2023**, *9* (1), 153. <https://doi.org/10.1038/s41524-023-01089-2>.
- (43) Yaffe, O.; Guo, Y.; Tan, L. Z.; Egger, D. A.; Hull, T.; Stoumpos, C. C.; Zheng, F.; Heinz, T. F.; Kronik, L.; Kanatzidis, M. G.; Owen, J. S.; Rappe, A. M.; Pimenta, M. A.; Brus, L. E. Local Polar Fluctuations in Lead Halide Perovskite Crystals. *Phys. Rev. Lett.* **2017**, *118* (13). <https://doi.org/10.1103/PhysRevLett.118.136001>.
- (44) Ferreira, A. C.; Paofai, S.; Létoublon, A.; Ollivier, J.; Raymond, S.; Hehlen, B.; Rufflé, B.; Cordier, S.; Katan, C.; Even, J.; Bourges, P. Direct Evidence of Weakly Dispersed and Strongly Anharmonic Optical Phonons in Hybrid Perovskites. *Commun. Phys.* **2020**, *3* (1), 48. <https://doi.org/10.1038/s42005-020-0313-7>.
- (45) Lanigan-Atkins, T.; He, X.; Krogstad, M. J.; Pajeroski, D. M.; Abernathy, D. L.; Xu, G. N. M. N.; Xu, Z.; Chung, D.-Y.; Kanatzidis, M. G.; Rosenkranz, S.; Osborn, R.; Delaire, O. Two-Dimensional Overdamped Fluctuations of the Soft Perovskite Lattice in CsPbBr<sub>3</sub>. *Nat. Mater.* **2021**, *20* (7), 977–983. <https://doi.org/10.1038/s41563-021-00947-y>.
- (46) Hehlen, B.; Bourges, P.; Rufflé, B.; Clément, S.; Vialla, R.; Ferreira, A. C.; Ecolivet, C.; Paofai, S.; Cordier, S.; Katan, C.; Létoublon, A.; Even, J. Pseudospin-Phonon Pretransitional Dynamics in Lead Halide Hybrid Perovskites. *Phys. Rev. B* **2022**, *105* (2), 024306. <https://doi.org/10.1103/PhysRevB.105.024306>.
- (47) Giustino, F. Electron-Phonon Interactions from First Principles. *Rev. Mod. Phys.* **2017**, *89* (1). <https://doi.org/10.1103/RevModPhys.89.015003>.
- (48) Iaru, C. M.; Brodu, A.; Van Hoof, N. J. J.; Ter Huurne, S. E. T.; Buhot, J.; Montanarella, F.; Buhbut, S.; Christianen, P. C. M.; Vanmaekelbergh, D.; De Mello Donega, C.; Rivas, J. G.; Koenraad, P. M.; Silov, A. Yu. Fröhlich Interaction Dominated by a Single Phonon Mode in CsPbBr<sub>3</sub>. *Nat. Commun.* **2021**, *12* (1), 5844. <https://doi.org/10.1038/s41467-021-26192-0>.
- (49) *Polarons in Ionic Crystals and Polar Semiconductors*; Devreese, J. T., Ed.; North-Holland Pub. Co [u.a.]: Amsterdam, 1972.
- (50) Miyata, K.; Meggiolaro, D.; Trinh, M. T.; Joshi, P. P.; Mosconi, E.; Jones, S. C.; De Angelis, F.; Zhu, X.-Y. Large Polarons in Lead Halide Perovskites. *Sci. Adv.* **2017**, *3* (8), e1701217. <https://doi.org/10.1126/sciadv.1701217>.
- (51) Neukirch, A. J.; Nie, W.; Blancon, J.-C.; Appavoo, K.; Tsai, H.; Sfeir, M. Y.; Katan, C.; Pedesseau, L.; Even, J.; Crochet, J. J.; Gupta, G.; Mohite, A. D.; Tretiak, S. Polaron Stabilization by Cooperative Lattice Distortion and Cation Rotations in Hybrid Perovskite Materials. *Nano Lett.* **2016**, *16* (6), 3809–3816. <https://doi.org/10.1021/acs.nanolett.6b01218>.
- (52) Ghosh, D.; Welch, E.; Neukirch, A. J.; Zakhidov, A.; Tretiak, S. Polarons in Halide Perovskites: A Perspective. *J. Phys. Chem. Lett.* **2020**, *11* (9), 3271–3286. <https://doi.org/10.1021/acs.jpcclett.0c00018>.
- (53) Yamada, Y.; Kanemitsu, Y. Electron-Phonon Interactions in Halide Perovskites. *NPG Asia Mater.* **2022**, *14* (1), 48. <https://doi.org/10.1038/s41427-022-00394-4>.
- (54) Zhang, H.; Park, N.-G. Polarons in Perovskite Solar Cells: Effects on Photovoltaic Performance and Stability. *J. Phys. Energy* **2023**, *5* (2), 024002. <https://doi.org/10.1088/2515-7655/acb96d>.

- (55) Guzelturk, B.; Winkler, T.; Van De Goor, T. W. J.; Smith, M. D.; Bourelle, S. A.; Feldmann, S.; Trigo, M.; Teitelbaum, S. W.; Steinrück, H.-G.; De La Pena, G. A.; Alonso-Mori, R.; Zhu, D.; Sato, T.; Karunadasa, H. I.; Toney, M. F.; Deschler, F.; Lindenberg, A. M. Visualization of Dynamic Polaronic Strain Fields in Hybrid Lead Halide Perovskites. *Nat. Mater.* **2021**, *20* (5), 618–623. <https://doi.org/10.1038/s41563-020-00865-5>.
- (56) Menéndez-Proupin, E.; Beltrán Ríos, C. L.; Wahnón, P. Nonhydrogenic Exciton Spectrum in Perovskite  $\text{CH}_3\text{NH}_3\text{PbI}_3$ . *Phys. Status Solidi RRL – Rapid Res. Lett.* **2015**, *9* (10), 559–563. <https://doi.org/10.1002/pssr.201510265>.
- (57) Toyozawa, Y.; Hermanson, J. Exciton-Phonon Bound State: A New Quasiparticle. *Phys. Rev. Lett.* **1968**, *21* (24), 1637–1641. <https://doi.org/10.1103/PhysRevLett.21.1637>.
- (58) Hermanson, J. C. Exciton-Phonon Bound State and the Vibronic Spectra of Solids. *Phys. Rev. B* **1970**, *2* (12), 5043–5051. <https://doi.org/10.1103/PhysRevB.2.5043>.
- (59) Pollmann, J.; Büttner, H. Upper Bounds for the Ground-State Energy of the Exciton-Phonon System. *Solid State Commun.* **1975**, *17* (9), 1171–1174. [https://doi.org/10.1016/0038-1098\(75\)90279-3](https://doi.org/10.1016/0038-1098(75)90279-3).
- (60) Pollmann, J.; Büttner, H. Effective Hamiltonians and Bindings Energies of Wannier Excitons in Polar Semiconductors. *Phys. Rev. B* **1977**, *16* (10), 4480–4490. <https://doi.org/10.1103/PhysRevB.16.4480>.
- (61) Kane, E. O. Pollmann-Büttner Variational Method for Excitonic Polarons. *Phys. Rev. B* **1978**, *18* (12), 6849–6855. <https://doi.org/10.1103/PhysRevB.18.6849>.
- (62) Lee, T.-D.; Pines, D. The Motion of Slow Electrons in Polar Crystals. *Phys. Rev.* **1952**, *88* (4), 960–961. <https://doi.org/10.1103/PhysRev.88.960>.
- (63) Lee, T. D.; Low, F. E.; Pines, D. The Motion of Slow Electrons in a Polar Crystal. *Phys. Rev.* **1953**, *90* (2), 297–302. <https://doi.org/10.1103/PhysRev.90.297>.
- (64) Haga, E. Self-Energy of Slow Polaron and Variational Method. *Prog. Theor. Phys.* **1955**, *13* (5), 555–557. <https://doi.org/10.1143/PTP.13.555>.
- (65) Aldrich, C.; Bajaj, K. K. Binding Energy of a Mott-Wannier Exciton in a Polarizable Medium. *Solid State Commun.* **1977**, *22* (2), 157–160. [https://doi.org/10.1016/0038-1098\(77\)90423-9](https://doi.org/10.1016/0038-1098(77)90423-9).
- (66) Feynman, R. P. Slow Electrons in a Polar Crystal. *Phys. Rev.* **1955**, *97* (3), 660–665. <https://doi.org/10.1103/PhysRev.97.660>.
- (67) Adamowski, J.; Gerlach, B.; Leschke, H. Treatment of the Exciton-Phonon Interaction via Functional Integration. I. Harmonic Trial Actions. *Phys. Rev. B* **1981**, *23* (6), 2943–2950. <https://doi.org/10.1103/PhysRevB.23.2943>.
- (68) Park, Y.; Limmer, D. T. Renormalization of Excitonic Properties by Polar Phonons. *J. Chem. Phys.* **2022**, *157* (10), 104116. <https://doi.org/10.1063/5.0100738>.
- (69) Alvertis, A. M.; Haber, J. B.; Li, Z.; Coveney, C. J. N.; Louie, S. G.; Filip, M. R.; Neaton, J. B. Phonon Screening and Dissociation of Excitons at Finite Temperatures from First Principles. **2023**. <https://doi.org/10.48550/ARXIV.2312.03841>.
- (70) Jin, Y.; Rusishvili, M.; Govoni, M.; Galli, G. Self-Trapped Excitons in Metal-Halide Perovskites Investigated by Time-Dependent Density Functional Theory. *J. Phys. Chem. Lett.* **2024**, *15* (12), 3229–3237. <https://doi.org/10.1021/acs.jpcclett.4c00209>.
- (71) Bai, Y.; Wang, Y.; Meng, S. *Ab Initio* Self-Trapped Excitons. *Phys. Rev. Lett.* **2024**, *133* (4), 046903. <https://doi.org/10.1103/PhysRevLett.133.046903>.

- (72) Dai, Z.; Lian, C.; Lafuente-Bartolome, J.; Giustino, F. Excitonic Polarons and Self-Trapped Excitons from First-Principles Exciton-Phonon Couplings. *Phys. Rev. Lett.* **2024**, *132* (3), 036902. <https://doi.org/10.1103/PhysRevLett.132.036902>.
- (73) Sio, W. H.; Verdi, C.; Poncé, S.; Giustino, F. *Ab Initio* Theory of Polarons: Formalism and Applications. *Phys. Rev. B* **2019**, *99* (23), 235139. <https://doi.org/10.1103/PhysRevB.99.235139>.
- (74) Bassani, F.; Geddo, M.; Iadonisi, G.; Ninno, D. Variational Calculations of Bipolaron Binding Energies. *Phys. Rev. B* **1991**, *43* (7), 5296–5306. <https://doi.org/10.1103/PhysRevB.43.5296>.
- (75) Mokross, F.; Büttner, H. The Exciton-neutral Donor and Biexciton Complexes in Polar Semiconductors. *Phys. Status Solidi B* **1979**, *94* (1), 107–114. <https://doi.org/10.1002/pssb.2220940111>.
- (76) Zheng, R.; Matsuura, M. Polaronic Effects on Excitons in Quantum Wells. *Phys. Rev. B* **1998**, *57* (3), 1749–1761. <https://doi.org/10.1103/PhysRevB.57.1749>.
- (77) Oshiro, K.; Akai, K.; Matsuura, M. Size Dependence of Polaronic Effects on an Exciton in a Spherical Quantum Dot. *Phys. Rev. B* **1999**, *59* (16), 10850–10855. <https://doi.org/10.1103/PhysRevB.59.10850>.
- (78) Beril, S. I.; Pokatilov, E. P.; Kalinovski, V. V. Coulomb Interaction and Polaronic Exciton States in Compositional Superlattices. *Phys. Status Solidi B* **1992**, *169* (2), 387–403. <https://doi.org/10.1002/pssb.2221690213>.
- (79) Licari, J. J.; Evrard, R. Electron-Phonon Interaction in a Dielectric Slab: Effect of the Electronic Polarizability. *Phys. Rev. B* **1977**, *15* (4), 2254–2264. <https://doi.org/10.1103/PhysRevB.15.2254>.
- (80) Baranowski, M.; Plochocka, P.; Su, R.; Legrand, L.; Barisien, T.; Bernardot, F.; Xiong, Q.; Testelin, C.; Chamarro, M. Exciton Binding Energy and Effective Mass of CsPbCl<sub>3</sub>: A Magneto-Optical Study. *Photonics Res.* **2020**, *8* (10), A50. <https://doi.org/10.1364/PRJ.401872>.
- (81) Sendner, M.; Nayak, P. K.; Egger, D. A.; Beck, S.; Müller, C.; Epding, B.; Kowalsky, W.; Kronik, L.; Snaith, H. J.; Pucci, A.; Lovrinčić, R. Optical Phonons in Methylammonium Lead Halide Perovskites and Implications for Charge Transport. *Mater. Horiz.* **2016**, *3* (6), 613–620. <https://doi.org/10.1039/C6MH00275G>.
- (82) Wakamura, K.; Noda, Y. Enhanced Interionic Forces above T<sub>c</sub> in ABX<sub>3</sub>-Type Superionic Conductors. *J. Phys. Chem. Solids* **2001**, *62* (11), 2027–2034. [https://doi.org/10.1016/S0022-3697\(01\)00046-4](https://doi.org/10.1016/S0022-3697(01)00046-4).
- (83) Cochran, W.; Cowley, R. A. Dielectric Constants and Lattice Vibrations. *J. Phys. Chem. Solids* **1962**, *23* (5), 447–450. [https://doi.org/10.1016/0022-3697\(62\)90084-7](https://doi.org/10.1016/0022-3697(62)90084-7).
- (84) Lyddane, R. H.; Sachs, R. G.; Teller, E. On the Polar Vibrations of Alkali Halides. *Phys. Rev.* **1941**, *59* (8), 673–676. <https://doi.org/10.1103/PhysRev.59.673>.
- (85) Yu, Z.-G. Rashba Effect and Carrier Mobility in Hybrid Organic–Inorganic Perovskites. *J. Phys. Chem. Lett.* **2016**, *7* (16), 3078–3083. <https://doi.org/10.1021/acs.jpcclett.6b01404>.
- (86) Wannier, G. H. The Structure of Electronic Excitation Levels in Insulating Crystals. *Phys. Rev.* **1937**, *52* (3), 191–197. <https://doi.org/10.1103/PhysRev.52.191>.
- (87) Dresselhaus, G. Effective Mass Approximation for Excitons. *J. Phys. Chem. Solids* **1956**, *1* (1–2), 14–22. [https://doi.org/10.1016/0022-3697\(56\)90004-X](https://doi.org/10.1016/0022-3697(56)90004-X).
- (88) Emin, D. Barrier to Recombination of Oppositely Charged Large Polarons. *J. Appl. Phys.* **2018**, *123* (5), 055105. <https://doi.org/10.1063/1.5019834>.

- (89) Baranowski, M.; Nowok, A.; Galkowski, K.; Dyksik, M.; Surrente, A.; Maude, D.; Zacharias, M.; Volonakis, G.; Stranks, S. D.; Even, J.; Maczka, M.; Nicholas, R.; Plochocka, P. Polaronic Mass Enhancement and Polaronic Excitons in Metal Halide Perovskites. *ACS Energy Lett.* **2024**, *9* (6), 2696–2702. <https://doi.org/10.1021/acsenergylett.4c00905>.
- (90) Devreese, J. T. Fröhlich Polarons. Lecture Course Including Detailed Theoretical Derivations. **2010**. <https://doi.org/10.48550/ARXIV.1012.4576>.
- (91) Sio, W. H.; Giustino, F. Unified *Ab Initio* Description of Fröhlich Electron-Phonon Interactions in Two-Dimensional and Three-Dimensional Materials. *Phys. Rev. B* **2022**, *105* (11), 115414. <https://doi.org/10.1103/PhysRevB.105.115414>.
- (92) Poglitsch, A.; Weber, D. Dynamic Disorder in Methylammoniumtrihalogenoplumbates (II) Observed by Millimeter-Wave Spectroscopy. *J. Chem. Phys.* **1987**, *87* (11), 6373. <https://doi.org/10.1063/1.453467>.
- (93) Onoda-Yamamuro, N.; Matsuo, T.; Suga, H. Dielectric Study of CH<sub>3</sub>NH<sub>3</sub>PbX<sub>3</sub> (X = Cl, Br, I). *J. Phys. Chem. Solids* **1992**, *53* (7), 935–939. [https://doi.org/10.1016/0022-3697\(92\)90121-S](https://doi.org/10.1016/0022-3697(92)90121-S).
- (94) Zacharias, M.; Volonakis, G.; Giustino, F.; Even, J. Anharmonic Lattice Dynamics via the Special Displacement Method. *Phys. Rev. B* **2023**, *108* (3), 035155. <https://doi.org/10.1103/PhysRevB.108.035155>.
- (95) Landau, L. D.; Pekar, S. I. Effective Mass of a Polaron. *Zhurnal Eksp. Teroreticheskoi Fiz.* **1948**, *18* (5), 419–423.
- (96) Devreese, J.; Evrard, R. Validity of Lee, Low and Pines Method in the Case of the Interaction of an Electron with a Single Lattice Oscillator. *Phys. Status Solidi B* **1963**, *3* (11), 2133–2142. <https://doi.org/10.1002/pssb.19630031118>.
- (97) Huybrechts, W. J. Internal Excited State of the Optical Polaron. *J. Phys. C Solid State Phys.* **1977**, *10* (19), 3761–3768. <https://doi.org/10.1088/0022-3719/10/19/012>.
- (98) Tokuda, N. A Variational Approach to the Polaron Problem. *J. Phys. C Solid State Phys.* **1980**, *13* (30), L851–L855. <https://doi.org/10.1088/0022-3719/13/30/006>.
- (99) Filippis, G. D.; Cataudella, V.; Marigliano Ramaglia, V.; Perroni, C. A.; Bercioux, D. Ground State Features of the Fröhlich Model. *Eur. Phys. J. B - Condens. Matter* **2003**, *36* (1), 65–73. <https://doi.org/10.1140/epjb/e2003-00317-x>.
- (100) Rapp, M.; Wagner, M. On the Contrast between the Lee–Low–Pines and the Generalized Fulton–Gouterman Transformation. *J. Chem. Phys.* **2000**, *113* (14), 5675–5685. <https://doi.org/10.1063/1.1290034>.
- (101) Burovski, E.; Fehske, H.; Mishchenko, A. S. Exact Treatment of Exciton-Polaron Formation by Diagrammatic Monte Carlo Simulations. *Phys. Rev. Lett.* **2008**, *101* (11), 116403. <https://doi.org/10.1103/PhysRevLett.101.116403>.
- (102) Fulton, R. L.; Gouterman, M. Vibronic Coupling. I. Mathematical Treatment for Two Electronic States. *J. Chem. Phys.* **1961**, *35* (3), 1059–1071. <https://doi.org/10.1063/1.1701181>.
- (103) Meyer, H. J. G. Interaction of Excitons with Lattice Vibrations in Polar Crystals I. *Physica* **1956**, *22* (1–5), 109–120. [https://doi.org/10.1016/S0031-8914\(56\)80015-3](https://doi.org/10.1016/S0031-8914(56)80015-3).
- (104) Haken, H. Zur Quantentheorie des Mehrelektronensystems im schwingenden Gitter. I. *Z. Für Phys.* **1956**, *146* (5), 527–554. <https://doi.org/10.1007/BF01333179>.
- (105) Haken, H. *Quantum Field Theory of Solids: An Introd.*; North-Holland Publ. Co: Amsterdam, 1978.
- (106) Iadonisi, G.; Bassani, F. Excitonic Polaron States and Optical Transitions. *Il Nuovo Cimento D* **1983**, *2* (5), 1541–1560. <https://doi.org/10.1007/BF02460231>.

- (107) Wang, S.; Matsuura, M. Wannier Exciton in a Polarizable Field. *Phys. Rev. B* **1974**, *10* (8), 3330–3337. <https://doi.org/10.1103/PhysRevB.10.3330>.
- (108) Iadonisi, G.; Bassani, F.; Strinati, G. Polaronic Effects on Exciton States with Different Angular Momenta. *Phys. Status Solidi B* **1989**, *153* (2), 611–622. <https://doi.org/10.1002/pssb.2221530219>.
- (109) Strinati, G. On the Excitonic-Polaron Theory in Angular Variables. *J. Math. Phys.* **1987**, *28* (4), 981–985. <https://doi.org/10.1063/1.527591>.
- (110) Behnke, G.; Büttner, H. The Exciton Dispersion in Polar Semiconductors. *Phys. Status Solidi B* **1978**, *90* (1), 53–59. <https://doi.org/10.1002/pssb.2220900105>.
- (111) Iadonisi, G.; Bassani, F. Polaronic Correction to the Exciton Effective Mass. *Il Nuovo Cimento D* **1987**, *9* (6), 703–714. <https://doi.org/10.1007/BF02457030>.
- (112) Bednarek, S.; Adamowski, J.; Suffczyński, M. Effective Hamiltonian for Few-Particle Systems in Polar Semiconductors. *Solid State Commun.* **1977**, *21* (1), 1–3. [https://doi.org/10.1016/0038-1098\(77\)91465-X](https://doi.org/10.1016/0038-1098(77)91465-X).
- (113) Bajaj, K. K. Effect of Electron-Phonon Interaction on the Binding Energy of a Wannier Exciton in a Polarizable Medium. *Solid State Commun.* **1974**, *15* (7), 1221–1224. [https://doi.org/10.1016/0038-1098\(74\)90055-6](https://doi.org/10.1016/0038-1098(74)90055-6).
- (114) Adamowski, J.; Bednarek, S.; Suffczyński, M. The Influence of the Lattice Polarization on the Biexciton Binding Energy. *Solid State Commun.* **1976**, *20* (8), 785–787. [https://doi.org/10.1016/0038-1098\(76\)90295-7](https://doi.org/10.1016/0038-1098(76)90295-7).
- (115) Adamowski, J.; Bednarek, S.; Suffczyński, M. Variational Wave Functions for the Biexciton in Polar Semiconductors. *Solid State Commun.* **1978**, *25* (2), 89–92. [https://doi.org/10.1016/0038-1098\(78\)90364-2](https://doi.org/10.1016/0038-1098(78)90364-2).
- (116) Christiansen, D.; Selig, M.; Malic, E.; Ernstorfer, R.; Knorr, A. Theory of Exciton Dynamics in Time-Resolved ARPES: Intra- and Intervalley Scattering in Two-Dimensional Semiconductors. *Phys. Rev. B* **2019**, *100* (20), 205401. <https://doi.org/10.1103/PhysRevB.100.205401>.
- (117) Chen, H.-Y.; Sangalli, D.; Bernardi, M. Exciton-Phonon Interaction and Relaxation Times from First Principles. *Phys. Rev. Lett.* **2020**, *125* (10), 107401. <https://doi.org/10.1103/PhysRevLett.125.107401>.
- (118) Sio, W. H.; Verdi, C.; Poncé, S.; Giustino, F. Polarons from First Principles, without Supercells. *Phys. Rev. Lett.* **2019**, *122* (24). <https://doi.org/10.1103/physrevlett.122.246403>.
- (119) Cudazzo, P.; Sponza, L.; Giorgetti, C.; Reining, L.; Sottile, F.; Gatti, M. Exciton Band Structure in Two-Dimensional Materials. *Phys. Rev. Lett.* **2016**, *116* (6), 066803. <https://doi.org/10.1103/PhysRevLett.116.066803>.
- (120) Britt, T. L.; Caruso, F.; Siwick, B. J. A Momentum-Resolved View of Polaron Formation in Materials. *Npj Comput. Mater.* **2024**, *10* (1). <https://doi.org/10.1038/s41524-024-01347-x>.
- (121) Fu, M.; Tamarat, P.; Trebbia, J.-B.; Bodnarchuk, M. I.; Kovalenko, M. V.; Even, J.; Lounis, B. Unraveling Exciton–Phonon Coupling in Individual FAPbI<sub>3</sub> Nanocrystals Emitting near-Infrared Single Photons. *Nat. Commun.* **2018**, *9* (1), 3318. <https://doi.org/10.1038/s41467-018-05876-0>.
- (122) Verbist, G.; Peeters, F. M.; Devreese, J. T. Extended Stability Region for Large Bipolarons through Interaction with Multiple Phonon Branches. *Ferroelectrics* **1992**, *130* (1), 27–34. <https://doi.org/10.1080/00150199208019532>.
- (123) Hellwarth, R. W.; Biaggio, I. Mobility of an Electron in a Multimode Polar Lattice. *Phys. Rev. B* **1999**, *60* (1), 299–307. <https://doi.org/10.1103/PhysRevB.60.299>.

- (124) Železný, V.; Kadlec, C.; Kamba, S.; Repčák, D.; Kundu, S.; Saidaminov, M. I. Infrared and Terahertz Studies of Phase Transitions in the  $\text{CH}_3\text{NH}_3\text{PbBr}_3$  Perovskite. *Phys. Rev. B* **2023**, *107* (17), 174113. <https://doi.org/10.1103/PhysRevB.107.174113>.
- (125) Gervais, F.; Piriou, B. Anharmonicity in Several-Polar-Mode Crystals: Adjusting Phonon Self-Energy of LO and TO Modes in  $\text{Al}_2\text{O}_3$  and  $\text{TiO}_2$  to Fit Infrared Reflectivity. *J. Phys. C Solid State Phys.* **1974**, *7* (13), 2374–2386. <https://doi.org/10.1088/0022-3719/7/13/017>.
- (126) Swierkowski, L.; Zawadzki, W.; Guldner, Y.; Rigaux, C. Two-Mode Resonant Polaron in the  $\text{Hg}_{0.72}\text{Cd}_{0.28}\text{Te}$  Semiconductor. *Solid State Commun.* **1978**, *27* (11), 1245–1247. [https://doi.org/10.1016/0038-1098\(78\)91152-3](https://doi.org/10.1016/0038-1098(78)91152-3).
- (127) Nash, K. J.; Skolnick, M. S.; Bass, S. J. Electron-Phonon Interactions in Indium Gallium Arsenide. *Semicond. Sci. Technol.* **1987**, *2* (6), 329–336. <https://doi.org/10.1088/0268-1242/2/6/002>.
- (128) Yamada, Y.; Mino, H.; Kawahara, T.; Oto, K.; Suzuura, H.; Kanemitsu, Y. Polaron Masses in  $\text{CH}_3\text{NH}_3\text{PbX}_3$  Perovskites Determined by Landau Level Spectroscopy in Low Magnetic Fields. *Phys. Rev. Lett.* **2021**, *126* (23), 237401. <https://doi.org/10.1103/PhysRevLett.126.237401>.
- (129) Zhao, D.; Skelton, J. M.; Hu, H.; La-o-vorakiat, C.; Zhu, J.-X.; Marcus, R. A.; Michel-Beyerle, M.-E.; Lam, Y. M.; Walsh, A.; Chia, E. E. M. Low-Frequency Optical Phonon Modes and Carrier Mobility in the Halide Perovskite  $\text{CH}_3\text{NH}_3\text{PbBr}_3$  Using Terahertz Time-Domain Spectroscopy. *Appl. Phys. Lett.* **2017**, *111* (20), 201903. <https://doi.org/10.1063/1.4993524>.
- (130) Nagai, M.; Tomioka, T.; Ashida, M.; Hoyano, M.; Akashi, R.; Yamada, Y.; Aharen, T.; Kanemitsu, Y. Longitudinal Optical Phonons Modified by Organic Molecular Cation Motions in Organic-Inorganic Hybrid Perovskites. *Phys. Rev. Lett.* **2018**, *121* (14), 145506. <https://doi.org/10.1103/PhysRevLett.121.145506>.
- (131) Lan, Y.; Dringoli, B. J.; Valverde-Chávez, D. A.; Ponseca, C. S.; Sutton, M.; He, Y.; Kanatzidis, M. G.; Cooke, D. G. Ultrafast Correlated Charge and Lattice Motion in a Hybrid Metal Halide Perovskite. *Sci. Adv.* **2019**, *5* (5), eaaw5558. <https://doi.org/10.1126/sciadv.aaw5558>.
- (132) Wang, J.; Motaharifar, E.; Murthy, L. N. S.; Higgins, M.; Barrera, D.; Daunis, T. B.; Zheng, Y.; Malko, A. V.; Ely, F.; Quevedo-Lopez, M.; Lee, M.; Hsu, J. W. P. Revealing Lattice and Photocarrier Dynamics of High-Quality  $\text{MAPbBr}_3$  Single Crystals by Far Infrared Reflection and Surface Photovoltage Spectroscopy. *J. Appl. Phys.* **2019**, *125* (2), 025706. <https://doi.org/10.1063/1.5072794>.
- (133) Boldyrev, K. N.; Anikeeva, V. E.; Semenova, O. I.; Popova, M. N. Infrared Spectra of the  $\text{CH}_3\text{NH}_3\text{PbI}_3$  Hybrid Perovskite: Signatures of Phase Transitions and of Organic Cation Dynamics. *J. Phys. Chem. C* **2020**, *124* (42), 23307–23316. <https://doi.org/10.1021/acs.jpcc.0c06103>.
- (134) Maeng, I.; Lee, S.; Han, E. Q.; Zhang, Y.; Oh, S. J.; Nakamura, M.; Yun, J.-H.; Wang, L.; Kwon, Y.-K.; Jung, M.-C. Unusual Terahertz-Wave Absorptions in  $\delta/\alpha$ -Mixed-Phase  $\text{FAPbI}_3$  Single Crystals: Interfacial Phonon Vibration Modes. *NPG Asia Mater.* **2021**, *13* (1), 75. <https://doi.org/10.1038/s41427-021-00343-7>.
- (135) Anikeeva, V. E.; Boldyrev, K. N.; Semenova, O. I.; Sukhikh, T. S.; Popova, M. N. Broad-Range High-Resolution Optical Spectroscopy of  $\text{CH}_3\text{NH}_3\text{PbBr}_3$  Hybrid Perovskite Single Crystals: Optical Phonons, Absorption Edge, Phase Transitions. *Opt. Mater. X* **2023**, *20*, 100259. <https://doi.org/10.1016/j.omx.2023.100259>.

- (136) Pérez-Osorio, M. A.; Milot, R. L.; Filip, M. R.; Patel, J. B.; Herz, L. M.; Johnston, M. B.; Giustino, F. Vibrational Properties of the Organic–Inorganic Halide Perovskite  $\text{CH}_3\text{NH}_3\text{PbI}_3$  from Theory and Experiment: Factor Group Analysis, First-Principles Calculations, and Low-Temperature Infrared Spectra. *J. Phys. Chem. C* **2015**, *119* (46), 25703–25718. <https://doi.org/10.1021/acs.jpcc.5b07432>.
- (137) La-o-vorakiat, C.; Salim, T.; Kadro, J.; Khuc, M.-T.; Haselsberger, R.; Cheng, L.; Xia, H.; Gurzadyan, G. G.; Su, H.; Lam, Y. M.; Marcus, R. A.; Michel-Beyerle, M.-E.; Chia, E. E. M. Elucidating the Role of Disorder and Free-Carrier Recombination Kinetics in  $\text{CH}_3\text{NH}_3\text{PbI}_3$  Perovskite Films. *Nat. Commun.* **2015**, *6*, 7903. <https://doi.org/10.1038/ncomms8903>.
- (138) La-o-vorakiat, C.; Xia, H.; Kadro, J.; Salim, T.; Zhao, D.; Ahmed, T.; Lam, Y. M.; Zhu, J.-X.; Marcus, R. A.; Michel-Beyerle, M.-E.; Chia, E. E. M. Phonon Mode Transformation Across the Orthorhombic–Tetragonal Phase Transition in a Lead Iodide Perovskite  $\text{CH}_3\text{NH}_3\text{PbI}_3$ : A Terahertz Time-Domain Spectroscopy Approach. *J. Phys. Chem. Lett.* **2016**, *7* (1), 1–6. <https://doi.org/10.1021/acs.jpcelett.5b02223>.
- (139) Frenzel, M.; Cherasse, M.; Urban, J. M.; Wang, F.; Xiang, B.; Nest, L.; Huber, L.; Perfetti, L.; Wolf, M.; Kampfrath, T.; Zhu, X.-Y.; Maehrlein, S. F. Nonlinear Terahertz Control of the Lead Halide Perovskite Lattice. *Sci. Adv.* **2023**, *9* (21), eadg3856. <https://doi.org/10.1126/sciadv.adg3856>.
- (140) Wu, X.; Tan, L. Z.; Shen, X.; Hu, T.; Miyata, K.; Trinh, M. T.; Li, R.; Coffee, R.; Liu, S.; Egger, D. A.; Makasyuk, I.; Zheng, Q.; Fry, A.; Robinson, J. S.; Smith, M. D.; Guzelturk, B.; Karunadasa, H. I.; Wang, X.; Zhu, X.; Kronik, L.; Rappe, A. M.; Lindenberg, A. M. Light-Induced Picosecond Rotational Disorder of the Inorganic Sublattice in Hybrid Perovskites. *Sci. Adv.* **2017**, *3* (7), e1602388. <https://doi.org/10.1126/sciadv.1602388>.
- (141) Cuthriell, S. A.; Panuganti, S.; Laing, C. C.; Quintero, M. A.; Guzelturk, B.; Yazdani, N.; Traore, B.; Brumberg, A.; Malliakas, C. D.; Lindenberg, A. M.; Wood, V.; Katan, C.; Even, J.; Zhang, X.; Kanatzidis, M. G.; Schaller, R. D. Nonequilibrium Lattice Dynamics in Photoexcited 2D Perovskites. *Adv. Mater.* **2022**, *34* (44), 2202709. <https://doi.org/10.1002/adma.202202709>.
- (142) Zhang, H.; Li, W.; Essman, J.; Quarti, C.; Metcalf, I.; Chiang, W.-Y.; Sidhik, S.; Hou, J.; Fehr, A.; Attar, A.; Lin, M.-F.; Britz, A.; Shen, X.; Link, S.; Wang, X.; Bergmann, U.; Kanatzidis, M. G.; Katan, C.; Even, J.; Blancon, J.-C.; Mohite, A. D. Ultrafast Relaxation of Lattice Distortion in Two-Dimensional Perovskites. *Nat. Phys.* **2023**, *19* (4), 545–550. <https://doi.org/10.1038/s41567-022-01903-6>.
- (143) Seiler, H.; Zahn, D.; Taylor, V. C. A.; Bodnarchuk, M. I.; Windsor, Y. W.; Kovalenko, M. V.; Ernstorfer, R. Direct Observation of Ultrafast Lattice Distortions during Exciton–Polaron Formation in Lead Halide Perovskite Nanocrystals. *ACS Nano* **2023**, *17* (3), 1979–1988. <https://doi.org/10.1021/acsnano.2c06727>.
- (144) Yazdani, N.; Bodnarchuk, M. I.; Bertolotti, F.; Masciocchi, N.; Fureraj, I.; Guzelturk, B.; Cotts, B. L.; Zajac, M.; Rainò, G.; Jansen, M.; Boehme, S. C.; Yarema, M.; Lin, M.-F.; Kozina, M.; Reid, A.; Shen, X.; Weathersby, S.; Wang, X.; Vauthey, E.; Guagliardi, A.; Kovalenko, M. V.; Wood, V.; Lindenberg, A. M. Coupling to Octahedral Tilts in Halide Perovskite Nanocrystals Induces Phonon-Mediated Attractive Interactions between Excitons. *Nat. Phys.* **2024**, *20* (1), 47–53. <https://doi.org/10.1038/s41567-023-02253-7>.
- (145) Matsuura, M.; Büttner, H. Optical Properties of Excitons in Polar Semiconductors: Energies, Oscillator Strengths, and Phonon Side Bands. *Phys. Rev. B* **1980**, *21* (2), 679–691. <https://doi.org/10.1103/PhysRevB.21.679>.

- (146) Miller, R. C.; Kleinman, D. A.; Tsang, W. T.; Gossard, A. C. Observation of the Excited Level of Excitons in GaAs Quantum Wells. *Phys. Rev. B* **1981**, *24* (2), 1134–1136. <https://doi.org/10.1103/PhysRevB.24.1134>.
- (147) Bastard, G.; Mendez, E. E.; Chang, L. L.; Esaki, L. Exciton Binding Energy in Quantum Wells. *Phys. Rev. B* **1982**, *26* (4), 1974–1979. <https://doi.org/10.1103/PhysRevB.26.1974>.
- (148) Matsuura, M.; Shinozuka, Y. A Wannier Exciton in a Quantum Well: Subband Dependence. *J. Phys. Soc. Jpn.* **1984**, *53* (9), 3138–3145. <https://doi.org/10.1143/JPSJ.53.3138>.
- (149) Blancon, J.-C.; Stier, A. V.; Tsai, H.; Nie, W.; Stoumpos, C. C.; Traoré, B.; Pedesseau, L.; Kepenekian, M.; Katsutani, F.; Noe, G. T.; Kono, J.; Tretiak, S.; Crooker, S. A.; Katan, C.; Kanatzidis, M. G.; Crochet, J. J.; Even, J.; Mohite, A. D. Scaling Law for Excitons in 2D Perovskite Quantum Wells. *Nat. Commun.* **2018**, *9* (1), 2254. <https://doi.org/10.1038/s41467-018-04659-x>.
- (150) Zheng, R.; Matsuura, M. Exciton Binding Energies in Polar Quantum Wells with Finite Potential Barriers. *Phys. Rev. B* **1998**, *58* (16), 10769–10777. <https://doi.org/10.1103/PhysRevB.58.10769>.
- (151) Matsuura, M. Effects of an Optical Phonon on Excitons in Quantum Wells. *Phys. Rev. B* **1988**, *37* (12), 6977–6982. <https://doi.org/10.1103/PhysRevB.37.6977>.
- (152) Zheng, R.; Matsuura, M. Exciton-Phonon Interaction Effects in Quantum Wells. *Phys. Rev. B* **1997**, *56* (4), 2058–2061. <https://doi.org/10.1103/PhysRevB.56.2058>.
- (153) Jin-Sheng, P. Electron-Phonon Interaction in Dielectric Interface Systems. *Phys. Status Solidi B* **1987**, *140* (2), 421–436. <https://doi.org/10.1002/pssb.2221400213>.
- (154) Senger, R. T.; Bajaj, K. K. Binding Energies of Excitons in Polar Quantum Well Heterostructures. *Phys. Rev. B* **2003**, *68* (20), 205314. <https://doi.org/10.1103/PhysRevB.68.205314>.
- (155) Senger, R. T.; Bajaj, K. K. Optical Properties of Confined Polaronic Excitons in Spherical Ionic Quantum Dots. *Phys. Rev. B* **2003**, *68* (4), 045313. <https://doi.org/10.1103/PhysRevB.68.045313>.
- (156) Pan, J. S.; Pan, H. B. Size-Quantum Effect of the Energy of a Charge Carrier in a Semiconductor Crystallite. *Phys. Status Solidi B* **1988**, *148* (1), 129–141. <https://doi.org/10.1002/pssb.2221480111>.
- (157) Martin, D. Integrals of Lommel's Type for Confluent Hypergeometric Functions. *Proc. Glasg. Math. Assoc.* **1952**, *1* (1), 28–31. <https://doi.org/10.1017/S2040618500032901>.

## Supplementary information:

### 1) Unitary transformation introducing a lattice distortion

$\widehat{W} = e^{\sum_{\vec{k}} (F_{\vec{k}}^* \hat{a}_{\vec{k}} - F_{\vec{k}} \hat{a}_{\vec{k}}^+)}$  includes a shift operator  $F_{\vec{k}}$  which can be understood as the amplitude of the lattice distortion around the charge carrier (the sign convention in the exponential taken here from PB is opposite to the one of LLP). Considering the general relation  $e^{-\hat{B}} \hat{A} e^{\hat{B}} = \hat{A} + [\hat{A}, \hat{B}] + \frac{1}{2!} [[\hat{A}, \hat{B}], \hat{B}] + \dots$ , phonon operators are shifted:  $\widehat{W}^+ \hat{a}_{\vec{k}} \widehat{W} = \hat{a}_{\vec{k}} - F_{\vec{k}}$  and  $\widehat{W}^+ \hat{a}_{\vec{k}}^+ \widehat{W} = \hat{a}_{\vec{k}}^+ - F_{\vec{k}}^*$

### 2) LLP first unitary transformation for the center of mass motion of a free polaron

$\hbar\vec{Q}$  is the eigenvalue of the total momentum of the polaron  $\hat{\wp} = \hat{p}_e + \sum_{\vec{k}} \hbar\vec{k} \hat{a}_{\vec{k}}^+ \hat{a}_{\vec{k}}$ .  $\hat{\wp}$  commutes with the e-ph Hamiltonian ( $[\hat{\wp}, \hat{H}_{e-ph}] = 0$ ), which shows that  $\hat{\wp}$  and  $\hat{H}_{e-ph}$  share the same eigenstates:  $\hat{H}_{e-ph}|\varphi\rangle = E|\varphi\rangle$  and  $\hat{\wp}|\varphi\rangle = \hbar\vec{Q}|\varphi\rangle$ . Next, a unitary transformation is introduced to remove explicitly the electron position and momentum:  $\hat{U} = e^{i(\vec{Q} - \sum_{\vec{k}} \hbar\vec{k} \hat{a}_{\vec{k}}^+ \hat{a}_{\vec{k}}) \cdot \vec{r}_e}$ , leading to  $\hat{U}^+ \hat{a}_{\vec{k}} \hat{U} = \hat{a}_{\vec{k}} e^{i\vec{k} \cdot \vec{r}_e}$ ,  $\hat{U}^+ \hat{a}_{\vec{k}}^+ \hat{U} = \hat{a}_{\vec{k}}^+ e^{-i\vec{k} \cdot \vec{r}_e}$ ,  $\hat{U}^+ \hat{\wp} \hat{U} = \hbar\vec{Q} + \hat{p}_e$ ,  $\hat{U}^+ \hat{p}_e \hat{U} = \hbar\vec{Q} + \hat{p}_e - \sum_{\vec{k}} \hbar\vec{k} \hat{a}_{\vec{k}}^+ \hat{a}_{\vec{k}}$  and to an expression where the electron position is already removed:

$$\hat{U}^+ \hat{H}_{e-ph} \hat{U} = \frac{(\hbar\vec{Q} + \hat{p}_e - \sum_{\vec{k}} \hbar\vec{k} \hat{a}_{\vec{k}}^+ \hat{a}_{\vec{k}})^2}{2m_e} + \sum_{\vec{k}} (g_{\vec{k}} \hat{a}_{\vec{k}} + g_{\vec{k}}^* \hat{a}_{\vec{k}}^+) + \hbar\omega_{LO} \sum_{\vec{k}} \hat{a}_{\vec{k}}^+ \hat{a}_{\vec{k}}.$$

Next, applying the unitary transformation to  $\hat{\wp}|\varphi\rangle = \hbar\vec{Q}|\varphi\rangle$  and to the eigenstates  $|\varphi_{CM}\rangle = \hat{U}^+|\varphi\rangle$ , one gets  $\hat{U}^+ \hat{\wp} |\varphi\rangle = \hat{U}^+ \hat{\wp} \hat{U} \hat{U}^+ |\varphi\rangle = (\hbar\vec{Q} + \hat{p}_e) |\varphi_{CM}\rangle$ , but also  $\hat{U}^+ \hbar\vec{Q} |\varphi\rangle = \hbar\vec{Q} |\varphi_{CM}\rangle$ , which shows that  $\hat{p}_e |\varphi_{CM}\rangle = 0$ . Then, the electron momentum can also be removed from the transformed Hamiltonian:

$$\hat{H}_{CM}^{LLP} = \hat{U}^+ \hat{H}_{e-ph} \hat{U} = \frac{(\hbar\vec{Q} - \sum_{\vec{k}} \hbar\vec{k} \hat{a}_{\vec{k}}^+ \hat{a}_{\vec{k}})^2}{2m_e} + \sum_{\vec{k}} (g_{\vec{k}} \hat{a}_{\vec{k}} + g_{\vec{k}}^* \hat{a}_{\vec{k}}^+) + \hbar\omega_{LO} \sum_{\vec{k}} \hat{a}_{\vec{k}}^+ \hat{a}_{\vec{k}}.$$

As a result, the description of the system moved from (electron+phonons) to (polaron+phonons) at the expense of additional second and fourth order terms related to the phonon population.

This expression can be alternatively expressed as:

$$\hat{H}_{CM}^{LLP} = \frac{\hbar^2 Q^2}{2m_e} + \hbar\Omega_{CM}^{LLP} \sum_{\vec{k}} \hat{a}_{\vec{k}}^+ \hat{a}_{\vec{k}} + \sum_{\vec{k}} [g_{\vec{k}} \hat{a}_{\vec{k}} + c. c] + \sum_{\vec{k}} \sum_{\vec{k}'} \frac{\hbar^2 \vec{k} \cdot \vec{k}'}{2M} \hat{a}_{\vec{k}}^+ \hat{a}_{\vec{k}'}^+ \hat{a}_{\vec{k}} \hat{a}_{\vec{k}'}.$$

$$\text{with } \hbar\Omega_{CM}^{LLP} = \hbar\omega_{LO} - \frac{\hbar^2}{M} \vec{k} \cdot \vec{Q} + \frac{\hbar^2 k^2}{2m_e}.$$

### 3) LLP second unitary transformation introducing the lattice distortion

$$\begin{aligned} \hat{H}^{LLP} (F_{\vec{k}}(\vec{Q})) &= \hat{W}^+ \hat{U}^+ \hat{H}_{e-ph} \hat{U} \hat{W} = \hat{W}^+ \hat{H}_{CM}^{LLP} \hat{W} = \frac{(\hbar\vec{Q} - \sum_{\vec{k}} \hbar\vec{k} (\hat{a}_{\vec{k}}^+ - F_{\vec{k}}^+) (\hat{a}_{\vec{k}} - F_{\vec{k}}))}{2m_e} + \\ &\sum_{\vec{k}} (g_{\vec{k}} (\hat{a}_{\vec{k}} - F_{\vec{k}}) + g_{\vec{k}}^* (\hat{a}_{\vec{k}}^+ - F_{\vec{k}}^*)) + \hbar\omega_{LO} \sum_{\vec{k}} (\hat{a}_{\vec{k}}^+ - F_{\vec{k}}^+) (\hat{a}_{\vec{k}} - F_{\vec{k}}). \end{aligned}$$

The new expression of the eigenstates is related to the initial one by  $|\psi\rangle = \hat{W}^+ |\varphi_{CM}\rangle = \hat{W}^+ \hat{U}^+ |\varphi\rangle$ . For a ‘free vacuum’ e-ph GS with zero (real) phonon such as  $|\psi_{GS}\rangle = \phi(\vec{Q})|0\rangle$ , only

$\hat{H}_{0_{ph}}^{LLP} (F_{\vec{k}}(\vec{Q}))$  needs to be considered:

$$\begin{aligned} E_{GS}(\vec{Q}) &= \langle \psi_{GS} | \hat{H}_{0_{ph}}^{LLP} (F_{\vec{k}}(\vec{Q})) | \psi_{GS} \rangle = \frac{\hbar^2 Q^2 - 2\vec{Q} \cdot (\sum_{\vec{k}} \hbar\vec{k} |F_{\vec{k}}(\vec{Q})|^2) + (\sum_{\vec{k}} \hbar\vec{k} |F_{\vec{k}}(\vec{Q})|^2)^2}{2m_e} - \\ &\sum_{\vec{k}} (g_{\vec{k}} F_{\vec{k}}(\vec{Q}) + c. c) + \sum_{\vec{k}} |F_{\vec{k}}(\vec{Q})|^2 (\hbar\omega_{LO} + \frac{\hbar^2 k^2}{2m_e}). \end{aligned}$$

The variational relation between the lattice distortion and  $g_{\vec{k}}$  is obtained by energy minimization

$$\frac{\partial E_{GS}(\vec{Q})}{\partial F_{\vec{k}}(\vec{Q})} = \frac{\partial E_{GS}(\vec{Q})}{\partial F_{\vec{k}}^*(\vec{Q})} = 0:$$

$$g_{\vec{k}} = F_{\vec{k}}^{*,min}(\vec{Q}) \left[ \hbar\omega_{LO} - \hbar^2 \frac{\vec{Q} \cdot \vec{k}}{m_e} + \frac{\hbar^2 k^2}{2m_e} + \frac{\hbar^2}{m_e} \vec{k} \cdot \sum_{\vec{k}'} \vec{k}' |F_{\vec{k}'}^{min}(\vec{Q})|^2 \right];$$

$$g_{\vec{k}}^* = F_{\vec{k}}^{min}(\vec{Q}) \left[ \hbar\omega_{LO} - \hbar^2 \frac{\vec{Q} \cdot \vec{k}}{m_e} + \frac{\hbar^2 k^2}{2m_e} + \frac{\hbar^2}{m_e} \vec{k} \cdot \sum_{\vec{k}'} \vec{k}' |F_{\vec{k}'}^{min}(\vec{Q})|^2 \right].$$

- Expressions valid at the bottom of the free polaron dispersion ( $\vec{Q} = \vec{0}$ ).

The non-linear term can be removed  $\sum_{\vec{k}} \vec{k} |F_{\vec{k}}^{min}(\vec{0})|^2 = \vec{0}$  because the system does not possess any preferential direction related to the distortion or the total momentum. In that case,  $F_{\vec{k}}^{min}(\vec{0}) =$

$\frac{g_{\vec{k}}^*}{\hbar\omega_{LO} + \frac{\hbar^2 k^2}{2m_e}}$  and the energy after integration is given by  $E_{GS}(\vec{0}) = \sigma_e^{LLP}(\vec{0}) = -\alpha_e \hbar\omega_{LO}$ . The

population of virtual phonons for the GS  $N_e^{LLP}(\vec{Q})$  is directly connected to the distortion  $F_{\vec{k}}^{min}(\vec{Q})$

of the lattice around the charge carrier through  $N_e^{LLP}(\vec{Q}) = \langle \varphi_{GS} | \sum_{\vec{k}} \hat{a}_{\vec{k}}^+ \hat{a}_{\vec{k}} | \varphi_{GS} \rangle =$

$\sum_{\vec{k}} |F_{\vec{k}}^{min}(\vec{Q})|^2$ , leading to a simple expression for  $\vec{Q} = \vec{0}$ :  $N_e^{LLP}(\vec{0}) = \frac{\alpha_e}{2}$ .

- Energy dispersion of the free polaron ( $\vec{Q} \neq \vec{0}$ ).

The non-linear term is vectorial and is therefore expected to be parallel to the preferential direction

in the system namely  $\vec{Q}$ :  $\sum_{\vec{k}} \vec{k} |F_{\vec{k}}^{min}(\vec{Q})|^2 = \eta \vec{Q}$ . One can integrate over the angle  $\theta$  between  $\vec{k}$

and  $\vec{Q}$ , before integration over the modulus of  $\vec{k}$ :

$$\begin{aligned} \eta &= \frac{\alpha_e(1-\eta)}{\pi q^3} \int_0^{+\infty} \frac{dK}{2K} \left( \frac{2Kq(1+K^2)}{(1+K^2)^2 - 4K^2q^2} - \frac{1}{2} \log \left( \frac{1+K^2+2Kq}{1+K^2-2Kq} \right) \right) \\ &= \frac{\alpha_e(1-\eta)}{2q^3} \left( \frac{q}{\sqrt{1-q^2}} - \text{asin}(q) \right) \end{aligned}$$

$$\text{with } K = \frac{\hbar k}{(2m_e \hbar \omega_{LO})^{1/2}} = R_e k \text{ and } q = \frac{\hbar Q(1-\eta)}{(2m_e \hbar \omega_{LO})^{1/2}} = R_e Q(1-\eta)$$

The expressions of the total energy and virtual phonon population are integrated over wavevector orientation and modulus.

$$E_{GS}(\vec{Q}) = \frac{\hbar^2 Q^2 (1-\eta)^2}{2m_e} + \frac{2\alpha_e \hbar \omega_{LO}}{\pi q} \int_0^{+\infty} \frac{dK}{2K} \left( \frac{2Kq(1+K^2)}{(1+K^2)^2 - 4K^2 q^2} - \log \left( \frac{1+K^2+2Kq}{1+K^2-2Kq} \right) \right),$$

$$N_e^{LLP}(\vec{Q}) = \frac{\alpha_e}{2\sqrt{1-q^2}}.$$

After simplification the total energy can be recasted in the original LLP form:

$$E_{GS}(\vec{Q}) = \frac{\hbar^2 Q^2 (1-\eta^2)}{2m_e} - \alpha_e \hbar \omega_{LO} \frac{\text{asin}(q)}{q}.$$

The two expressions for  $\eta$  and  $E_{GS}(\vec{Q})$  can be expressed for small  $q$  values thanks to  $\text{asin}(q) \approx$

$$q + \frac{q^3}{6} \text{ and } \eta \approx \frac{\alpha_e(1-\eta)}{2q^3} \left( \frac{q^3}{3} \right) = \frac{\alpha_e(1-\eta)}{6} \text{ yielding the final expression of LLP for the energy}$$

dispersion including a self-energy term and a correction over the charge carrier mass:

$$E_{GS}(\vec{Q}) \approx -\alpha_e \hbar \omega_{LO} + \frac{\hbar^2 Q^2}{2m_e(1+\frac{\alpha_e}{6})} + \dots,$$

$$N_e^{LLP}(\vec{Q}) \approx \frac{\alpha_e}{2} \left( 1 + \frac{R_e^2 Q^2}{2(1+\frac{\alpha_e}{6})^2} + \dots \right).$$

#### 4) Iadonisi's approach to PB's model for zero phonon and $\vec{Q} = \vec{0}$ :

To perform a partial summation of the exact solution proposed as a series by Iadonisi and coworkers and expressed in the main text using Whittaker functions, it is interesting to start with Lommel integrals for the Whittaker functions:<sup>157</sup>

$$\begin{aligned}
& M_{\frac{1}{\tilde{\zeta}}, l+\frac{1}{2}}(2\tilde{\zeta}\tilde{r}) \int_{\tilde{r}}^{+\infty} W_{\frac{1}{\tilde{\zeta}}, l+\frac{1}{2}}(2\tilde{\zeta}\tilde{u}) M_{0, l+\frac{1}{2}}(2is_e\tilde{k}\tilde{u}) d\tilde{u} \\
& + W_{\frac{1}{\tilde{\zeta}}, l+\frac{1}{2}}(2\tilde{\zeta}\tilde{r}) \int_0^{\tilde{r}} M_{\frac{1}{\tilde{\zeta}}, l+\frac{1}{2}}(2\tilde{\zeta}\tilde{u}) M_{0, l+\frac{1}{2}}(2is_e\tilde{k}\tilde{u}) d\tilde{u} = \left( \frac{2\tilde{\zeta}\Gamma(2(l+1))}{(\tilde{\zeta}^2 + s_e^2\tilde{k}^2)\Gamma(l+1-\frac{1}{\tilde{\zeta}})} \right) M_{0, l+\frac{1}{2}}(2is_e\tilde{k}\tilde{r}) + \\
& \frac{1}{(\tilde{\zeta}^2 + s_e^2\tilde{k}^2)} \left( M_{\frac{1}{\tilde{\zeta}}, l+\frac{1}{2}}(2\tilde{\zeta}\tilde{r}) \int_{\tilde{r}}^{+\infty} W_{\frac{1}{\tilde{\zeta}}, l+\frac{1}{2}}(2\tilde{\zeta}\tilde{u}) M_{0, l+\frac{1}{2}}(2is_e\tilde{k}\tilde{u}) \frac{2}{\tilde{u}} d\tilde{u} \right. \\
& \left. + W_{\frac{1}{\tilde{\zeta}}, l+\frac{1}{2}}(2\tilde{\zeta}\tilde{r}) \int_0^{\tilde{r}} M_{\frac{1}{\tilde{\zeta}}, l+\frac{1}{2}}(2\tilde{\zeta}\tilde{u}) M_{0, l+\frac{1}{2}}(2is_e\tilde{k}\tilde{u}) \frac{2}{\tilde{u}} d\tilde{u} \right).
\end{aligned}$$

where the Jacobian of the  $(M, W)$  Whittaker functions is introduced in the first term after analytical calculations of the partial Lommel integrals. Next, it is necessary to connect Whittaker and Bessel functions:

$$M_{0, l+\frac{1}{2}}(2is_e\tilde{k}\tilde{r}) = i^{l+1} 2^{2l+\frac{3}{2}} \Gamma\left(l + \frac{3}{2}\right) (s_e\tilde{k}\tilde{r})^{1/2} J_{l+\frac{1}{2}}(s_e\tilde{k}\tilde{r})$$

and finally, to perform partial infinite summations through:

$$e^{is_e\tilde{k}\tilde{r}\cos(\theta)} = \sum_{l=0}^{+\infty} i^l \sqrt{\frac{\pi}{2}} (2l+1) J_{l+\frac{1}{2}}(s_e\tilde{k}\tilde{r}) (s_e\tilde{k}\tilde{r})^{-1/2} P_l(\cos(\theta)).$$

The leading first term of  $F_{\vec{k}}(\vec{r})$  has a form which is now close to the ones of PB and Kane:

$$\frac{g_{\vec{k}}^*}{\hbar\omega_{LO}} \left( \frac{1}{(\tilde{R}_e^2 + \tilde{R}_h^2 + 1 + \tilde{R}_e^2\tilde{k}^2)} e^{-is_h\vec{k}\cdot\vec{r}} - \frac{1}{(\tilde{R}_e^2 + \tilde{R}_h^2 + 1 + \tilde{R}_h^2\tilde{k}^2)} e^{is_e\vec{k}\cdot\vec{r}} \right)$$

and the second term leads to a better convergence as a function of  $l$  than the initial series:

$$\frac{g_{\vec{k}}^*}{\hbar\omega_{LO}} \sum_{l=0}^{+\infty} \left( (-1)^{l+1} \int_0^{+\infty} \left( e^{\tilde{r}-\tilde{u}} - 1 + \frac{2}{\tilde{u}(\tilde{\zeta}^2 + s_e^2 \tilde{k}^2)} \right) \left( \frac{\tilde{u}}{s_e \tilde{k} \tilde{r}^2} \right)^{\frac{1}{2}} M_{\frac{\tilde{\zeta}}{2}, l + \frac{1}{2}}^1(2\tilde{\zeta}\tilde{r}) M_{\frac{\tilde{\zeta}}{2}, l + \frac{1}{2}}^2(2\tilde{\zeta}\tilde{u}) J_{l + \frac{1}{2}}(s_e \tilde{k} \tilde{u}) d\tilde{u} \right. \\ \left. + \int_0^{+\infty} \left( e^{\tilde{r}-\tilde{u}} - 1 + \frac{2}{\tilde{u}(\tilde{\zeta}^2 + s_h^2 \tilde{k}^2)} \right) \left( \frac{\tilde{u}}{s_h \tilde{k} \tilde{r}^2} \right)^{\frac{1}{2}} M_{\frac{\tilde{\zeta}}{2}, l + \frac{1}{2}}^1(2\tilde{\zeta}\tilde{r}) M_{\frac{\tilde{\zeta}}{2}, l + \frac{1}{2}}^2(2\tilde{\zeta}\tilde{u}) J_{l + \frac{1}{2}}(s_h \tilde{k} \tilde{u}) d\tilde{u} \right) \\ \times \left( \frac{(-i)^l \sqrt{\frac{\pi}{8}} (2l+1) \Gamma(l+1 - \frac{1}{\tilde{\zeta}}) P_l(\cos(\theta))}{(\tilde{R}_e^2 + \tilde{R}_h^2) \tilde{\zeta} \Gamma(2(l+1))} \right)$$

### 5) Energy dispersion of the excitonic polaron ( $\vec{Q} \neq \vec{0}$ )

- PB Hamiltonian for a GS with zero-phonon

After two successive unitary transformations the Hamiltonian related to the interaction between an exciton and an optical polar phonon reads:

$$\hat{H}_{PB} \left( F_{\vec{k}}(\vec{Q}, \vec{r}) \right) = \hat{W}^+ \hat{U}^+ \hat{H}_{X-ph} \hat{U} \hat{W} = \hat{H}_{0_{ph}}^{PB} + \hat{H}_{1_{ph}}^{PB} + \hat{H}_{2_{ph}}^{PB} + \hat{H}_{3_{ph}}^{PB} + \hat{H}_{4_{ph}}^{PB},$$

where  $\hat{H}_{n_{ph}}^{PB} \left( F_{\vec{k}}(\vec{Q}, \vec{r}) \right)$  are the n-phonon contributions to the Hamiltonian. The explicit expression of the  $0_{ph}$  contribution is:

$$\hat{H}_{0_{ph}}^{PB} \left( F_{\vec{k}}(\vec{Q}, \vec{r}) \right) = E_g + \frac{\hbar^2 Q^2 - 2\hbar^2 \vec{Q} \cdot \sum_{\vec{k}} \vec{k} |F_{\vec{k}}(\vec{Q}, \vec{r})|^2 + \hbar^2 \left| \sum_{\vec{k}} \vec{k} |F_{\vec{k}}(\vec{Q}, \vec{r})|^2 \right|^2}{2M} + \frac{(\hat{p} + \mu \vec{j})^2 + \hbar^2 |\nabla F_{\vec{k}}(\vec{Q}, \vec{r})|^2}{2\mu} -$$

$$\sum_{\vec{k}} (\rho_{\vec{k}} g_{\vec{k}} F_{\vec{k}}(\vec{Q}, \vec{r}) + c.c) + \sum_{\vec{k}} |F_{\vec{k}}(\vec{Q}, \vec{r})|^2 \left( \hbar\omega_{LO} + \frac{\hbar^2 k^2}{2M} \right).$$

$$\text{with } \vec{j} = \frac{F_{\vec{k}}^*(\vec{Q}, \vec{r}) (-i\hbar \nabla F_{\vec{k}}(\vec{Q}, \vec{r})) + c.c}{2\mu}.$$

- Analytic calculation for  $m_e = m_h$  with PB functional. Virtual phonon population.

The virtual phonon population for a 1S exciton can be computed thanks to  $N_{1S}(\vec{0}) = \langle \phi_{1S}(\vec{r}) | \sum_{\vec{k}} |F_{\vec{k}}^{min}(\vec{r}, \vec{0})|^2 | \phi_{1S}(\vec{r}) \rangle$ . When a PB functional is used for  $m_e = m_h$ , this expression

can be expressed as a single integral:  $N_{1S}^{PB}(\vec{0}) = N_{1S}^{PBpref} \int_0^{+\infty} d\tilde{k} \frac{(1-\tilde{G}_{1S})^3}{(1+\tilde{R}_{pol}^2 \tilde{k}^2 - \tilde{G}_{1S})}$  with  $\tilde{G}_{1S} =$

$\frac{1}{(1+(\frac{\tilde{k}}{2})^2)}$  and  $N_{1S}^{PBpref} = \frac{2a_B^{vac} R_{yvac}}{\pi \varepsilon^* a_B^{eff} \hbar \omega_{LO}}$ . After analytical integration over  $\tilde{k} = k a_B^{eff}$ , we find:

$$\frac{N_{1S}^{PB}(\vec{0})}{N_{1S}^{PBpref}} = 2\pi \left( \frac{1}{\sqrt{-\lambda_+}} - \frac{1}{\sqrt{-\lambda_-}} \right) \left( g_1 - g_2 \frac{\lambda_+ + \lambda_- + 2g_3}{\lambda_+ - \lambda_-} \right) + \pi g_2 g_3 \left( \frac{1}{(-\lambda_+)^{3/2}} + \frac{1}{(-\lambda_-)^{3/2}} \right) +$$

$$\pi g_2 \left( \frac{1}{\sqrt{-\lambda_+}} + \frac{1}{\sqrt{-\lambda_-}} \right) - \pi, \quad \text{with } \eta = 4\tilde{R}_{pol}^2, \quad \lambda_{\pm} = \frac{1}{2\eta} \left( -(1+2\eta) \pm \sqrt{1-4\eta} \right), \quad g_1 = \frac{1+\frac{1}{\eta^2}}{\lambda_+ - \lambda_-},$$

$$g_2 = \frac{\eta^2 + 2\eta - 1}{\eta^3 (\lambda_+ - \lambda_-)^2}, \quad g_3 = \frac{2\eta^2 + 3\eta - 2}{\eta^2 + 2\eta - 1}.$$

- Self-energies in the weak-coupling regime.

Within PB's model, the general expression for the single carrier self-energies is:

$$\sigma_{e(h),1S}(\vec{0}) = -\sum_{\vec{k}} \frac{|g_{\vec{k}}|^2}{\hbar \omega_{LO}} \left( 2f_{e(h),\vec{k}}^{min}(\vec{0}) - (1 + R_{e(h)}^2 k^2) f_{e(h),\vec{k}}^{min}(\vec{0})^2 \right).$$

In the weak-coupling regime,  $f_{e(h),\vec{k}}^{min}(\vec{0}) \approx \frac{1}{(1+R_{e(h)}^2 k^2)}$ . The expression of self-energies is

simplified to:  $\sigma_{e(h),1S}(\vec{0}) = -\sum_{\vec{k}} \frac{|g_{\vec{k}}|^2}{\hbar \omega_{LO}} f_{e(h),\vec{k}}^{min}(\vec{0})$ . Using  $\alpha_{e(h)} = \frac{e^2}{8\pi \varepsilon_0 \hbar \omega_{LO} R_{e(h)} \varepsilon^*}$  and  $\int_0^{+\infty} \frac{dK}{(1+K^2)} =$

$\frac{\pi}{2}$ , one finally obtains  $\sigma_{e(h),1S}(\vec{0}) = -\alpha_{e(h)} \hbar \omega_{LO}$

- Semi-analytic calculation for  $m_e = m_h$  with PB functional. Center of mass motion.

Internal excitonic polaron energy.

Analyzing the effects of the excitonic polaron center of mass motion on the excitonic polaron more complex than in the case of free polarons.<sup>61,110</sup> Using PB approach, we propose here a semi-analytic calculation for  $m_e = m_h$ . This assumption, which is well suited for halide perovskites, leads to several simplifications in the above expression, including first  $\vec{j} = \vec{0}$ . Next, the Hamiltonian is applied to the exciton GS with zero-phonon:  $E_{GS}(\vec{Q}) = \langle \phi_{1S}(\vec{r}) | \hat{H}_{PB}^0 (F_{\vec{k}}(\vec{Q}, \vec{r})) | \phi_{1S}(\vec{r}) \rangle$ . According to PB,  $F_{\vec{k}}(\vec{Q}, \vec{r})$  is parameterized through:  $F_{\vec{k}}(\vec{Q}, \vec{r}) \approx \frac{g_{\vec{k}}^*}{\hbar\omega_{LO}} (f_{e,\vec{k}}(\vec{Q})e^{-is_h\vec{k}\cdot\vec{r}} - f_{h,\vec{k}}(\vec{Q})e^{is_e\vec{k}\cdot\vec{r}})$  and the energy is minimized against  $f_{e,\vec{k}}(\vec{Q})$  and  $f_{h,\vec{k}}(\vec{Q})$ . For  $m_e = m_h$ ,  $\alpha_e = \alpha_h = \alpha$  and  $f_{e,\vec{k}}^{min}(\vec{Q}) = f_{h,\vec{k}}^{min}(\vec{Q}) = f_{e(h),\vec{k}}^{min}(\vec{Q})$ , we achieve a simplification of PB parameters:  $f_{e(h),\vec{k}}^{min}(\vec{Q}) = \frac{1-G_{1S}(\vec{k}, a_B^{eff})}{1+K^2-\vec{q}\cdot\vec{k}-G_{1S}(\vec{k}, a_B^{eff})}$  with  $\vec{K} = R_{pol}\vec{k}$ ,  $\vec{q} = R_{pol}\vec{Q} (1 - \eta - G_{1S}(\vec{k}, a_B^{eff}))$  and  $\eta\vec{Q} = \langle \phi_{1S}(\vec{r}) | \sum_{\vec{k}} \vec{k} | F_{\vec{k}}^{min}(\vec{Q}, \vec{r}) |^2 | \phi_{1S}(\vec{r}) \rangle$ . The expression of the energy of the GS becomes:

$$\begin{aligned}
E_{1S}(a_B^{eff}, \vec{Q}) &= E_g + \frac{\hbar^2 Q^2 (1 - \eta)^2}{2M} + \frac{\hbar^2}{2\mu a_B^{eff^2}} - \frac{e^2}{4\pi\epsilon_0\epsilon_\infty a_B^{eff}} \\
&+ \frac{\alpha_e \hbar\omega_{LO}}{\pi q} \int_0^{+\infty} \frac{4dK}{K} (1 - G_{1S})^2 \left( \frac{Kq(1 + K^2 - G_{1S})}{(1 + K^2 - G_{1S})^2 - K^2 q^2} \right. \\
&\left. - \log \left( \frac{1 + K^2 + Kq - G_{1S}}{1 + K^2 - Kq - G_{1S}} \right) \right) \\
\eta &= \frac{\alpha_e (1 - \eta)}{\pi q^3} \int_0^{+\infty} \frac{4dK}{K} (1 - G_{1S})^3 \left( \frac{Kq(1 + K^2 - G_{1S})}{(1 + K^2 - G_{1S})^2 - K^2 q^2} \right. \\
&\left. - \frac{1}{2} \log \left( \frac{1 + K^2 + Kq - G_{1S}}{1 + K^2 - Kq - G_{1S}} \right) \right)
\end{aligned}$$

For small Q values, the two expressions above can be approximated by:

$$E_{1S}(a_B^{eff}, \vec{Q}) \approx E_{1S}(a_B^{eff}, \vec{0}) + \frac{\hbar^2 Q^2 (1 - \eta)^2}{2M} + \frac{\alpha \hbar^2 Q^2}{2M} (I_3(a_B^{eff}) - \eta I_2(a_B^{eff}))$$

with the internal excitonic polaron energy

$$E_{1S}(a_B^{eff}, \vec{0}) = E_g + \frac{\hbar^2}{2\mu a_B^{eff2}} - \frac{e^2}{4\pi\epsilon_0\epsilon_\infty a_B^{eff}} - \frac{e^2}{2\pi^2\epsilon_0\epsilon^* R_{pol}} \int_0^{+\infty} dK \frac{(1 - G_{1S})^2}{(1 + K^2 - G_{1S})}$$

and

$$\eta \approx \frac{\alpha I_4(a_B^{eff})}{1 + \alpha I_3(a_B^{eff})}$$

where several integrals have a similar form:

$$I_n(a_B^{eff}) = \int_0^{+\infty} \frac{8K^2 dK}{3\pi} \left( \frac{(1 - G_{1S})^n}{(1 + K^2 - G_{1S})^3} \right) \text{ and } G_{1S} = \frac{1}{\left( 1 + \left( \frac{K}{2R_{pol}} \right)^2 \right)^2}. \text{ Numerical integrations can be}$$

easily performed to get  $M_{PB}$  for any  $\alpha$  value:

$$\frac{M^{PB}}{M} = \frac{1}{(1 - \eta)^2 + \alpha (I_3(a_B^{eff}) - \eta I_2(a_B^{eff}))}$$

In the weak coupling limit  $G_{1S} \rightarrow 0$  and  $\alpha \rightarrow 0$ , using  $\int_0^{+\infty} \frac{K^2 dK}{(1 + K^2)^3} = \frac{\pi}{16}$ ,  $I_n(a_B^{eff}) \rightarrow \frac{1}{6}$ . One can

check that the effective mass for the center of mass motion is consistent with LLP model for free

polarons and renormalized to  $\frac{M^{PB}}{M} \approx \left( 1 + \frac{\alpha}{6} \right) \approx \frac{M^{LLP}}{M}$

$$\text{with } M^{LLP} = m_e^{LLP} + m_h^{LLP}$$

**6) Toyozawa's analysis of the Fröhlich interaction in cubic, polar and harmonic lattices with more than one longitudinal optical mode**

In the harmonic approximation:  $\frac{1}{\varepsilon_\infty} - \frac{1}{\varepsilon(\omega)} = \sum_\nu \frac{2\omega_{LO,\nu}\varepsilon_0 k^2 |g_{\vec{k},\nu}^-|^2}{\hbar e^2 (\omega_{LO,\nu}^2 - \omega^2)}$ .

Considering the longitudinal modes as poles of the dielectric constant  $\varepsilon(\omega_{LO,\nu}) = 0$  and expanding  $\frac{1}{\varepsilon(\omega)}$  close to  $\omega = \omega_{LO,\nu}$  in this expression ( $\omega = \omega_{LO,\nu} + \delta, \delta \rightarrow 0$ ):

$$k^2 |g_{\vec{k},\nu}^-|^2 = \frac{\hbar e^2}{\varepsilon_0 \left. \frac{\partial \varepsilon}{\partial \omega} \right|_{\omega_{LO,\nu}}}$$

Considering the inverse of the generalized LST equation:  $\frac{\varepsilon_\infty}{\varepsilon(\omega)} = \prod_\nu \left( \frac{\omega_{TO,\nu}^2 - \omega^2}{\omega_{LO,\nu}^2 - \omega^2} \right)$ , and expanding it

$$\text{close to } \omega = \omega_{LO,\nu}: \left. \frac{\partial \varepsilon}{\partial \omega} \right|_{\omega_{LO,\nu}} = \varepsilon_\infty \left( \frac{\omega_{LO,\nu}}{\omega_{LO,\nu}^2 - \omega_{TO,\nu}^2} \right) \prod_{\mu \neq \nu} \left( \frac{\omega_{LO,\nu}^2 - \omega_{LO,\mu}^2}{\omega_{LO,\nu}^2 - \omega_{TO,\mu}^2} \right)$$

**7) Analysis of Gervais multimode expression for cubic, polar and harmonic lattices with more than one longitudinal optical mode:**

Considering the generalized LST equation:  $\frac{\varepsilon(\omega)}{\varepsilon_\infty} = \prod_\nu \left( \frac{\omega_{LO,\nu}^2 - \omega^2}{\omega_{TO,\nu}^2 - \omega^2} \right)$ , and expanding it close to  $\omega =$

$$\omega_{TO,\nu} \ (\omega = \omega_{TO,\nu} + \delta, \delta \rightarrow 0): \varepsilon(\omega_{TO,\nu} + \delta) \approx \varepsilon_\infty \frac{\omega_{LO,\nu}^2 - \omega_{TO,\nu}^2}{-2\omega_{TO,\nu}\delta} \prod_{\mu \neq \nu} \left( \frac{\omega_{TO,\nu}^2 - \omega_{LO,\mu}^2}{\omega_{TO,\nu}^2 - \omega_{TO,\mu}^2} \right)$$

Starting from  $\varepsilon(\omega) = \varepsilon_\infty + \sum_\nu \frac{\omega_{TO,\nu}^2 \Delta\varepsilon_\nu}{\omega_{TO,\nu}^2 - \omega^2}$ ,<sup>125</sup> expanded close to  $\omega = \omega_{TO,\nu}$ :

$$\varepsilon(\omega_{TO,\nu} + \delta) \approx \frac{\Delta\varepsilon_\nu \omega_{TO,\nu}^2}{-2\omega_{TO,\nu}\delta}$$

which shows that  $\Delta\varepsilon_\nu = \varepsilon_\infty \left( \frac{\omega_{LO,\nu}^2}{\omega_{TO,\nu}^2} - 1 \right) \prod_{\mu \neq \nu} \left( \frac{\omega_{TO,\nu}^2 - \omega_{LO,\mu}^2}{\omega_{TO,\nu}^2 - \omega_{TO,\mu}^2} \right)$

### 8) A simplified model for a Fröhlich bipolaron

A simplified model for a bipolaron (two equivalent charges, i.e. two holes or two electrons numbered 1 and 2 and abbreviated as *bip*) at the same level of theory than PB approach for excitonic polaron leads to the effective Hamiltonian:

$$\hat{H}_{bip} = E_g + \frac{\hat{p}^2}{2M} + \frac{\hat{p}^2}{2\mu} + \frac{e^2}{4\pi\epsilon_0\epsilon_\infty r} + \hbar\omega_{LO} \sum_{\vec{k}} \hat{a}_{\vec{k}}^+ \hat{a}_{\vec{k}} + \sum_{\vec{k}} \left[ \rho_{\vec{k}} e^{i\vec{k}\cdot\vec{R}} g_{\vec{k}} \hat{a}_{\vec{k}} + c.c \right],$$

where<sup>74</sup>:  $\rho_{\vec{k}} = e^{is_1\vec{k}\cdot\vec{r}} + e^{-is_2\vec{k}\cdot\vec{r}}$  with  $s_1 = s_2 = \frac{1}{2}$

A simplified variational approach can be based on a PB-like functional (see Bassani et al<sup>74</sup> for a complete approach):

$$F_{\vec{k}}(\vec{r}) \approx \frac{g_{\vec{k}}^*}{\hbar\omega_{LO}} \left( f_{1,\vec{k}}^{min} e^{-is_1\vec{k}\cdot\vec{r}} + f_{2,\vec{k}} e^{is_2\vec{k}\cdot\vec{r}} \right)$$

$$E_{1S}(a_B^{eff}, \vec{0}) = \left\langle \phi_{bip,1S}(\vec{r}) \left| E_g + \frac{p^2}{2\mu} + \frac{e^2}{4\pi\epsilon_0\epsilon_\infty r} + V_{latt} \left( \vec{r}, f_{1,\vec{k}}^{min}(\vec{0}), f_{2,\vec{k}}^{min}(\vec{0}) \right) \right| \phi_{bip,1S}(\vec{r}) \right\rangle +$$

$$\sigma_{1,1S} \left( f_{1,\vec{k}}^{min}(\vec{0}), f_{2,\vec{k}}^{min}(\vec{0}) \right) + \sigma_{2,1S} \left( f_{1,\vec{k}}^{min}(\vec{0}), f_{2,\vec{k}}^{min}(\vec{0}) \right) \quad (49)$$

including a lattice mediated attractive interaction to the electron-electron (or hole-hole) effective repulsion:

$$V_{latt}^{PB} \left( \vec{r}, f_{1,\vec{k}}^{min}(\vec{0}), f_{2,\vec{k}}^{min}(\vec{0}) \right) = 2 \sum_{\vec{k}} \frac{|g_{\vec{k}}|^2}{\hbar\omega_{LO}} \left( -f_{1,\vec{k}}^{min}(\vec{0}) - f_{2,\vec{k}}^{min}(\vec{0}) + \right.$$

$$\left. f_{1,\vec{k}}^{min}(\vec{0}) f_{2,\vec{k}}^{min}(\vec{0}) \right) \cos(\vec{k}\cdot\vec{r}) \quad (50)$$

and a sum of self-energy corrections  $\sigma_{1,1S}(\vec{0}) + \sigma_{2,1S}(\vec{0})$  in the presence of the bipolaron with:

$$\sigma_{1(2),1S}(\vec{0}) = -\sum_{\vec{k}} \frac{|g_{\vec{k}}|^2}{\hbar\omega_{LO}} \left( 2f_{1(2),\vec{k}}^{min}(\vec{0}) - (1 + R_{1(2)}^2 k^2) f_{1(2),\vec{k}}^{min}(\vec{0})^2 \right).$$

For a 1S trial bipolaron wavefunction such as  $\phi_{1S}(\vec{r}) = \frac{e^{-r/a_B^{eff}}}{a_B^{eff3/2} \pi^{1/2}}$  (see Bassani et al<sup>74</sup> for a complete approach), the expressions of  $f_{1(2),\vec{k},1S}(\vec{0})$  can be simplified:  $f_{e(h),\vec{k},1S}(\vec{0}) = \frac{1+G_{1S}(\vec{k},a_B^{eff})}{1+R_{pol}^2 k^2 + G_{1S}(\vec{k},a_B^{eff})}$  and the total energy :

$$E_{1S}(a_B^{eff}, \vec{0}) = E_g + \frac{\hbar^2}{2\mu a_B^{eff2}} + \frac{e^2}{4\pi\epsilon_0\epsilon_\infty a_B^{eff}} - \frac{e^2}{2\pi^2\epsilon_0\epsilon^* R_{pol}} \int_0^{+\infty} dK \frac{(1+G_{1S})^2}{(1+K^2+G_{1S})} \text{ with } \vec{K} = R_{pol}\vec{k}.$$

Effective interaction and self-energies have been merged in a single integral.

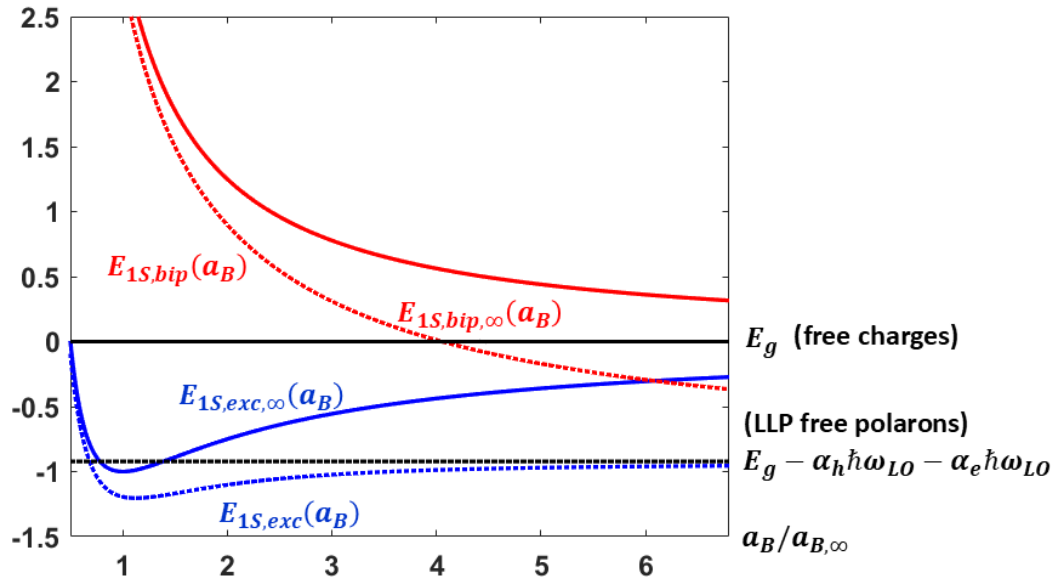


Figure S1. Illustration of the calculation of 1S excitonic polaron binding energy and bipolaron variational calculation for MAPbI<sub>3</sub>. The variation of internal excitonic polaron (Wannier exciton with  $\epsilon_{eff} = \epsilon_\infty$ ) energy is represented by a dotted (straight) blue curve as a function of the Bohr radius. The Bohr radius is scaled by its value at the minimum energy for a Wannier exciton with  $\epsilon_{eff} = \epsilon_\infty$ . The energies are scaled with the Rydberg energy of a Wannier exciton with  $\epsilon_{eff} = \epsilon_\infty$ . The binding energies are computed at the energy minima by subtracting the energy for free carriers

or free polarons. The minimum energy for free carriers (band gap) is taken as a reference to define the vertical axis. The minimum energy for free polarons is lowered by self-energy terms computed within LLP theory. The variations of the energies for a pair of free charges or a bipolaron are illustrated respectively by a straight or a dotted red line.

### 9) Adamowski, Bednarek and Suffczynski (ABS) approximation to PB's model

The full expression of the effective interaction within PB's model can be integrated thanks to the ABS approximation. For  $m_e = m_h$ , a variational form is assumed for  $f_{e(h),\vec{k}}(\vec{0})$ :

$$f_{e(h),\vec{k}}(\vec{0}) \approx \frac{\lambda\rho}{1+(\rho R_{pol})^2 k^2}. \text{ These coefficients can be introduced into the general expression}$$

of the effective interaction leading to:

$$V_{latt,m_e=m_h}^{ABS}(\vec{r}, \vec{0}) = \frac{e^2}{2\pi^2 \varepsilon_0 \varepsilon^*} \int_0^{+\infty} \frac{\sin(kr)}{kr} dk \left( \frac{2\lambda\rho}{1 + \rho^2 R^2 k^2} - \frac{\lambda^2 \rho^2}{(1 + \rho^2 R^2 k^2)^2} \right)$$

which can be further integrated to yield:

$$\tilde{V}_{latt,m_e=m_h}^{ABS}(\vec{r}, \vec{0}) = \frac{V_{latt,m_e=m_h}^{ABS}(\vec{r}, \vec{0})}{\frac{e^2}{4\pi\varepsilon_0\varepsilon^*R_{pol}}} = \frac{1}{\rho} \left( \frac{(2\lambda\rho - \lambda^2\rho^2)(1 - e^{-\tilde{r}/\rho})}{\tilde{r}/\rho} + \frac{\lambda^2\rho^2 e^{-\tilde{r}/\rho}}{2} \right)$$

The general expression of self-energies can be integrated analytically as well leading to:

$$\sigma_{e(h)}(\vec{0}) = -2\alpha\hbar\omega_{LO} \left( \lambda - \frac{\lambda^2(1 + \rho^2)}{4\rho} \right)$$

Finally, assuming a 1S trial excitonic polaron wavefunction such as  $\phi_{1S}(\vec{r}) = \frac{e^{-r/a_B^{eff}}}{a_B^{eff3/2} \pi^{1/2}}$ :

$$\begin{aligned} \frac{E_{1S}(a_B^{eff}, \vec{0})}{Ry_{vac}} &= \frac{a_B^{vac2}}{\mu a_B^{eff2}} - \frac{2a_B^{vac}}{\epsilon_\infty a_B^{eff}} - \frac{4a_B^{vac}}{\epsilon^* R_{pol}} \left( \lambda - \frac{\lambda^2(1+\rho^2)}{4\rho} \right) \\ &+ \frac{2a_B^{vac}}{\epsilon^* a_B^{eff}} \left( (2\lambda\rho - \lambda^2\rho^2) \left( 1 - \frac{1}{\left(1 + \frac{a_B^{eff}}{2\rho R_{pol}}\right)^2} \right) \right. \\ &\left. + \frac{\lambda^2\rho^2 a_B^{eff}}{2\rho R_{pol} \left(1 + \frac{a_B^{eff}}{2\rho R_{pol}}\right)^3} \right) \end{aligned}$$

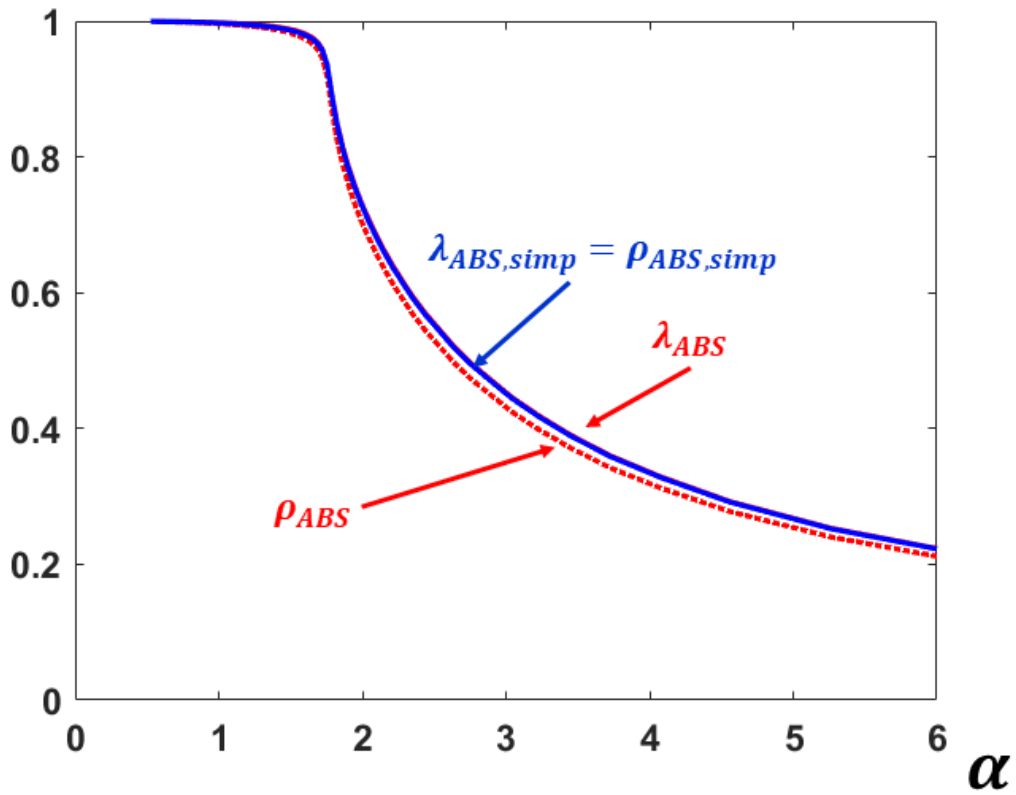


Figure S2. Variation of ABS  $\lambda$  (straight red line) and  $\rho$  (dotted red line) variational parameters as a function of  $\alpha$  for model parameters relevant to MAPbI<sub>3</sub>. The result of a simplified version of the ABS method with a single adjustable parameter ( $\lambda = \rho$ ) is indicated by the blue line.

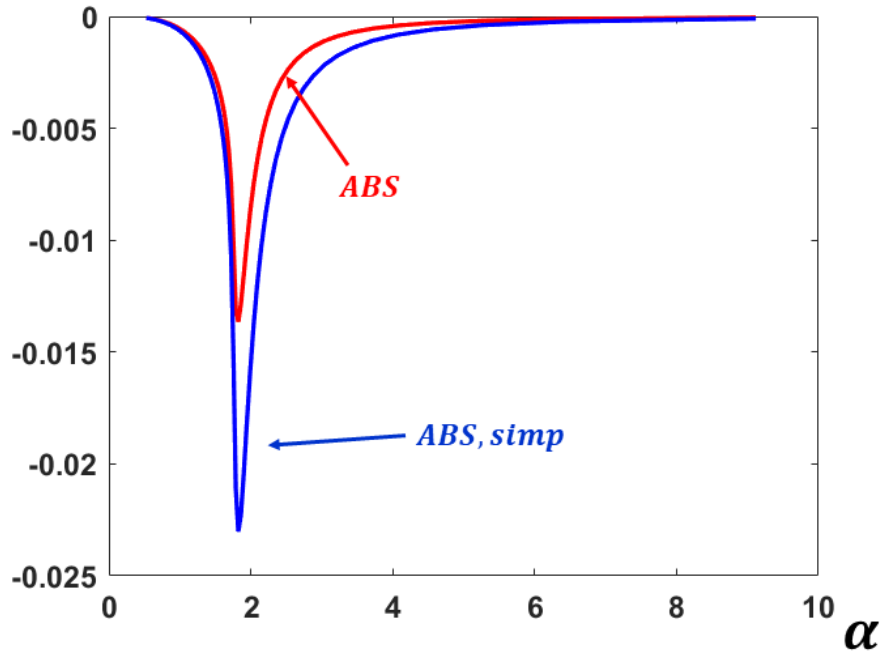


Figure S3. ABS relative error (red line) on the excitonic polaron binding energy by comparison to PB's model as a function of  $\alpha$  for model parameters relevant to MAPbI<sub>3</sub>. The relative error obtained by a simplified version of the ABS method with a single adjustable parameter is indicated by the blue line.

### 10) Computation of multiband Huang-Rhys factors ( $S$ ) within the MPB model

In the dipolar electric approximation within PB's framework, the matrix element for a direct optical transition from the crystal ground state  $|GS\rangle$  to an excitonic polaron state  $|\phi_n(\vec{r}), n_{\vec{k}}\rangle$  characterized

by a wavefunction  $\phi_n(\vec{r})$  ( $n=1S, 2S, \dots$ ) for the relative electron motion and the creation of  $n_{\vec{k}}$  phonons at position  $\vec{k}$  in the dispersion of the LO optical phonon branch is given by:<sup>106,145</sup>

$$\langle GS | \hat{H}_{D.E} | \phi_n(\vec{r}), n_{\vec{k}} \rangle \approx \vec{e} \cdot \vec{M}_{c,v} \psi_n(\vec{0}) \langle 0_{ph} | \hat{W}(\vec{0}) | n_{\vec{k}} \rangle \delta \left( E(\phi(\vec{r}), n_{\vec{k}}) + \frac{\hbar^2 k_{opt}^2}{2M} - \hbar\omega \right)$$

where  $\hbar\omega$  and  $\vec{e}$  are the energy and polarization of the incoming photon,  $\vec{M}_{c,v}$  is the dipolar matrix element between the mono-electronic Bloch functions in the conduction and valence bands,  $0_{ph}$  stands for the absence of thermal phonon population and  $\hat{W}(\vec{r})$  is the unitary transformation of the PB model. The light dispersion can be neglected ( $k_{opt} \approx 0$ ) and  $E(\phi_n(\vec{r}), n_{\vec{k}}) \approx E_n(a_B^{eff}, \vec{0}) + n_{\vec{k}} \hbar\omega_{\vec{k}}$ <sup>106</sup>

For the MPB model, we introduced a generalized unitary transformation  $\hat{S}(\vec{r}) = e^{\sum_{\vec{k},\nu} (F_{\vec{k},\nu}^*(\vec{r}) \hat{a}_{\vec{k},\nu} - F_{\vec{k},\nu}(\vec{r}) \hat{a}_{\vec{k},\nu}^\dagger)}$  assuming independent lattice distortions produced by the various polar optical modes  $\nu$ .

- zero-phonon line ( $0_{ph}$ )

To estimate the amplitude of the zero-phonon line of the 1S excitonic polaron within the MPB model:

$$I_{1S,0_{ph}} \propto |M_{1S,0_{ph}}|^2 \delta(E_{1S}(a_B^{eff}, \vec{0}) - \hbar\omega)$$

$$M_{1S,0_{ph}} = \langle GS | \hat{H}_{D.E} | \phi_{1S}(\vec{r}), 0_{ph} \rangle \approx \vec{e} \cdot \vec{M}_{c,v} \phi_{1S}(\vec{0}) \langle 0_{ph} | \hat{W}(\vec{0}) | 0_{ph} \rangle$$

$$\langle 0_{ph} | \hat{W} | 0_{ph} \rangle = \left\langle 0_{ph} \left| e^{\sum_{\vec{k},\nu} (F_{\vec{k},\nu}^*(\vec{0}) \hat{a}_{\vec{k},\nu} - F_{\vec{k},\nu}(\vec{0}) \hat{a}_{\vec{k},\nu}^\dagger)} \right| 0_{ph} \right\rangle$$

Introducing  $\hat{A} = \sum_{\vec{k},\nu} F_{\vec{k},\nu}^* (\vec{0}) \hat{a}_{\vec{k},\nu}$  and  $\hat{B} = -\sum_{\vec{k},\nu} F_{\vec{k},\nu} (\vec{0}) \hat{a}_{\vec{k},\nu}^+$ , we find  $[\hat{A}, \hat{B}] = -S$  with

$S = \sum_{\nu} S_{\nu} = \sum_{\vec{k},\nu} |F_{\vec{k},\nu}(\vec{0})|^2$ . Using the relations  $e^{\hat{A}+\hat{B}} = e^{\hat{A}} e^{\hat{B}} e^{-\frac{1}{2}[\hat{A},\hat{B}]}$  and  $e^{\hat{A}} e^{\hat{B}} = e^{\hat{B}} e^{\hat{A}} e^{-[\hat{B},\hat{A}]}$ ,

which are valid since  $[\hat{A}, \hat{B}]$  commutes with  $\hat{A}$  and  $\hat{B}$ :

$$\langle 0_{ph} | \hat{S} | 0_{ph} \rangle = e^{-\frac{S}{2}} \text{ and } |M_{1S,0_{ph}}|^2 \propto e^{-S}$$

$$\text{because } e^{\hat{A}} |0_{ph}\rangle = \sum_{n=0}^{+\infty} \frac{1}{n!} \left( \sum_{\vec{k},\nu} F_{\vec{k},\nu}^* (\vec{0}) \hat{a}_{\vec{k},\nu} \right)^n |0_{ph}\rangle = |0_{ph}\rangle$$

- one-phonon replica ( $1_{\vec{k},\nu}$ )

The amplitude of a one phonon replica, phonon branch  $\nu$  at wavevector  $\vec{k}$  of energy  $\hbar\omega_{\vec{k},\nu}$ , for the

1S excitonic polaron is  $I_{1S,1_{\vec{k},\nu}} \propto |M_{1S,1_{\vec{k},\nu}}|^2 \delta(E_{1S}(a_B^{eff}, \vec{0}) + \hbar\omega_{\vec{k},\nu} - \hbar\omega)$  with:

$$M_{1S,1_{\vec{k},\nu}} \approx \vec{e} \cdot \vec{M}_{c,\nu} \phi_{1S}(\vec{0}) \langle 0_{ph} | \hat{W}(0) | 1_{\vec{k},\nu} \rangle$$

Using the same transformation:

$$e^{\hat{A}} |1_{\vec{k},\nu}\rangle = \sum_{n=0}^{+\infty} \frac{1}{n!} \left( \sum_{\vec{k},\nu} F_{\vec{k},\nu}^* (\vec{0}) \hat{a}_{\vec{k},\nu} \right)^n \hat{a}_{\vec{k},\nu}^+ |0_{ph}\rangle = F_{\vec{k},\nu}^* (\vec{0}) |0_{ph}\rangle$$

$\langle 0_{ph} | \hat{S} | 1_{\vec{k},\nu} \rangle = e^{-\frac{S}{2}} \langle 0_{ph} | e^{\hat{B}} e^{\hat{A}} | 1_{\vec{k},\nu} \rangle = e^{-\frac{S}{2}} F_{\vec{k},\nu}^* (\vec{0})$ , the ratio of  $I_{1S,1_{\vec{k},\nu}}$  and  $I_{1S,0_{ph}}$  is given by:

$$\frac{|M_{1S,1_{\vec{k},\nu}}|^2}{|M_{1S,0_{ph}}|^2} = |F_{\vec{k},\nu}(\vec{0})|^2$$

For a phonon branch  $\nu$  without dispersion ( $\hbar\omega_{\vec{k},\nu} = \hbar\omega_\nu$ ), it is possible to sum over  $\vec{k}$  the one phonon replica  $I_{1S,1\nu}$  contributions observed at  $\hbar\omega \approx E_{1S}(a_B^{eff}, \vec{0}) + \hbar\omega_\nu$  :

$$\frac{I_{1S,1\nu}}{I_{1S,0ph}} = \frac{\sum_{\vec{k}} |M_{1S,1\vec{k},\nu}|^2}{|M_{1S,0ph}|^2} = S_\nu = \sum_{\vec{k}} |F_{\vec{k},\nu}(\vec{0})|^2$$

- two-phonons replica ( $2_\nu: 1_{\vec{k}_1,\nu}, 1_{\vec{k}_2,\nu}$ )

To compute the two-phonon replica for the same phonon branch  $\nu$ , it is necessary to consider two contributions ( $\frac{1}{2}$  in the following expression to avoid double-counting):

$$I_{1S,2\nu} \propto \frac{1}{2} \sum_{\vec{k}_1} \sum_{\vec{k}_2 \neq \vec{k}_1} \left| \langle 0_{ph} | \hat{S} | 1_{\vec{k}_1,\nu}; 1_{\vec{k}_2,\nu} \rangle \right|^2 \delta \left( E_{1S}(a_B^{eff}, \vec{0}) + \hbar\omega_{\vec{k}_1,\nu} + \hbar\omega_{\vec{k}_2,\nu} - \hbar\omega \right) \\ + \sum_{\vec{k}_1} \left| \langle 0_{ph} | \hat{S} | 2_{\vec{k}_1,\nu} \rangle \right|^2 \delta \left( E_{1S}(a_B^{eff}, \vec{0}) + 2\hbar\omega_{\vec{k}_1,\nu} - \hbar\omega \right)$$

with  $|1_{\vec{k}_1,\nu}; 1_{\vec{k}_2,\nu}\rangle = \hat{a}_{\vec{k}_1,\nu}^+ \hat{a}_{\vec{k}_2,\nu}^+ |0_{ph}\rangle$  and  $|2_{\vec{k}_1,\nu}\rangle = \frac{\hat{a}_{\vec{k}_1,\nu}^{+2}}{\sqrt{2}} |0_{ph}\rangle$

$$\langle 0_{ph} | \hat{S} | 1_{\vec{k}_1,\nu}; 1_{\vec{k}_2,\nu} \rangle = e^{-\frac{S}{2}} \langle 0_{ph} | e^{\hat{B}} e^{\hat{A}} | 1_{\vec{k}_1,\nu}; 1_{\vec{k}_2,\nu} \rangle = e^{-\frac{S}{2}} F_{\vec{k}_1,\nu}^*(\vec{0}) F_{\vec{k}_2,\nu}^*(\vec{0})$$

$$\langle 0_{ph} | \hat{S} | 2_{\vec{k}_1,\nu} \rangle = e^{-\frac{S}{2}} \langle 0_{ph} | e^{\hat{B}} e^{\hat{A}} | 2_{\vec{k}_1,\nu} \rangle = \frac{e^{-\frac{S}{2}}}{\sqrt{2}} F_{\vec{k}_1,\nu}^*(\vec{0})^2$$

Using:

$$\left\langle 0_{ph} \left| \frac{\hat{a}_{\vec{k}_1,\nu}^{+2} \hat{a}_{\vec{k}_1,\nu}^{+2}}{2} \right| 0_{ph} \right\rangle = \left\langle 0_{ph} \left| \frac{\hat{a}_{\vec{k}_1,\nu}^{+2} \hat{a}_{\vec{k}_1,\nu}^+}{2} \right| 1_{\vec{k}_1,\nu} \right\rangle = \left\langle 0_{ph} \left| \frac{\hat{a}_{\vec{k}_1,\nu}^{+2}}{\sqrt{2}} \right| 2_{\vec{k}_1,\nu} \right\rangle = \left\langle 0_{ph} \left| \hat{a}_{\vec{k}_1,\nu} \right| 1_{\vec{k}_1,\nu} \right\rangle = 1$$

Considering an optical phonon branch without dispersion, the ratio of the two-phonon replica observed at  $\hbar\omega \approx E_{1S}(a_B^{eff}, \vec{0}) + 2\hbar\omega_\nu$  to the one of the zero-phonon line at observed at  $\hbar\omega \approx E_{1S}(a_B^{eff}, \vec{0})$  is:

$$S_{2\nu} = \frac{I_{1S,2\nu}}{I_{1S,0\nu}} = \frac{(S_\nu)^2}{2}$$

- two-phonons overtone ( $1_{\vec{k}_1, \nu_1}, 1_{\vec{k}_2, \nu_2}, \nu_1 \neq \nu_2$ )

$$I_{1S,1\nu_1,1\nu_2} \propto \sum_{\vec{k}_1} \sum_{\vec{k}_2} \left| \langle 0_\nu | \hat{S} | 1_{\vec{k}_1, \nu_1}; 1_{\vec{k}_2, \nu_2} \rangle \right|^2 \delta(E_{1S}(a_{B,eff}, \vec{0}) + \hbar\omega_{\vec{k}_1, \nu_1} + \hbar\omega_{\vec{k}_2, \nu_2} - \hbar\omega)$$

leading for phonon branches without dispersion to:

$$\frac{I_{1S,1\nu_1,1\nu_2}}{I_{1S,0ph}} = S_{\nu_1} S_{\nu_2}$$

- sum rule for the MPB model

Summing all the contributions of the phonon replica and overtones for the various phonon branches leads to a sum rule similar to the one predicted for the PB model: <sup>106,145</sup>

$$e^{-S} e^S = e^{-S} \sum_{n=0}^{+\infty} \frac{1}{n!} \left( \sum_{\nu} S_{\nu} \right)^n = e^{-S} \left( 1 + \left( \sum_{\nu} S_{\nu} \right) + \frac{1}{2} \left( \sum_{\nu} S_{\nu} \right)^2 + \dots \right)$$

where the contributions of the zero-phonon line, the one-phonon replica and the two-phonon lines (replica+overtones) appear progressively.